University of Illinois at Urbana-Champaign

Air Conditioning and Refrigeration Center A National Science Foundation/University Cooperative Research Center

Effect of Shorter Compressor On/Off Cycle Times on A/C System Performance

S. M. Ilic, C. W. Bullard, and P. S. Hrnjak

ACRC CR-43 December 2001

For additional information:

Air Conditioning and Refrigeration Center
University of Illinois
Mechanical & Industrial Engineering Dept.
1206 West Green Street
Urbana, IL 61801

(217) 333-3115

Prepared for
Copeland Corporation

The Air Conditioning and Refrigeration Center was founded in 1988 with a grant from the estate of Richard W. Kritzer, the founder of Peerless of America Inc. A State of Illinois Technology Challenge Grant helped build the laboratory facilities. The ACRC receives continuing support from the Richard W. Kritzer Endowment and the National Science Foundation. The following organizations have also become sponsors of the Center.

Alcan Aluminum Corporation
Amana Refrigeration, Inc.
Arçelik A. S.
Brazeway, Inc.
Carrier Corporation
Copeland Corporation
Dacor
Daikin Industries, Ltd.
Delphi Harrison Thermal Systems
General Motors Corporation
Hill PHOENIX
Honeywell, Inc.
Hydro Aluminum Adrian, Inc.
Ingersoll-Rand Company
Invensys Climate Controls
Kelon Electrical Holdings Co., Ltd.
Lennox International, Inc.
LG Electronics, Inc.
Modine Manufacturing Co.
Parker Hannifin Corporation
Peerless of America, Inc.
Samsung Electronics Co., Ltd.
Tecumseh Products Company
The Trane Company
Valeo, Inc.
Visteon Automotive Systems
Wolverine Tube, Inc.
York International, Inc.

For additional information:

Air Conditioning & Refrigeration Center
Mechanical & Industrial Engineering Dept.
University of Illinois
1206 West Green Street
Urbana, IL 61801

217 333 3115

Abstract

Effects of compressor on/off cycle times shorter than typical a/c heat exchanger thermal time constant (~1 min) were examined as a method of cooling capacity regulation. Short compressor on/off cycle times enable the use of heat exchangers continuously throughout entire off-cycle, thus reducing on-cycle temperature lift and increasing COP compared to conventional cycling.

Experiments were done for a typical residential a/c system for run time fractions from 0.3 to 1.0, and cycle periods from 10 to 80 seconds. The objective was to understand how pulsed refrigerant flow from the compressor affects performance of the other components. Refrigerant side heat transfer resistance, pressure drop, and magnitude and curvature of heat exchanger surface temperature fluctuations were identified as the most influential factors affecting system performance. Virtually identical effects were observed for wet and dry coil experiments.

Results at a run time fraction of 0.56 were compared to continuous (simulating variable speed) operation of a smaller compressor providing the same cooling capacity. Cycling the compressor at cycle periods of 10-80 sec degraded the performance of other components enough to reduce COP by approximately 2.5-7.5%, respectively. The corresponding COP loss for conventional long-cycling was 11.5%, all on the condenser side, because evaporator surface temperature was held constant to ensure that sensible and latent capacities were comparable. Comparisons of actual variable speed and cycling strategies must also account for parasitic power such as inverter losses and differences in fan and blower power.

Table of Contents

Page

Abstract ii

List of Figures v

List of Tables vii

Nomenclature viii

Chapter 1: Introduction 1

1.1 Background 1

1.2 Purpose 2

Chapter 2: Experimental facility, test matrix and procedure 3

2.1 Experimental facility 3

2.2 Test procedure 4

2.3 Test matrix 5

Chapter 3: Analysis of factors affecting short-cycling performance 7

3.1 Evaluating short-cycling performance 7

3.2 Factors affecting short-cycling efficiency 8

3.2.1 Refrigerant side heat transfer 8

3.2.2 Pressure drop 8

3.2.3 Thermal capacitance (heat exchanger metal temperature nonlinearity) 8

3.3 Analysis of short-cycling experiments 9

3.3.1 Automobile a/c system experiments 9

3.3.2 Residential a/c system experiments 10

3.4 Effect of evaporator thermal capacitance 17

3.4.1 Model validation using the experimental measurements 18

3.4.2 Effect of changing the design variables hA_{air} and C_m 20

3.5 Wet coil performance under short-cycling 23

3.6 Open vs. closed valve operation 26

Chapter 4: Short-cycling comparison to continuous operation 29

4.1 Short-cycling losses at $\dot{m}$=0.56 compared to continuous operation 29

4.2 Lift degradation terms breakdown for t=0, 10 and 80 seconds at $\dot{m}$=0.56 31

4.3 Lift loss for t=10 and 80 seconds at $\dot{m}$=0.56 34

4.3.1 Losses due to short-cycling at τ=10 seconds 35

4.3.2 Losses due to short-cycling at longer cycle periods (τ=80 seconds) 36

4.4 Short-cycling comparison to conventional cycling 37

Chapter 5: Conclusions 38
5.1 Defining an ideal baseline for comparing capacity regulation methods 38
5.2 Factors affecting short-cycling COP degradation 38
5.2.1 Refrigerant side heat transfer resistance 38
5.2.2 Pressure drop 39
5.2.3 Heat exchanger thermal capacitance 39
5.2.4 Other effects 39
5.3 Short-cycling compared to variable-speed meeting ~1/2 of design load 40
5.3.1 Losses for 10-second cycle period 40
5.3.2 Losses for 80-second cycle period 40
5.4 Short-cycling compared to conventional cycling 41
References 42
Appendix A: Short-cycling experiments on R134a mobile a/c system 43
A.1 Purpose 43
A.2 Experimental setup 43
A.3 Experiment description 43
A.4 Experimental results and analysis 44
A.5 Conclusions 49
Appendix B: Experimental setup for residential a/c system 51
B.1 A/C refrigeration loop and components 51
B.2 Environmental chambers and evaporator wind tunnel 55
B.3 Measured parameters 55
B.3.1 Measured parameters providing information about COP 56
B.4 Data acquisition 58
B.4.1 Data acquisition system 59
B.4.2 Slow data sampling for instantaneous display 60
B.4.3 Fast data sampling 62
Appendix C: Short-cycling experiments at 26.7/27.7^{o} C (80/82^{o} F) 65
C.1 Dry coil experiments 65
C.1.1 Short-cycling losses at μ=0.57 compared to continuous operation 65
C.1.2 Temperature lift degradation breakdown for τ=0, 50 seconds at μ=0.57 67
C.1.3 Lift loss for τ=10 and 50 seconds at μ=0.57 68
C.1.4 Short-cycling comparison to conventional cycling 69
C.2 Wet coil experiments at 26.7/27.7 C (80/82 F) 70
APPENDIX D: Temperature lift degradation for open vs. closed valve 72

List of Figures

Page

Figure 2.1 The change in capacity and air flow rate with run time fraction 4
Figure 3.1 Automotive a/c system efficiency comparison; variable speed vs. short-cycling 9
Figure 3.2 COP degradation with cycle period for experiments at μ=0.5 10
Figure 3.3 The saturation temperature lift increase with τ for experiments at μ=0.5 10
Figure 3.4 Lift degradation term increase with cycle period for experiments at μ=0.5 11
Figure 3.5 Lift degradation term as a function of cycle period and run time fraction 12
Figure 3.6 Temperature lift as a function of μ for τ=10 sec 13
Figure 3.7 Lift degradation term as a function of μ for τ=10 sec 13
Figure 3.8 Refrigerant heat transfer part of temperature lift degradation term, ΔT_e(rht) 14
Figure 3.9 Refrigerant pressure drop part of lift degradation term, $\Delta T_e(\Delta P)$ 15
Figure 3.10 Nonlinear evaporator metal temperature, $T_{m,e}$, oscillations at μ=0.5 and τ=50 sec 16
Figure 3.11 Metal temperature nonlinearity part of a COP loss term, ΔT_e(nonlin) 16
Figure 3.12 Lift degradation term divided into three parts for μ=0.5 and τ=50 sec 17
Figure 3.13 Experimentally obtained values of $hA_{air,e}$ for the range of μ and τ 19
Figure 3.14 Experimentally obtained values of C_m for the range of μ and τ 19
Figure 3.15 The model results comparison to the experimental results at μ=0.5 and τ=80 sec 20
Figure 3.16 Calculated evaporator metal temperature 21
Figure 3.17 Influence of halving C_m 22
Figure 3.18 Influence of doubling $hA_{air,e}$ 22
Figure 3.19 COP degradation with cycle period for dry coil experiments 24
Figure 3.20 COP degradation with cycle period for wet coil experiments 24
Figure 3.21 On-cycle average saturation temperatures for dry coil experiments 25
Figure 3.22 On-cycle average saturation temperatures for wet coil experiments 25
Figure 3.23 Evaporator metal and dew point temperature at μ=0.3 and τ=80 sec 26
Figure 3.24 Refrigerant mass flow rate into the evaporator overlaid for OV and CV 27
Figure 3.25 Evaporator and condenser saturation temperatures overlaid for OV and CV 28
Figure 4.1 Saturation temperature lift and degradation terms increase with τ 29
Figure 4.2 Coefficient of performance decrease with τ 30
Figure 4.3 Evaporator side lift degradation term increase with τ 31
Figure 4.4 Condenser side lift degradation term increase with τ 31
Figure 4.5 Lift degradation term breakdown on evaporator side 32
Figure 4.6 Lift degradation term breakdown on condenser side 32
Figure 4.7 Evaporator degradation term for VS operation (τ=0) 33
Figure 4.8 Evaporator degradation term for SC at τ=10 sec 33
Figure 4.9 Evaporator degradation term for SC at τ=80 sec 34
Figure 4.10 Breakdown of the lift loss term on evaporator side 34
Figure 4.11 Breakdown of the lift loss term on condenser side 35
Figure 4.12 Evaporator pressure drop at τ=10 sec (short-cycling) and τ=0 sec (continuous) 35

Figure 4.13 COP comparison to conventional cycling....37
Figure A.1 Experiment results for short-cycling (SC) and variable speed (VS) capacity regulation method....46
Figure A.2 Change of compressor work and evaporator capacity for SC at τ=10 sec and VS....46
Figure A.3 Change of coefficient of performance of cycle for SC at τ=10 sec and VS....47
Figure A.4 Saturation temperatures averaged over on-cycle for VS and SC....48
Figure A.5 Change in evaporator and condenser saturation temperatures for two cycles of short-cycling operation at μ=0.35 and τ=10 sec....48
Figure A.6 Change in evaporator and condenser saturation temperatures for two cycles (τ=10 seconds) for run time fractions μ=0.8, 0.6 and 0.35....49
Figure B.1 Residential a/c facility for short-cycling....52
Figure B.2 1st slow sampling and averaging program screen shot....60
Figure B.3 2nd Slow sampling and averaging program screen shot....61
Figure B.4 3rd slow sampling and averaging program screen shot....61
Figure B.5 4th slow sampling and averaging program screen shot....62
Figure B.6 5th slow sampling and averaging program screen shot....62
Figure B.7 1st screen shot of entire fast sampling and averaging program....63
Figure B.8 2nd screen shot of fast sampling and averaging program....63
Figure B.9 E1313A Direct I/O control panel, configuration panel....64
Figure B.10 E1313A Direct I/O control panel, engineering units panel....64
Figure B.11 E1313A Direct I/O control panel, scan-list panel....64
Figure B.12 E1313A Direct I/O control panel, trigger panel....64
Figure C.1 Saturation temperature lift and degradation terms increase with τ....65
Figure C.2 Coefficient of performance decrease with τ....66
Figure C.3 Evaporator side lift degradation term increase with τ....66
Figure C.4 Condenser side lift degradation term increase with τ....67
Figure C.5 Lift degradation term breakdown on evaporator side....67
Figure C.6 Lift degradation term breakdown on condenser side....68
Figure C.7 Breakdown of the lift loss term on evaporator side....68
Figure C.8 Breakdown of the lift loss term on condenser side....69
Figure C.9 COP comparison to conventional cycling....69
Figure C.10 Saturation temperature lift and degradation terms increase with τ....70
Figure C.11 Coefficient of performance decrease with τ....71
Figure D.1 Evaporator metal and saturation temperature for CV....73
Figure D.2 Evaporator metal and saturation temperature for OV....73
Figure D.3 Evaporator superheat for CV....74
Figure D.4 Evaporator superheat for OV....74
Figure D.5 Evaporator pressure drop overlaid for OV and CV operation....75

List of Tables

Page

Table 2.2 Test matrix for automotive a/c system experiments 6
Table 3.1 Temperature lift degradation breakdown 12
Table 3.2 Experimental results compared for OV and CV operation 27
Table A.1 Experimental results for short-cycling and variable speed capacity regulation method 44
Table A.2 Condenser and evaporator saturation temperatures for VS and SC operation (τ=10s) 47
Table B.1 Short-cycling parameters and instruments used for measurements 53
Table D.1 Lift degradation term and its components for OV and CV operation 72

Nomenclature

A	area, m^2
AMTD	arithmetic mean temperature difference
c	specific heat, kJ/kg-K
C	thermal capacitance $(\dot{m} * c)$, kJ/K
COP	coefficient of performance
ΔT	temperature difference, °C
ΔT_c	condenser side degradation term, °C
ΔT_e	evaporator side degradation term, °C
ΔT_{sat}	temperature lift (cond-evap saturation temperature difference), °C
ΔP	pressure drop, kPa
Δu	internal energy difference.
h	heat transfer coefficient, kW/m^2-K
hA	product of heat transfer coefficient and corresponding area (h*A)
$\dot{Q}_e$	evaporator capacity, kW
$\dot{Q}_{ref}$	refrigerant side heat transfer rate, kW
t	time, s
u	internal energy, kJ/kg-K
$\dot{V}$	volumetric air flow rate, cfm or m^3/s
W	power, kW
x	refrigerant quality

Greek

μ	run time fraction
τ	cycle period, s
ρ	density, kg/m^3

Subscripts

air	air
avg	average (mean)
c	condenser
cp	compressor
cv	closed valve
e	evaporator
f	fin
in	in
init	initial
m	metal
max	maximum
mean	arithmetic mean with respect to surface

min	minimum
off	off-cycle
on	on-cycle
out	out
ov	open valve
ref	refrigerant
sat	saturation
sc	short-cycling
t	tube
vs	variable speed

Chapter 1: Introduction

1.1 Background

There is a need for capacity regulation in any air-conditioning system in order to maintain specified room comfort as sensible and latent loads change. Most residential air-conditioning (a/c) systems in North America are designed to meet the maximum heat load, sized to operate continuously at a specified design condition. During its lifetime an a/c system seldom operates at design conditions. In order to meet actual loads, less than the maximum, they usually operate in cycles of on and off operation, where the cycle length is determined by a deadband thermostat controlling indoor room temperature.

A typical residential thermostat characteristic corresponds to approximately 3 cycles per hour at 50% system load, as discussed by Parken et al. (1977). For example, for a moderate summer day in which heat load is 50% of maximum (design) heat load, residential a/c system is on about 50% of time, and off about 50% of time. If cycle duration is 20 minutes, then it is turned off after about 10 min, stays off 10 minutes and is turned on again. For a different summer day, average evaporator capacity and compressor power, over the cycle period, are reduced by reducing compressor run time fraction. In this conventional cycling (CC) type of capacity regulation using long cycling, both evaporator capacity and compressor power have maximum values during a large portion of on-cycle and minimum values during a large portion of off-cycle. The heat exchangers (evaporator and condenser) are practically inactive during off-cycles that exceed the heat exchanger thermal time constant. This causes very high pressure lift during a large portion of the on-cycle and thus low efficiency.

In addition, long cycling efficiency is affected by cyclic losses. A significant amount of work has been done in determining and quantifying cyclic losses in refrigeration systems. Refrigerant migration and component thermal masses have been identified as the important contributors to cycling losses in the work of Coulter and Bullard (1997), Krause and Bullard (1996), Wang and Wu (1990), Mulroy and Didion (1985), Murphy and Goldschmidt (1986).

One alternative to the capacity regulation by long cycling is variable speed (VS) capacity regulation, in which the system runs continuously, but at lower compressor speed. The room thermostat is connected to the compressor controller such that when the heat load increases (indoor temperature increases) compressor speed increases maintaining constant indoor temperature, while the compressor operates all the time. A heat transfer surface area of heat exchangers is used in whole period of continuous operation reducing pressure lift and achieving high cycle efficiencies. The findings of Bahel and Zubair (1989), Tassou et al. (1983), Marquand et al. (1984), Toshiba (1987), Umezu and Suma (1984) show that VS systems can achieve seasonal energy savings of 15% to 40%. The cost of using VS capacity regulation method is high due to a need for inverter for changing compressor speed.

Another way of regulating system capacity during the year is by cycling a compressor using shorter on/off cycle times than typical a/c heat exchanger thermal time constant (~ 1 min). Thus, the compressor short-cycling (SC) is characterized by short cycles of compressor on and off operation having duration on the order of seconds (5-20 sec). The room thermostat would regulate the run time fraction of short-cycling similarly to regulating speed during the variable speed regulation method. Thus, when the heat load increases (indoor temperature increases) run

time fraction increases maintaining constant indoor temperature. Heat exchangers are used in whole period of short-cycling operation, reducing pressure lift during the on-cycle and ideally achieving the cycle efficiency of VS capacity regulation method. The initial cost of using short-cycling capacity regulation method is potentially lower, since there is no need for inverter. Even though the short-cycling may seem as a special case of a conventional long-cycling, its performance and regulation are almost the same as during the variable speed operation. There are several important similarities to the variable speed operation. Firstly, the room thermostat doesn't regulate directly the cycle period (as in the long-cycling), but run time fraction similar to the way compressor speed is regulated in variable speed system. Secondly, the evaporator airflow requirements for compressor short-cycling are essentially the same as for a variable-speed compressors. Since the heat exchangers are used during the whole cycle period, evaporator blower operates all the time, ideally at a speed adjusted to enable independent control of humidity. In contrast, during the long-cycling operation, the fan and blower operate only during the on-cycle, and in some instances during the short initial phase of the off-cycle during which there is still potential for exchange of heat at the condenser and evaporator. Finally, the evaporator and condenser saturation temperatures cycle with a small amplitude around almost the same average temperature as in the variable speed operation during the short-cycling operation, which provides for almost the same on-cycle pressure lift in between variable speed and short-cycling and thus almost the same energy efficiency. In the limit as cycle period is reduced to zero, short-cycling becomes indistinguishable (viewed from the perspective of heat exchangers' response, not compressor) from VS. By increasing cycle period significantly, short-cycling operation becomes equal to the conventional long-cycling operation with the evaporator blower constantly operating.

1.2 Purpose

The purpose of this report is to experimentally explore a method of capacity regulation involving compressor on/off cycle times shorter than typical a/c heat exchanger thermal time constant, Experiments were conducted in a conventional residential-scale split a/c system. The factors causing compressor short-cycling efficiency losses are identified and quantified. The experimental facility, test procedure and test matrices will be described in Chapter 2. After introducing the procedures used for evaluation of short-cycling performance in Chapter 3, the factors important for the evaluation will be explained: 1) refrigerant side heat transfer resistance, 2) pressure drop and 3) the heat exchanger thermal capacitance. Chapter 4 presents an experimental comparison between short-cycling and continuous operation for meeting an equal and constant load, and analyzes the effect of cycle period on system performance. Conclusions are presented in Chapter 5.

Appendix A compares SC and VS operation in automotive a/c system. With our residential a/c apparatus, it was not possible to compare SC with VS operation without resorting to use of different compressors and then sorting out the effects of their different efficiencies. Therefore, to compare SC and VS operation in a controlled fashion, some preliminary experiments were conducted using an automotive a/c systems. Experimental results showing almost the same efficiency of SC and VS method in automotive a/c system is presented in Appendix A (and excerpt in section 3.3.1). A description of the residential a/c system facility is presented in Appendix B. Appendix C and D present figures with experimental data related to residential a/c experiments, which were not included in the Chapters for the clarity of presentation purposes.

Chapter 2: Experimental facility, test matrix and procedure

2.1 Experimental facility

The main components of a residential air conditioning system tested were condenser, evaporator, compressor and expansion valve. The heat exchangers (condenser and evaporator) were taken from a two-ton, R-22, unitary rooftop air conditioning system (Trane model TCH024100A). Indoor and outdoor heat exchangers for this system are made of copper tubing and plate fins, and were placed in separate environmental chambers. The heat exchangers were not modified from the original unitary a/c design in any way, but compressor, piping and expansion device were replaced. A Copeland's two-ton hermetic scroll compressor (Copeland model ZR22K3-TF5) was fitted with a dynamic solenoid valve to enable more precise measurement and system control during the experiments. The valve ensured that no refrigerant vapor leaked back to the evaporator during the off-cycle, and eliminated power inputs during the off-cycle. The compressor was connected to a switch and timer that controlled lengths of on and off compressor operation during short-cycling.

The existing commercial implementation of this concept has the mechanical clutch mechanism installed in the compressor for the purpose of engaging and disengaging scrolls, enabling power efficient short-cycling without high starting currents and potential reliability risks which exist when a switch is used. A switch was used in our experiment since our focus has been on the influence of short-cycling on the rest of the system, not compressor. The high starting currents were excluded from the analyses presented in this report. The measured start-up power peak lasted about 0.2 seconds and accounted for about 0.5 – 10 % of the cycle-average measured power, for the longest (56 sec) and shortest (3 sec) on-cycles, respectively.

In addition, the system was designed to enable liquid flow into the evaporator during the whole off-cycle, by adding receiver holding enough liquid refrigerant to last during off-cycles of up to 40 seconds.

A manually adjusted expansion device replaced the original TXV to enable more precise control of the experiments by eliminating the uncontrollable lags inherent in TXV's. A solenoid valve was installed upstream of the expansion device to enable comparison of two operating modes: 1) valve continuously open; and 2) valve synchronized with compressor to isolate evaporator from condenser during off-cycle. The latter mode has been found to be an efficient strategy in conventional cycling experiments, reported by Wang and Wu (1989).

Fast data scanning speed is needed to capture quick changes in measured parameters during short-cycling. All data was taken with data acquisition system which was programmed for scanning a group of more than 50 parameters in 0.2 seconds. The data acquisition system carried special 7 Hz fixed filters capable of filtering electrical noise from thermocouple measurements. The filters were installed since electric noise produces huge errors on thermocouple readings at very fast scanning rates without filters. The temperatures, pressures, powers and flow rates were measured throughout the facility. The air side and surface temperatures were measured by T-type thermocouples, and the refrigerant side temperatures were measured by T-type immersion thermocouple probes. Thermocouples were adjusted for tare values to provide the same output at the room temperature. The uncertainty in thermocouple measurement is estimated to be +-0.1^{o} C, using manufacturer's specifications. Low range, 0 to 1" water (+/-0.4% FS), differential air pressure transducer was used for measuring the air side pressure drop across the nozzle. The refrigerant pressures and pressure drops were measured by using absolute 0 to 500 psia (+/-0.1 % FS)

and differential 0 to 50 psid (+/-0.25% FS) pressure transducers. Watt transducers 0 to 8 kW (+/-0.5% FS) measured the compressor, blower and heater powers. Coriolis type 0 to 680 kg/h (+/-0.15% of reading) mass flow meter, consisting of sensor and transmitter was used for measuring the refrigerant mass flow rate.

2.2 Test procedure

For clarity of presentation, this report presents results from experiments performed with dry indoor coil, at 80° F (26.7° C) indoor air, and 95° F (35° C) outdoor air temperatures used for evaluation of the short-cycling performance. The results at other experimental conditions will be presented in appendices. There is no significant difference in the COP loss analysis, for the wet and dry coil experiments, as long as the evaporator surface temperature remained lower than the dew point temperature at the end of the off-cycle. Results for a wet coil tests will be presented in section 3.5.

The main method of regulating the evaporator capacity in short-cycling systems is the regulation of run time fraction. The air flow rate over evaporator was decreased along with run time fraction (capacity), in order to maintain the evaporator surface temperature at about 12° C during all experiments, as would be required during actual wet coil operation. This enabled approximately the same latent/sensible load split during the wet indoor coil surface experiments at different evaporator capacities. Figure (2.1) shows that the percent reduction from the design air flow rate was almost the same as the percent change in the evaporator capacity due to the requirement to maintain constant evaporator surface temperature. The evaporator design air flow rate was $\dot{V}$ = 800 cfm (0.378 m^3/s). The air flow rate over the condenser was kept constant for all experiments at $\dot{V}$ = 2500 cfm (1.180 m^3/s).

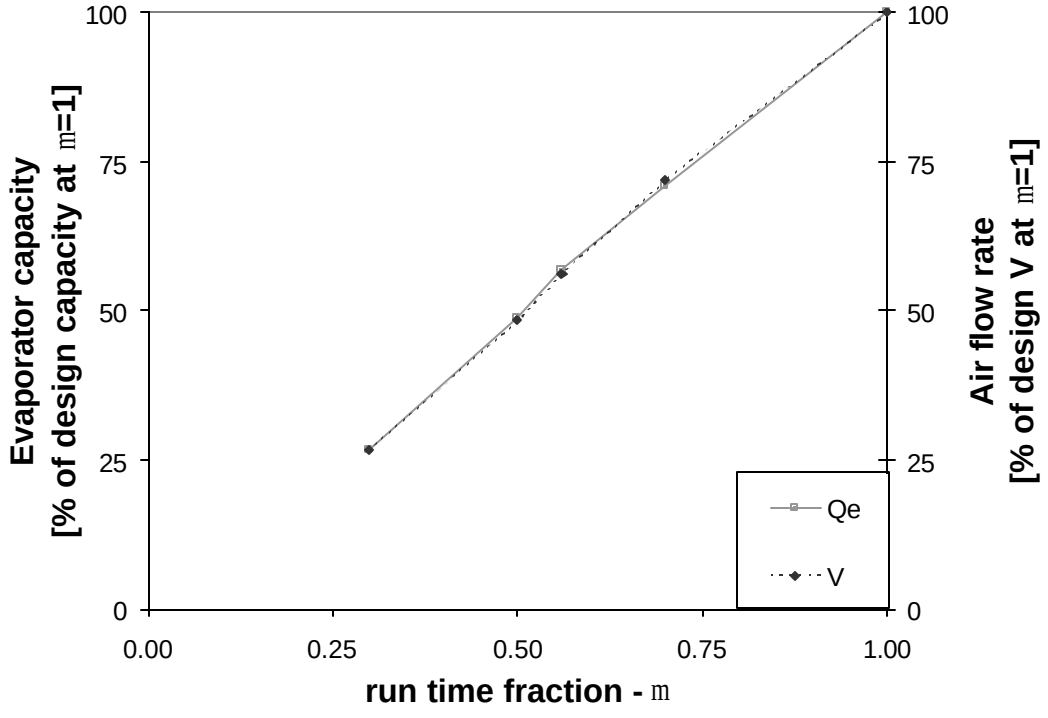

Figure 2.1 The change in capacity and air flow rate with run time fraction

An EEV was installed in the system and adjusted manually to achieve the desired fixed opening for each operating condition. A fixed opening proved capable of providing the desired average on-cycle superheat at the evaporator exit (of about 4^{o} C) for experimental points at short-cycle periods (τ~10 sec). However, during longer cycle periods (τ~60 sec) the fixed opening caused large fluctuations of superheat (1 – 15^{o} C), with especially large superheat at the end of on-cycle, causing significant degradation of evaporator capacity. A fast-responding EEV, which would maintain constant superheat at the exit of evaporator during whole cycle period was not available. Therefore to ensure that evaporator performance was repeatable, an expansion device opening was found which enabled maintenance of the two-phase refrigerant evaporator exit throughout the whole on-cycle for each experimental point. This eliminated the evaporator capacity degradation. To protect compressor from liquid slugging a tape heater was installed on the suction line. In a real system, a fast-responding EEV would serve this purpose with no additional energy input. Variation in average on-cycle suction superheat of 5 to 11^{o} C was observed for the whole test matrix due to use of fixed orifice and tape heater instead of more suitable fast EEV.

The analysis presented in Chapter 4 of the report compares short-cycling experiments done at run time fraction of 0.56 to continuous operation to meet a load of about 4.0 kW. Continuous operation was achieved by installing a nominal one-ton rotary compressor (Kenmore a/c unit, model 253.8783110, with compressor part# A445513).

2.3 Test matrix

The experiments were done in automotive and residential a/c lab. The a/c systems in these two labs are described in Appendices A and B respectively.

The residential a/c system experiments were conducted at several conditions: at $80/95^{o}$ F (indoor/outdoor air temperature) with dry and wet coil; at $80/82^{o}$ F with dry and wet coil. The test matrix listing all run time fractions and cycle periods run at these conditions is shown in Table 2.1.

The test matrix was designed to provide information on short-cycling performance at various cycle periods and run time fractions. The compressor was short-cycled at run time fractions (μ=0.56, 0.57 or 0.58 depending on running conditions) to match exactly the capacity achieved during the continuous compressor operation. These short-cycling experiments can therefore be compared to continuous operation.

Table 2.1 Test matrix for residential a/c system experiments

80/95°F								
run time fraction	cycle period [sec]							
	10		30		50		80	
	dry	wet	dry	wet	dry	wet	dry	wet
1	x	x	x	x	x	x	x	
0.7	x	x	x		x		x	
0.56 (0.57 wet)	x	x	x	x	x	x	x	
0.5	x	x	x	x	x	x	x	
0.3	x	x	x	x	x	x	x	x

80/82°F								
run time fraction	cycle period [sec]							
	10		30		50		80	
	dry	wet	dry	wet	dry	wet	dry	wet
0.57 (0.58 wet)	x	x		x	x	x		x

Before designing the residential a/c experiments, an initial set of experiments were conducted on an automotive a/c system using both short-cycling and variable-speed capacity regulation method. The design compressor speed was chosen. The system was run at various run time fractions and cycle periods at the design on-cycle compressor speed during short-cycling operation. During the variable speed operation, the system was run at several compressor speeds lower than the design speed and the efficiencies of the two methods were compared. The test matrix listing all run time fractions, cycle periods (for short-cycling) and speeds (for variable-speed) is shown in Table (2.2). Those results, detailed in Appendix A, showed that short-cycling system efficiency could indeed approach that of variable-speed system. They also revealed that the built-in time lags of a TXV rendered it unsuitable for conducting repeatable experiments on short-cycling system.

Table 2.2 Test matrix for automotive a/c system experiments

Short-cycling				Variable-speed	
run time fraction	cycle period [sec]			compressor speed [rpm]	
	5	10	15		
1	x	x	x	1700	x
0.8	x	x	x	1350	x
0.6	x	x	x	1000	x
0.35	x	x	x	700	x

Chapter 3: Analysis of factors affecting short-cycling performance

3.1 Evaluating short-cycling performance

Widespread reliance on cycling as the preferred method for modulating capacity in a/c systems has resulted in a large body of literature that defines cycling "losses" by comparing cycling COP to the steady state COP at 100% capacity. Today, with the increasing use of variable-speed and variable-capacity compressors, it is appropriate to redefine the baseline, and measure COP degradation from a condition closer to the thermodynamic ideal. This will facilitate definitions and comparisons of a wide variety of systems, in terms of their cycling period τ, and their capacity factor μ, as the evaporator capacity decreases with run time fraction).

To meet a given heating or cooling load, an ideal vapor-compression system must operate continuously to minimize temperature lift, pumping just enough refrigerant to provide the needed capacity. The thermodynamically ideal (Carnot) cycle operates between the indoor and outdoor ambient temperatures. The more realistic "ideal" baseline system operates – continuously – between heat source and sink temperatures defined by the tube temperatures of real heat exchangers, which have finite size and finite airflow rate. This ideal system would be sized to meet the maximum load, and its steady state operation can be represented generally as a limiting case of a system cycling at the range of capacities (run time fractions), $\mu \leq 1$ and $\tau \rightarrow 0$. On the other hand a conventional cycling system would operate at the same capacity to meet the same load, but at a cycling period $\tau \sim O$ (30 min) that reflects the thermal capacitance of the conditioned space. This chapter focuses on short-cycling systems having the same capacity, but $\tau \sim O$ (10 sec) reflecting the thermal capacitance of the heat exchangers.

The time-averaged on-cycle temperature lift for all three systems (ideal baseline operation, conventional cycling and short-cycling) will be different. The lowest ideal temperature lift is defined by the difference in between the heat source and sink tube temperatures for the ideal baseline system where refrigerant side $\Delta T = 0$. The highest temperature lift exists for the conventional cycling operation. The refrigerant saturation temperatures follow those of the heat source and sink, namely the heat exchanger surface that is in contact with the refrigerant. Due to their relatively small thermal capacitance, real heat exchangers generally achieve thermal equilibrium with the indoor and outdoor air during the first few minutes of the off-cycle. Therefore during conventional cycling, little heat is transferred from the air to the refrigerant during the off-cycle, requiring large on-cycle air side ΔT's to achieve the required capacity. Since the compressor operates only during the on-cycle, large on-cycle air-side ΔT's lead to high on-cycle temperature lift, causing conventional cycling systems to have the highest power requirement for the same capacity and the lowest efficiency. The purpose of short-cycling is to exploit the thermal capacitance of the heat exchangers to minimize the magnitude of oscillation of the source and sink temperatures, around those of the steady-state ideal system. That magnitude is much smaller than in the extreme case of conventional cycling.

Viewed from the air side, the requirement for sensible and latent cooling capacities to be the same for all three systems implies that the cycle time averaged sink (evaporator) temperatures must be the same while the blower is operating. Since the numerator of COP is therefore constant, the amount of degradation depends solely on the power, which in turn is a function of on-cycle temperature lift. The energy efficiency will therefore be inversely proportional to the magnitude of the temperature lift. Therefore to compare short-cycling system efficiencies with

those of variable-speed, we monitor the difference between the whole-cycle mean tube (metal) temperature and the on-cycle mean saturation temperature in the evaporator and condenser ($\Delta T_e = T_{m,e} - T_{sat,e,on}$ and $\Delta T_c = T_{sat,c,on} - T_{m,c}$). The larger the defined difference, which causes the temperature lift degradation (therefore called lift degradation term), the greater the COP degradation relative to the ideal condition.

3.2 Factors affecting short-cycling efficiency

For the case of steady state operation with a variable-speed or variable-displacement compressor, the existence of finite refrigerant side ΔT is one factor increasing the on-cycle temperature lift, and thereby degrading COP relative to the ideal case where $\Delta T_{ref} = 0$. The other factor is refrigerant pressure drop, which increases temperature lift by $\Delta T_{sat}(\Delta P_{ref})$.

3.2.1 Refrigerant side heat transfer

During short-cycling, on-cycle refrigerant side heat transfer rate must be greater, by almost a factor of $1/\mu$ (due to low refrigerant side heat transfer rate during the off-cycle), than in the case of continuous operation at the same capacity. However the penalty in terms of on-cycle ΔT_{ref} need not increase by the same amount ($1/\mu$), if the on-cycle refrigerant side heat transfer coefficient is larger. The full-speed operation of a short-cycling compressor may increase on-cycle refrigerant mass flux enough to ameliorate the COP degradation due to low off-cycle heat transfer rate.

3.2.2 Pressure drop

Another factor influencing COP degradation is refrigerant pressure drop, which increases temperature lift by $\Delta T_{sat}(\Delta P_{ref})$. Since pressure drop in a crossflow heat exchanger also increases capacity, the net effect of pressure drop on system temperature lift, in the case of constant capacity can be approximated by $\Delta T_{sat}(\Delta P_{ref}/2)$. The degradation due to the on-cycle refrigerant pressure drop, $\Delta P_{ref,on}$, is expected to be greater than for continuous operation at the same capacity, due to the higher mass flux.

3.2.3 Thermal capacitance (heat exchanger metal temperature nonlinearity)

Thermal capacitance is another factor affecting COP degradation during cycling, independent of the factors described above. In all cases of cycling with $\tau > 0$, the source and sink (tube) temperatures will oscillate around the same mean in order to maintain a fixed capacity. However, the on-cycle mean tube temperatures could be significantly different from the whole-cycle mean temperatures depending on the thermal capacitance of the heat exchangers. Since refrigerant saturation temperatures follow the oscillations of the tube temperatures, COP may be affected to the extent that on-cycle average surface temperatures significantly differ from the whole-cycle average, thus increasing the temperature lift. For those average saturation temperatures to be equal, the tube temperature oscillations must be linear. They are not, due to the inherently exponential nature of the heat transfer process (Figure 3.17). The worst case of nonlinearity occurs for the "step function like" tube temperature oscillations in conventional long-cycling; the on-cycle average saturation temperature is far greater than whole-cycle average. At the opposite extreme, very short cycling exploits the thermal capacitance of the heat exchangers, having almost linear tube temperature oscillations minimizing the effects of exponential nature. The linearity of those oscillations

would eliminate the difference between on-cycle and whole-cycle mean tube temperatures which are equal to the tube temperatures of the steady-state ideal system (Figures 3.15 and 3.16).

3.3 Analysis of short-cycling experiments

The pressure lift integrated over the on-cycle (difference between condenser and evaporator saturation pressure) of the short-cycling operation is the main parameter for evaluating short-cycling performance. The higher the pressure lift, the higher compressor work required for compressing a unit of refrigerant mass. The evaporator capacity determines the refrigerant mass flow rate required. Thus, for two systems operating at the same capacity (the same refrigerant mass flow rate), the system with the higher integrated on-cycle pressure lift would consume more power and be less efficient.

3.3.1 Automobile a/c system experiments

With our residential a/c apparatus, it was not possible to compare short-cycling with variable-speed operation without resorting to use of different compressors and then sorting out the effects of their different efficiencies. Therefore, to compare short-cycling and variable-speed operation in a controlled fashion, some preliminary experiments were conducted using an automotive a/c systems. These initial experiments were done with clutch-cycling an automotive scroll compressor in R134a automotive a/c system at three run time fractions (μ=0.8, 0.6 and 0.35). Run time fraction μ=1 (100% on) was chosen as the design, maximum capacity operation at 1700 rpm. Short-cycling could therefore be compared directly to the variable-speed capacity regulation method, since the compressor in the system was driven by a variable speed electric motor. The capacity during variable speed experiments was regulated by changing compressor speed to 1350 rpm, 1000 rpm and 700 rpm.

The results shown in Figure 3.1 show that short-cycling achieved almost the same efficiency as variable speed operation at lower than design capacities, which is significantly higher than achieved in conventional long-cycling which would be close to that observed at μ=1.

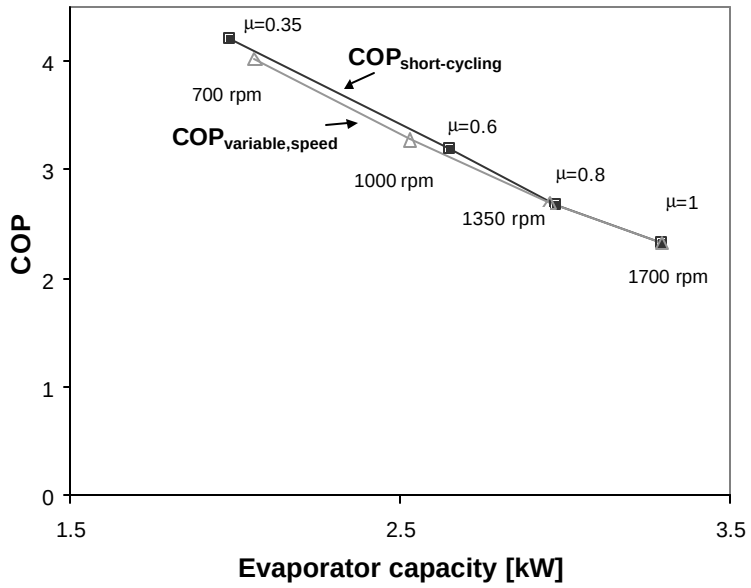

Figure 3.1 Automotive a/c system efficiency comparison; variable speed vs. short-cycling

3.3.2 Residential a/c system experiments

The focus of analysis in the next sections will be on the factors influencing the increase in pressure lift at a given capacity of short-cycling operation. The range of capacities is achieved by changing run time fraction of the short-cycling residential a/c system.

To illustrate how COP decreases with pressure lift during short-cycling operation, Figures (3.2) and (3.3) show the COP and saturation temperature lift respectively, for experiments at μ=0.5 (50% on time) and several cycle periods (τ=10–80 sec) with dry evaporator surface at indoor/outdoor temperature 80/95^{o} F.

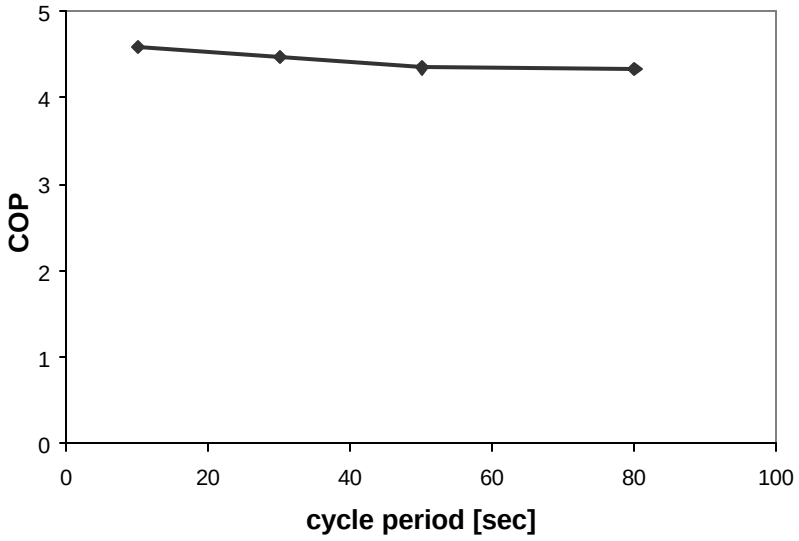

Figure 3.2 COP degradation with cycle period for experiments at μ=0.5

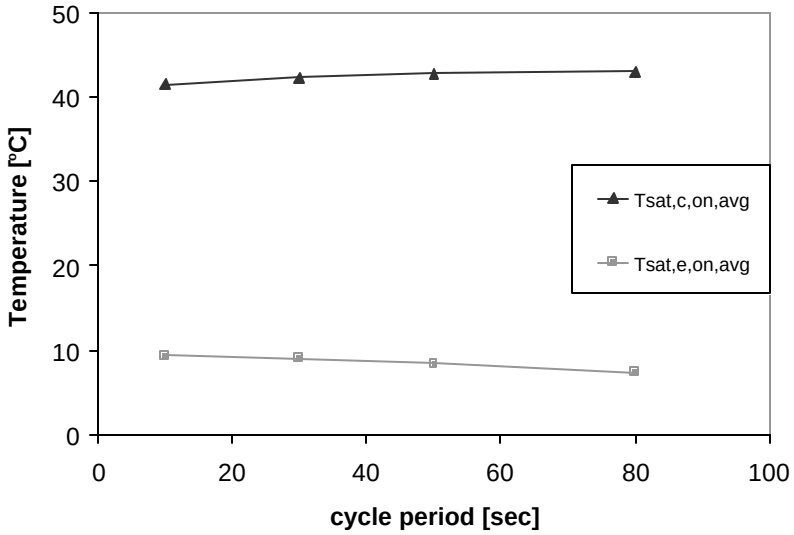

Figure 3.3 The saturation temperature lift increase with τ for experiments at μ=0.5

3.3.2.1 The lift degradation term as a basis for evaluating the system efficiency

The short-cycling operation will be evaluated by comparing it to the ideal system baseline operation. The ideal system baseline operation is defined as continuous operation at the same capacity, between heat source and sink temperatures defined by the tube temperatures of real heat exchangers. In other words the ideal baseline case corresponds to VS operation with infinite refrigerant side heat transfer coefficients causing zero refrigerant side temperature differences. Actual variable-speed system would fall short of this ideal due to its finite h_{ref}. An ideal baseline defined in this manner allows both variable-speed and short-cycling systems to be compared in terms of their increased pressure lift caused by finite h_{ref}, ΔP_{ref} and other factors.

The system efficiencies were compared by monitoring the difference between the whole-cycle mean tube temperature ($T_{m,avg}$) and the on-cycle mean saturation temperature ($T_{sat,on,avg}$) in the evaporator and condenser. The larger those differences, the greater the temperature lift and COP degradation relative to the ideal condition at a given capacity. Figure 3.4 shows the same evaporator and condenser saturation temperatures (shown in Figure 3.2), with an overlay showing the whole-cycle mean heat exchanger metal temperature for experiments at μ=0.5 (about 50% of design capacity) and several cycle periods (τ=10–80 sec).

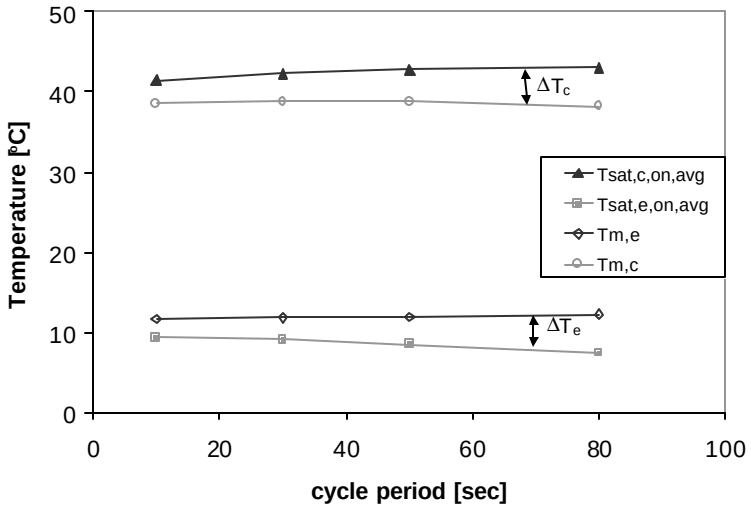

Figure 3.4 Lift degradation term increase with cycle period for experiments at μ=0.5

The factors affecting short-cycling efficiency will be analyzed on the evaporator side. The same mechanisms and processes influence the establishment of higher on-cycle condenser saturation temperature. We will focus on the evaporator side temperature lift degradation term ($\Delta T_e = T_{m,e,avg} - T_{sat,e,on,avg}$) and its components in next paragraphs in order to explain the mechanisms causing the COP degradation during short-cycling operation.

The third (bold) column of Table 3.1 shows the values of the evaporator side lift degradation term (ΔT_e) for the set of experiments at various run time fractions and cycle periods with dry evaporator surface at indoor/outdoor temperature 80/95^o F.

Table 3.1 Temperature lift degradation breakdown

80/95°F					
run time	cycle period	ΔT_e	ΔT_e(ht)	ΔT_e(nonlin)	ΔT_e(ΔP)
fraction	[sec]	**[°C]**	[°C]	[°C]	[°C]
1	0	**2.7**	2.1	0.0	0.6
0.7	10	**2.5**	2.0	0.0	0.5
0.7	30	**2.7**	2.1	0.1	0.5
0.7	50	**3.2**	2.3	0.3	0.5
0.7	80	**3.6**	2.4	0.7	0.5
0.5	10	**2.3**	1.9	0.0	0.4
0.5	30	**2.8**	2.2	0.1	0.5
0.5	50	**3.5**	2.5	0.4	0.6
0.5	80	**4.8**	3.1	1.2	0.5
0.3	10	**2.0**	1.7	0.0	0.4
0.3	30	**2.7**	2.2	0.0	0.5
0.3	50	**3.3**	2.5	0.3	0.6
0.3	80	**4.3**	3.0	0.7	0.6

Figure 3.5 shows the lift degradation term as a function of cycle period for four run time fractions. It can be seen that the lift degradation term increases with the cycle period for a given run time fraction.

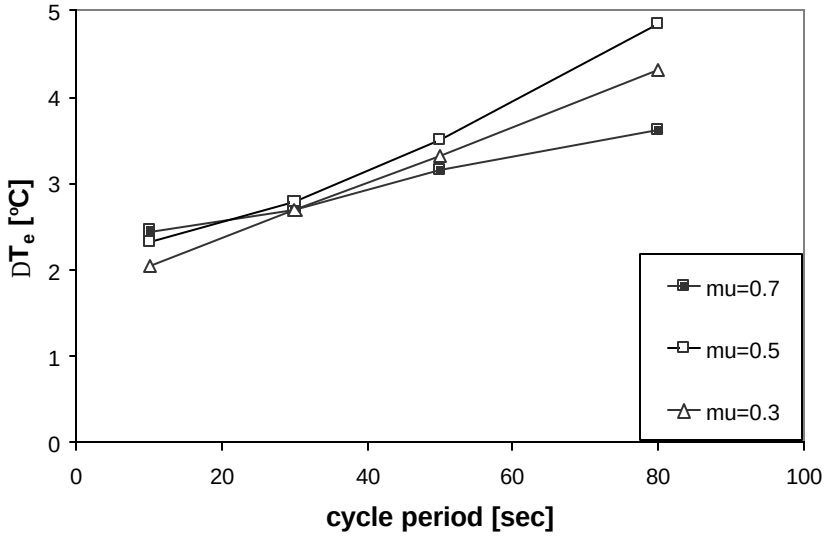

Figure 3.5 Lift degradation term as a function of cycle period and run time fraction

Figure (3.6) shows how on-cycle temperature lift decreases at lower run time fractions. Therefore a given value of the lift degradation term (ΔT_e) will have a proportionally greater effect on COP at lower capacities.

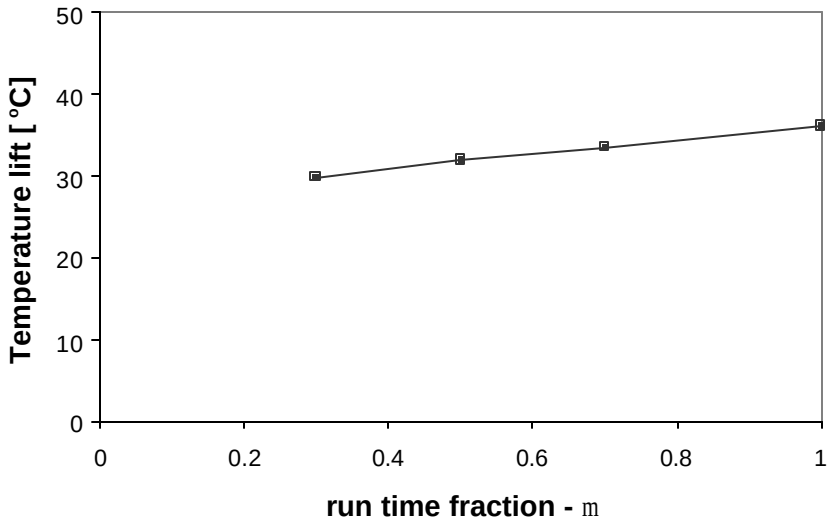

Figure 3.6 Temperature lift as a function of μ for τ=10 sec

The absolute value of the degradation term of about 3 C at various μ, shown in Figure 3.7, represents higher percentage of saturation temperature lift at low than at high run time fractions and thus hurts performance more.

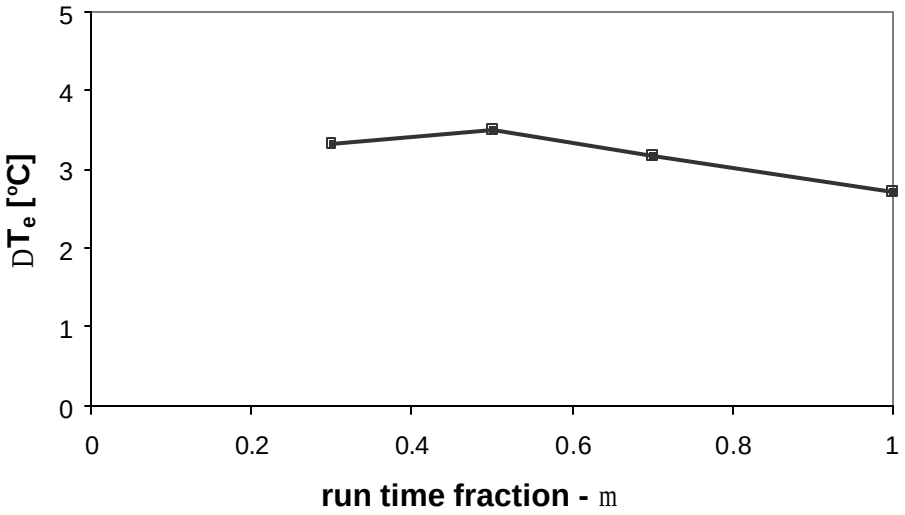

Figure 3.7 Lift degradation term as a function of μ for τ=10 sec

Therefore the short-cycling COP loss is actually greatest for small run time fraction (at lower capacities), despite the fact that experimental results show a larger evaporator temperature lift degradation at μ=0.5 than at μ=0.3, might appear to suggest a different conclusion.

3.3.2.2 Separating the lift degradation term

The lift degradation term was separated into three terms, each representing one major factor increasing the temperature lift (columns 4 to 6 in Table 3.1): refrigerant side heat transfer resistance [$\Delta T_e(rht)$], pressure drop [$\Delta T_e(\Delta P)$] and nonlinearity term [$\Delta T_e(nonlin)$]. Equations 3.1 to 3.4 show that mathematical sum of these three degradation terms is equal to total degradation of temperature lift.

$$T_{m,e,avg} - T_{sat,e,on,avg} = \Delta T_e(rht) + \Delta T_e(\Delta P) + \Delta T_e(nonlin) \quad (3.1)$$

where:

$$\Delta T_e(rht) = T_{m,e,on,avg} - T_{sat,e,mean,on,avg} \quad (3.2)$$

$$\Delta T_e(\Delta P) = T_{sat,e,mean,on,avg} - T_{sat,e,on,avg} \quad (3.3)$$

$$\Delta T_e(nonlin) = T_{m,e,avg} - T_{m,e,on,avg} \quad (3.4)$$

3.3.2.2.1 The refrigerant side heat transfer term -- ?Te(rht) The existence of finite on-cycle refrigerant side temperature difference, $\Delta T_{ref}(t) = T_{m,on}(t) - T_{sat,on}(t)$, is one factor increasing the average on-cycle temperature lift, thereby degrading COP relative to the baseline ideal case where $\Delta T_{ref} = 0$.

The mean evaporator surface temperature was obtained as an area-weighted average of 12 surface thermocouples located on return bends. The corresponding mean saturation temperature with respect to evaporator surface, $T_{sat,e,mean} = T_{sat,e} + \Delta T_e(\Delta P_e/2)$, was obtained by monitoring the exit saturation pressure and the total pressure drop across the evaporator. Figure 3.8 shows the refrigerant side heat transfer lift degradation term increasing slightly with cycle period, at four run time fractions.

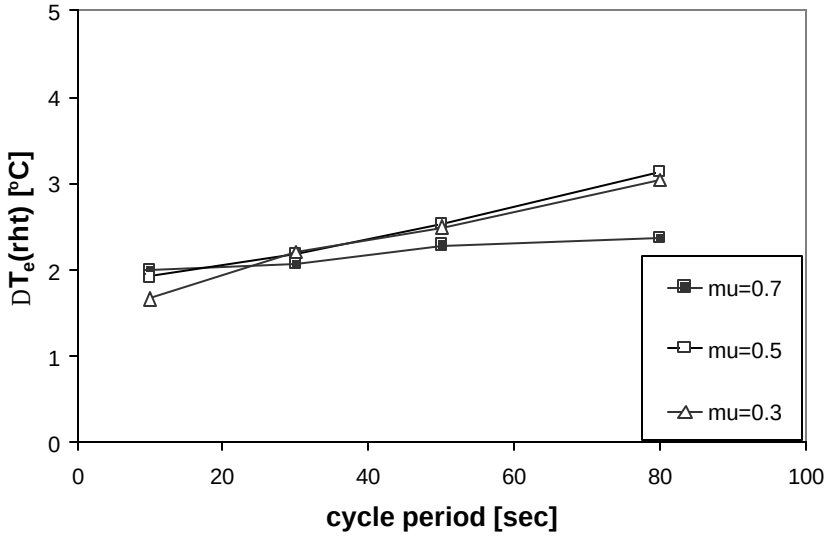

Figure 3.8 Refrigerant heat transfer part of temperature lift degradation term, $\Delta T_e(rht)$

3.3.2.2.2 The pressure drop term -- ?Te(?P) The evaporator mean saturation temperature with respect to surface, $T_{sat,e,mean}$, is defined such that it does not depend on the refrigerant side pressure drop. However, the effect of evaporator pressure drop on the compressor suction pressure is exactly half of the refrigerant side pressure drop (difference between evaporator mean and exit pressure). The equation $P_{sat,e,out} = P_{sat,e,mean} - \Delta P_e/2$ can be written in terms of temperatures used in equation 3.3, $T_{sat,e} = T_{sat,e,mean} - \Delta T_e(\Delta P_e/2)$. The evaporator exit pressure was measured and used as the indicator of the temperature lift in this analysis. The compressor inlet pressure is real representative of the temperature lift, therefore the chosen pressure drop term $\Delta P_e/2$, omits the system-specific suction line pressure drop, which is proportional to it.

Figure 3.9 shows that the pressure drop term was almost constant for the set of cycle periods, as expected due to the almost constant on-cycle refrigerant mass flux resulting from the constant on-cycle compressor speed. For the same reason, the temperature lift degradation term due to the pressure drop is also nearly independent of run time fraction.

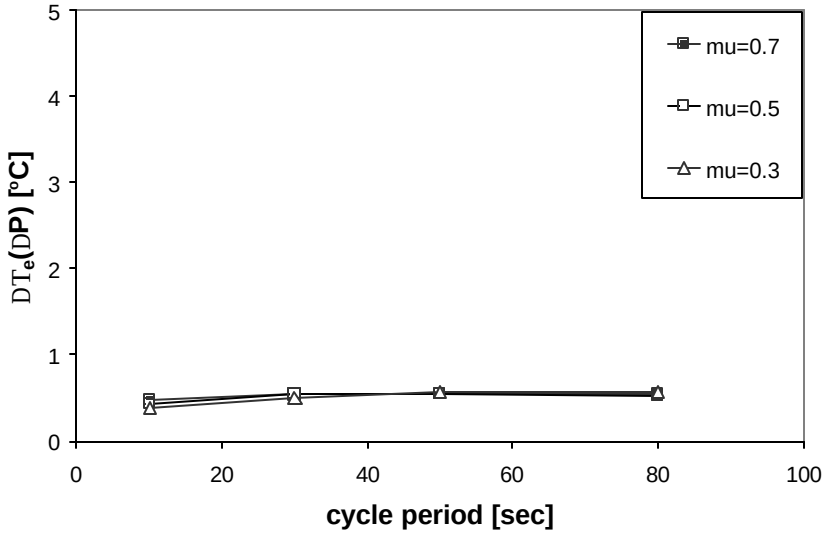

Figure 3.9 Refrigerant pressure drop part of lift degradation term, $\Delta T_e(\Delta P)$

3.3.2.2.3 The metal temperature nonlinearity term -- ?Te(nonlin) Due to the inherently exponential nature of the heat transfer process, the evaporator metal temperature during the off-cycle will approach the air temperature nonlinearly. The same phenomenon occurs during the on-cycle as the metal temperature is pulled down towards the steady-state refrigerant saturation temperature. Short-cycling truncates these processes, but the fundamental asymmetry remains. As a result, the on-cycle average metal temperature is always less than the whole-cycle average, as shown in Figure 3.10. Since the compressor sees only the lower on-cycle metal temperature, there is a penalty in pressure lift for long cycle periods where the nonlinearities are the greatest.

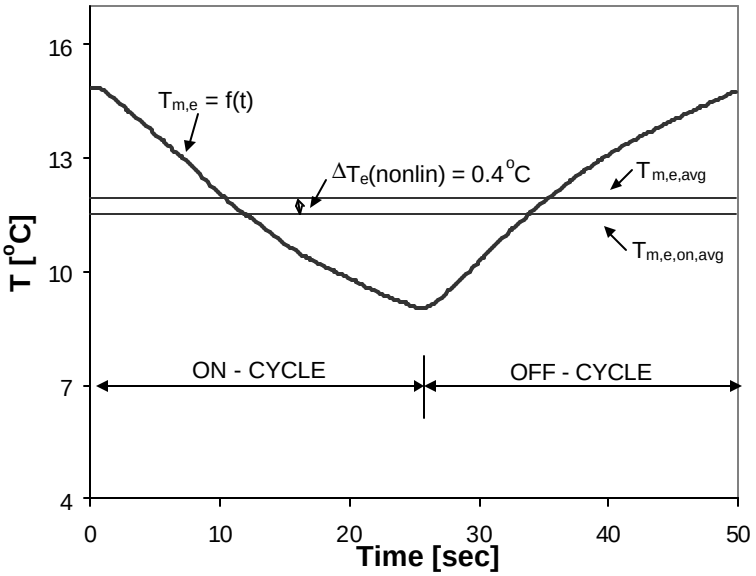

Figure 3.10 Nonlinear evaporator metal temperature, $T_{m,e}$, oscillations at μ=0.5 and τ=50 sec

Figure (3.11) shows how this loss significantly increases with cycle period, more than was observed for the pressure drop and refrigerant heat transfer terms. The effect of evaporator metal thermal mass on the nonlinearity of the temperature fluctuations is explored in Section 3.4.2.

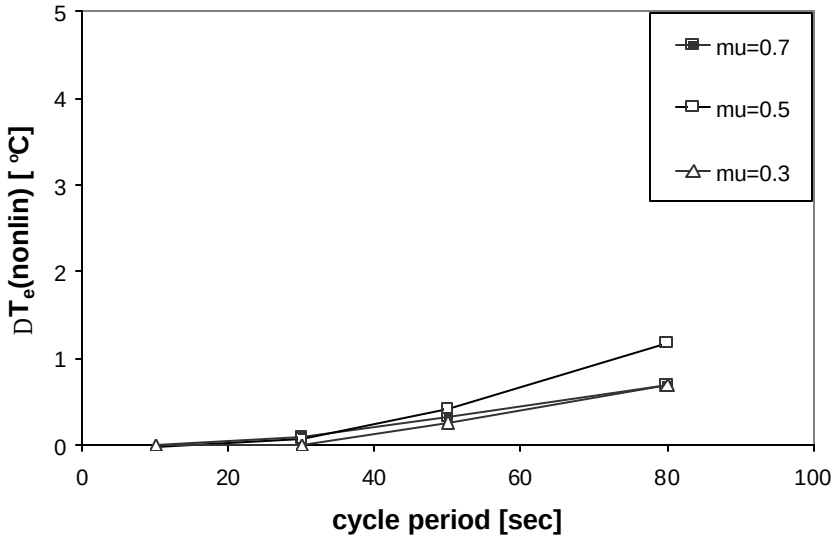

Figure 3.11 Metal temperature nonlinearity part of a COP loss term, ΔT_e(nonlin)

All three lift degradation terms are illustrated in Figure 3.12, for cycle period τ=50 sec and run time fraction μ=0.5.

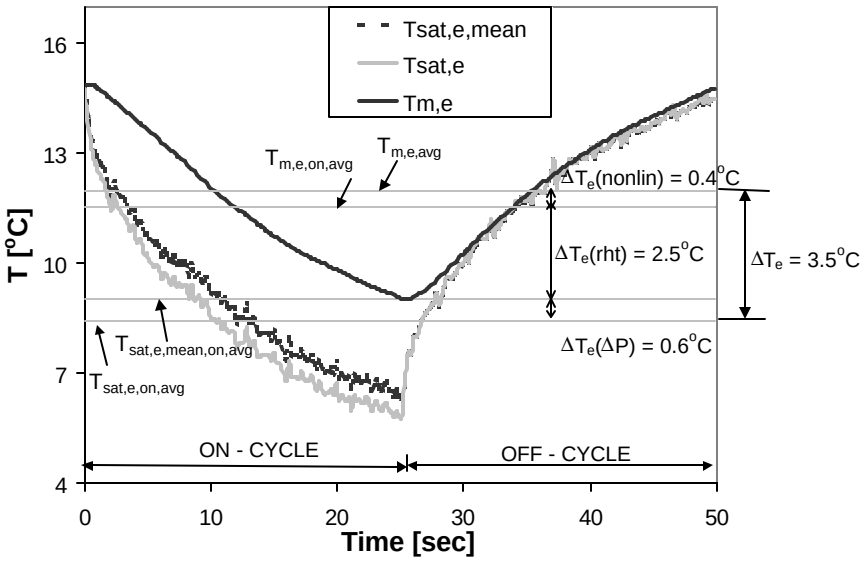

Figure 3.12 Lift degradation term divided into three parts for μ=0.5 and τ=50 sec

3.4 Effect of evaporator thermal capacitance

To understand the significance of parameters influencing the nonlinearity of the evaporator metal temperature fluctuation, represented by the difference in between the entire cycle and on-cycle average metal temperature, the dynamics of the evaporator metal temperature fluctuation during the compressor on and off-cycle were modeled as a 1st order, lumped capacitance system. The model validity will be checked by comparing it with the experimental results.

It has been shown that the nonlinearity part of the temperature lift degradation term becomes dominant as the cycling period increases. It is possible that heat exchanger having relatively large thermal capacitance, may be able to minimize COP degradation at longer cycle periods than a less massive one.

Equation 3.5 describes the change of evaporator metal temperature as a function of the air side and refrigerant side heat transfer rates. The resistance of the copper and aluminum to internal heat conduction is assumed to be small compared to convective resistance of the air side heat transfer, so the metal can be assumed to be isothermal throughout.

$$C_m * \left(\frac{dT_m}{dt}\right) = \dot{Q}_{air} - \dot{Q}_{ref} \qquad (3.5)$$

The thermal capacitance $C_m = c_t * m_t + c_f * m_f$ = 14 kJ/K (about 60% tubes, 40% fins) was calculated from the dimensions of evaporator fins and tubes, assuming the densities and specific heats of copper and aluminum to be 0.356 kJ/kg-K and 0.886 kJ/kg-K respectively. The heat transfer rate from the air to the evaporator metal, during both compressor off and on-cycles, is approximated using a simple arithmetic mean temperature difference model,

$$\dot{Q}_{air} = hA_{air,e} * AMTD \qquad (3.6)$$

where $hA_{air,e}$ [kW/K] is product of the air side heat transfer coefficient and evaporator surface area averaged over entire evaporator surface and AMTD = $[(T_{air,in} + T_{air,out})/2 - T_m]$ is arithmetic mean temperature difference, which is solved simultaneously at each time step with the air side energy balance using equation (3.7).

$$\dot{Q}_{air} = r_{air} * \dot{V}_{air} * c_p * (T_{air,in} - T_{air,out}) \tag{3.7}$$

Equations 3.8 and 3.9 describe the refrigerant side heat transfer rate from the evaporator metal to the refrigerant during the off and on-cycles, respectively.

$$\dot{Q}_{ref,off} = \dot{m}_{ref} * \frac{u_{ref,off} - u_{ref,init,off}}{t_{off}} \tag{3.8}$$

$$\dot{Q}_{ref,on} = \frac{\dot{Q}_{e,avg}}{m} \tag{3.9}$$

where

$$\dot{Q}_{e,avg} = \dot{Q}_{ref,on} * m + \dot{Q}_{ref,off} * (1 - m) \tag{3.10}$$

is the evaporator heat transfer rate averaged over the entire cycle period, and m_{ref} and $u_{ref,init,off}$ are the refrigerant mass and internal energy in the evaporator at the end of the on-cycle. It is clear from the experimental data (e.g. Figure 3.12) that the off-cycle heat transfer rate between the tube and refrigerant is almost negligible, reaching only ~15% of on-cycle heat transfer rate in the worst case (μ=0.7, τ=10 sec). Therefore we assume that all refrigerant side heat transfer occurs during the on-cycle at a constant rate equal to the $\dot{Q}_{e,avg}/\mu$, as indicated by the nearly constant on-cycle temperature difference, T_m- $T_{sat,e}$. Note that the slight on-cycle temperature difference increase is offset by a slight decrease in refrigerant mass flow rate through the compressor as suction pressure declines. In addition, data also show that the off-cycle refrigerant internal energy term $m_{ref}*\Delta u/t_{off}$ varies between 3.5 to 4.5 % of the metal thermal capacitance term depending on μ, suggesting the dominance of $hA_{air,e}/C_m$ term in equation 3.11.

The model governing equations are therefore written for off and on-cycle respectively:

$$\frac{dT_m}{dt} = \frac{hA_{air} * (T_{air,avg} - T_m)}{C_m} + m_{ref} * \frac{(u_{ref,off} - u_{ref,init,off})}{t_{off}} / C_m \tag{3.11}$$

$$\frac{dT_m}{dt} = \frac{hA_{air} * (T_{air,avg} - T_m) - \frac{\dot{Q}_{e,avg}}{m}}{C_m} \tag{3.12}$$

3.4.1 Model validation using the experimental measurements

The validity of the model will be checked by comparing it with the experimentally obtained evaporator metal temperature during the on and off-cycle.

The average $hA_{air,e}$ for entire evaporator was determined from dry coil steady state (μ=1 at 80/95^o F) data to be 0.94 kW/K. The average $hA_{air.e}$ was determined from experimental data by integrating the term $\dot{Q}_{air}$/AMTD

over entire cycle period at a given μ, where $\dot{Q}_{air}$ was obtained from the air side energy balance. Since air flow rate varied for μ<1, the dry coil experimental data in Figure 3.13 were used as inputs in calculations.

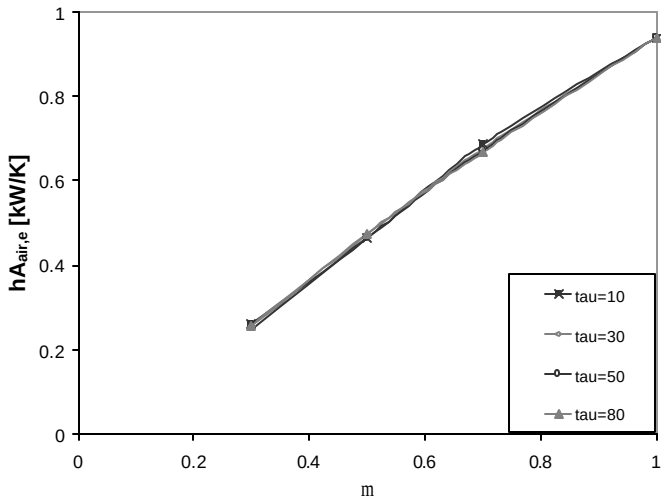

Figure 3.13 Experimentally obtained values of $hA_{air,e}$ for the range of μ and τ

The $hA_{air,e}$ shown in Figure 3.13 changed due to change in air flow rate at each run time fraction, following relation: $hA_{air,e}(\mu)/hA_{air,e}(\mu=1)=0.99*[V_{air}(\mu)/V_{air}(\mu=1)]^{1.024}$, which can be derived from experimental data.

Due to the uncertainty of the fin and tube thickness measurements, the calculated C_m value of 14 kJ/K is estimated be accurate within +/- 15%. In Figure 3.14, it is compared to the evaporator thermal capacitance, C_m, obtained from 12 dry coil experiments. The C_m value for each experiment has been calculated using the equation $\dot{Q}_{e,off}/(T_{m,max}-T_{m,min})$, where $\dot{Q}_{e,off}$ is the off-cycle air side evaporator capacity and $T_{m,max}-T_{m,min}$ is the amplitude of the evaporator metal temperature fluctuation for each experiment. These results appear consistent with the 14 kJ/K estimated independently from the evaporator dimension.

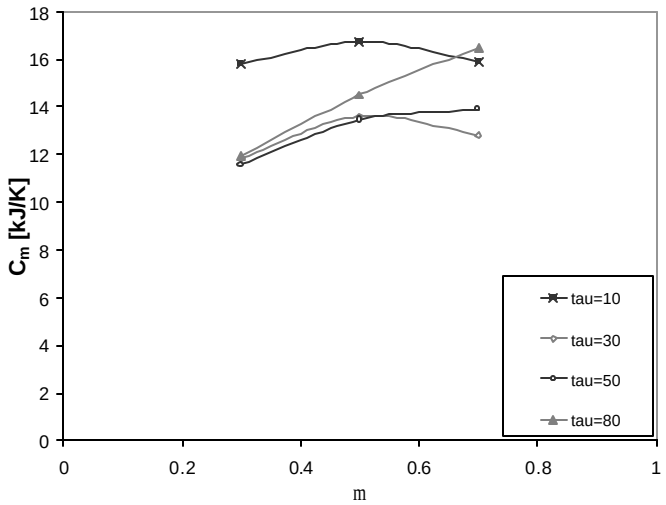

Figure 3.14 Experimentally obtained values of C_m for the range of μ and τ

The area-weighted average evaporator metal temperature used in the preceding calculations was obtained from insulated surface thermocouples located at 12 different spots on evaporator tubes (U-bends). There is uncertainty of about (1 +/- 0.1^o C) in choosing this area weighted average temperature as the representative of the entire evaporator temperature due to +/- 0.1^o C uncertainty of each tube temperature measurement, and +1^o C due to possible variations between the difference of the average fin (not measured) and average tube temperatures, since fins account for about 40% of total evaporator thermal capacitance.

The validity of the model is illustrated by comparing it with the experimentally obtained fluctuation of the evaporator tube temperature for the experiment done at run time fraction (μ=0.5 and τ=80 sec) in Figure 3.15. The initial metal temperature for the model was set to be equal to measured metal temperature at the beginning of the off-cycle. The overlaid experimental and model results can be seen in Figure 3.15.

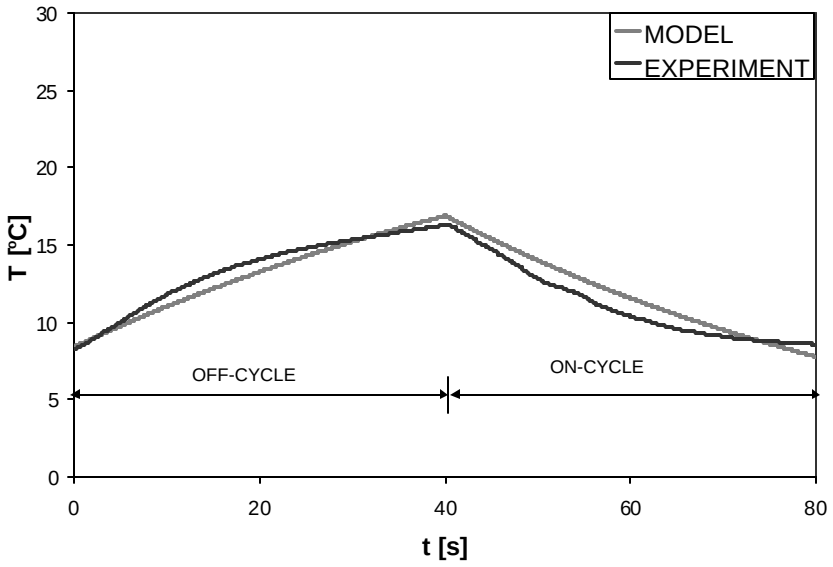

Figure 3.15 The model results comparison to the experimental results at μ=0.5 and τ=80 sec

The model overpredicted the metal temperature at the end of off-cycle by 0.5^o C, and underpredicted the metal temperature at the end of on-cycle by 1^o C for this experimental point. It also tended to underpredict the curvature of the metal temperature fluctuation, especially for the long cycle period experiments (80 seconds). The measured evaporator metal temperature lies within the range of uncertainties explained in previous paragraphs including: 1+0.1^o C uncertainty in picking the area-weighted average; 15% uncertainty on estimating the off-cycle (and thus on-cycle) heat transfer rate; and 15% uncertainty in obtaining the accurate C_m value.

3.4.2 Effect of changing the design variables hA_{air} and C_m

The lumped capacitance model will now be used to help in understanding the influence of changing the design variables hA_{air} and C_m on the temperature lift, for the design problem where the average heat exchanger capacity is given (given run time fraction). The analysis will be done for fixed cycle period, since it has been shown that the temperature lift increases with the cycle period.

Change in the hA_{air} and C_m, for a given heat exchanger capacity and cycle period, affects the temperature lift in two ways, by affecting change in:

1) Air side ΔT
2) 2) Nonlinearity of the heat exchanger metal temperature, represented by the difference between the full cycle and on-cycle average metal temperatures, which is affected primarily by: the magnitude of the metal temperature oscillation, and the quotient hA_{air}/C_m, defining the exponential rate, and thus the curvature of the metal temperature oscillation.

The higher the air side ΔT and nonlinearity, the higher temperature lift, and thus lower COP. The higher the magnitude of the metal temperature oscillation, the higher nonlinearity. The air side ΔT is affected by changing hA_{air} only. Decreasing C_m increases magnitude of metal temperature oscillations, while air side ΔT stays constant. Increasing hA_{air} decreases air side ΔT, while magnitude of oscillations stays constant.

The evaporator air side ΔT, $\Delta T_{air,e}=15^o$ C, and evaporator metal temperature nonlinearity, $\Delta T_e(nonlin)=T_{m,e,avg}-T_{m,e,on,avg}=0.45^o$ C, for the case of $\mu=0.5$ and $\tau=80$ seconds, was calculated using model, and it is shown in Figure 3.16, for values $C_m=14$ kJ/K and $hA_{air,e}= 0.47$ kW/K.

Two cases will be analyzed at $\mu=0.5$; $\tau=80$:

1) Halving C_m while maintaining $hA_{air,e}$ the same (doubling the quotient $hA_{air,e}/C_m$)
2) Doubling $hA_{air,e}$ by changing air side heat transfer coefficient, $h_{air,e}$, while air side surface area remains constant, and hence C_m remains constant (also doubles quotient $hA_{air,e}/C_m$)

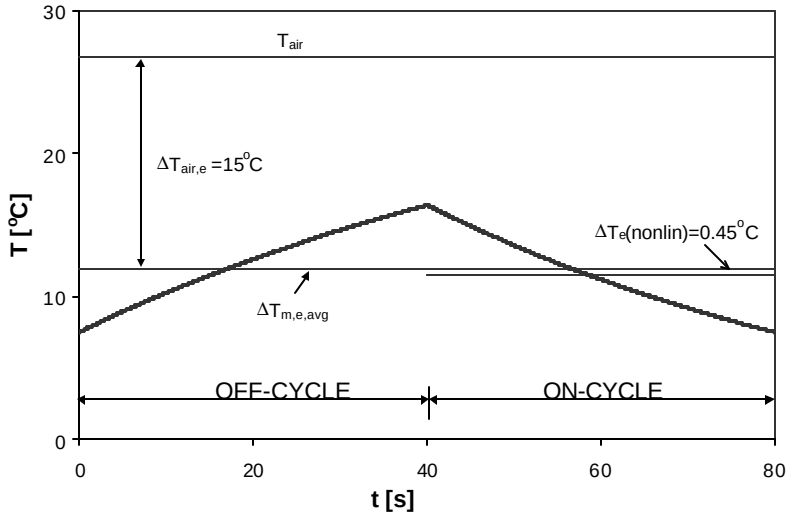

Figure 3.16 Calculated evaporator metal temperature

3.4.2.1 Halving C_m while maintaining $hA_{air,e}$ constant

Figure 3.17 shows that decreasing thermal capacitance by a factor of two (assuming a less "thermally massive" evaporator installed) increases $\Delta T_e(nonlin)$ from 0.45^o C to 1.6^o C, while the whole-cycle average evaporator metal temperature stays unchanged, thus air side ΔT remains constant ($\Delta T_{air,e}=15^o$ C). For this compressor, such a 1^o C increase in temperature lift, caused on the evaporator side, decreases COP about 2%. The reason for the increase in nonlinearity is in increased magnitude of metal temperature fluctuation, caused by halving

C_m. The increase in $hA_{air,e}/C_m$ caused additional increase in nonlinearity due to increase in the exponential rate, and thus increased curvature of the metal temperature oscillation.

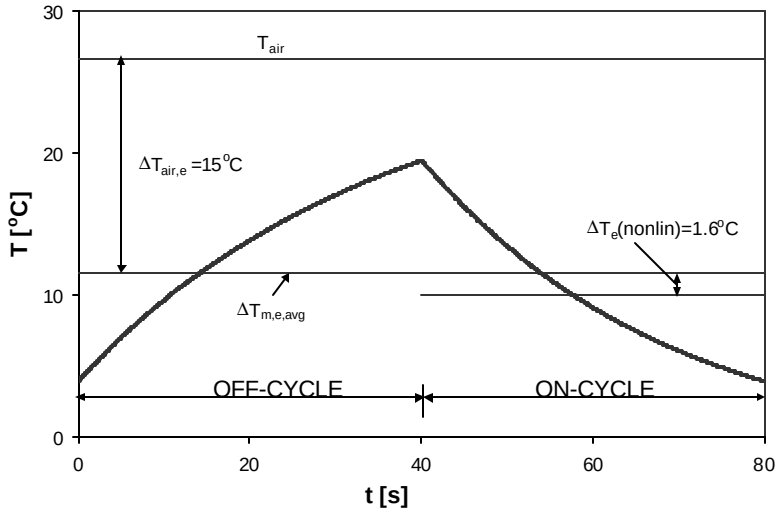

Figure 3.17 Influence of halving C_m

3.4.2.2 Doubling $hA_{air,e}$ while maintaining C_m constant

One way to imagine this scenario is that $h_{air,e}$ is varied, while A and C_m remain constant. In this case the designer focuses on fin surface enhancements by changing fin surface geometry, while air flow rate increases to maintain constant capacity, thus additionally increasing $h_{air,e}$ without changing size or mass of heat exchanger. Figure (3.18) shows that increasing $hA_{air,e}$ in this fashion by a factor of two increases ΔT_e(nonlin) only slightly from 0.45^o C to 0.9^o C, while decreasing ΔT_{air} significantly, from 15^o C to 7.5^o C.

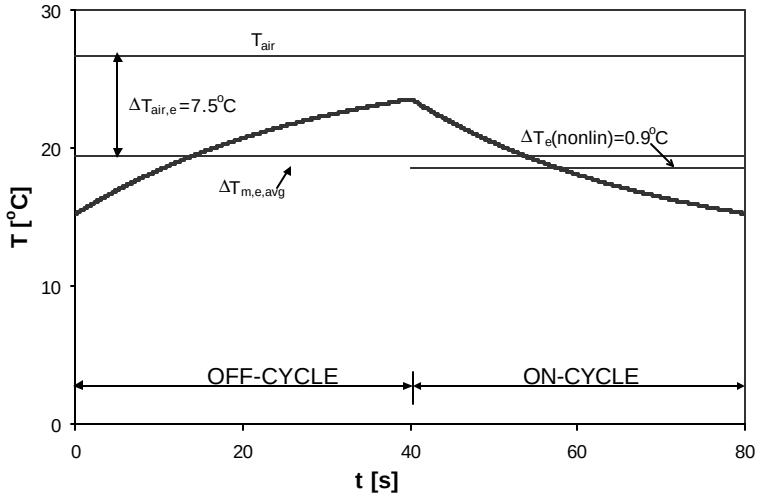

Figure 3.18 Influence of doubling $hA_{air,e}$

In this case, the magnitude of oscillations was unchanged because Cm remained constant. Since the quotient $hA_{air,e}/C_m$ was doubled, the curvature of the metal temperature oscillation increased. Constant C_m maintained the same magnitude of metal temperature oscillations.

It is shown that doubling hA_{air} increases nonlinearity, due to increase in exponential rate quotient hA_{air}/C_m, while maintaining the same metal temperature oscillation magnitude. In addition to this small increase in temperature lift due to nonlinearity (a few tenths of a degree), doubling hA_{air} causes the significant temperature lift decrease of approximately 7.5° C (compared Figures 3.16 and 3.18). Therefore, whenever design requirements allow, hA_{air} should be as high as possible, due to dominance of beneficial effect of reducing air side ΔT over the effect of small increase in nonlinearity.

The time constant of a simple lumped capacitance system is $(hA_{air}/C_m)^{-1}$, but it is clear that the COP degradation of this air conditioning system is more sensitive to a halving of the denominator than to a doubling of the numerator. When C_m is halved, the temperature lift penalty due to nonlinearity increases significantly due to two additive effects: increased magnitude of metal temperature oscillations, and increased exponential rate quotient hA_{air}/C_m, while air side ΔT stays the same. On the other hand, when hA_{air} is doubled, the air side ΔT is significantly reduced and nonlinearity slightly increased. The effect on temperature lift nonlinearity is smaller than observed when C_m was halved, since magnitude of oscillations was smaller, leaving only doubled exponential rate quotient to influence increase in nonlinearity.

Doubling $hA_{air,e}$ in this example would significantly increase time averaged metal temperature, from 12° C to 19° C, and would make dehumidification impossible. Therefore, analysis of doubling $hA_{air,e}$ on evaporator side is unrealistic because dehumidification is important part of design requirements. However, the same effect can be exploited on the condenser side.

3.5 Wet coil performance under short-cycling

Dry coil experiments at 80/95° F, were used as a basis for the analysis done in previous sections of Chapter 3. The air flow rate over evaporator for dry coil experiments was decreased with run time fraction to maintain the cycle-average evaporator surface temperature at 12° C, equal to the surface temperature at dry coil design condition at μ=1. A nearly identical set of wet surface experiments was conducted at the standard capacity rating condition (80/95/67° F), where the 67° F wet bulb temperature corresponds to the 50% inlet air relative humidity which ensures that the surface is fully wet. Results of these experiments are presented here. Additional results for 80/82° F dry and wet coil experiments are presented in Appendix C.

The purpose of the wet surface experiments was to determine whether the latent load had any effect on COP degradation caused by short-cycling. The air flow rate over the evaporator was changed for each run time fraction in order to maintain the whole-cycle average evaporator metal temperature at the 12.5° C needed to achieve the same ~25/75% latent/sensible load split at all operating conditions. Since this sensible heat ratio serves as a widely accepted target throughout the industry, it was decided to conduct these wet surface experiments at 12.5° C instead of the 12° C that had been chosen arbitrarily for the earlier dry surface experiments.

Almost the same COP degradation for wet and dry experiments was expected since the refrigerant sees only the constant tube wall temperature, which is nearly identical for both cases.

There is no significant difference in COP degradation observed, for the wet and dry coil experiments, as shown in Figures 3.19 and 3.20. Virtually identical increases in on-cycle temperature lift for wet and dry coil experiments caused essentially identical decreases in COP. The experimental results showing an increase in the on-cycle temperature lift with cycle period, for a given run time fraction, are presented for both dry and wet coil experiments in Figure 3.21 and 3.22, respectively.

The evaporator surface temperature remained lower than the 15.5 C dew point temperature throughout cycle as shown in Figure 3.23 for the longest cycle period (80 sec), which was the primary reason for almost identical COP degradation with cycle period for wet and dry coil experiments.

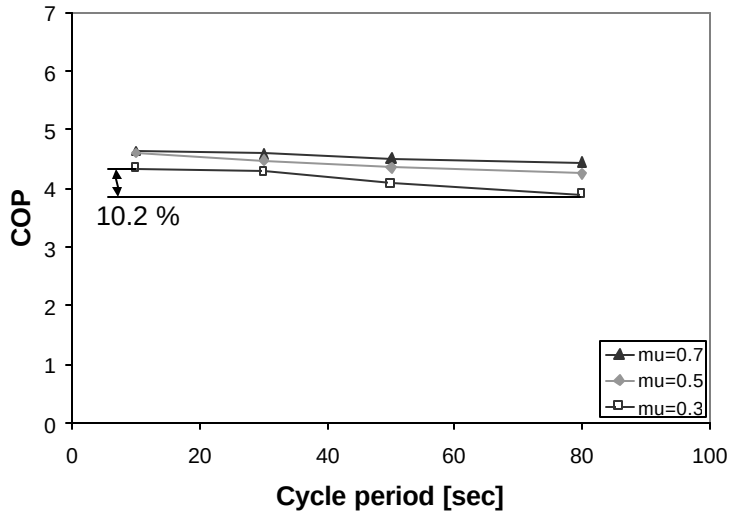

Figure 3.19 COP degradation with cycle period for dry coil experiments

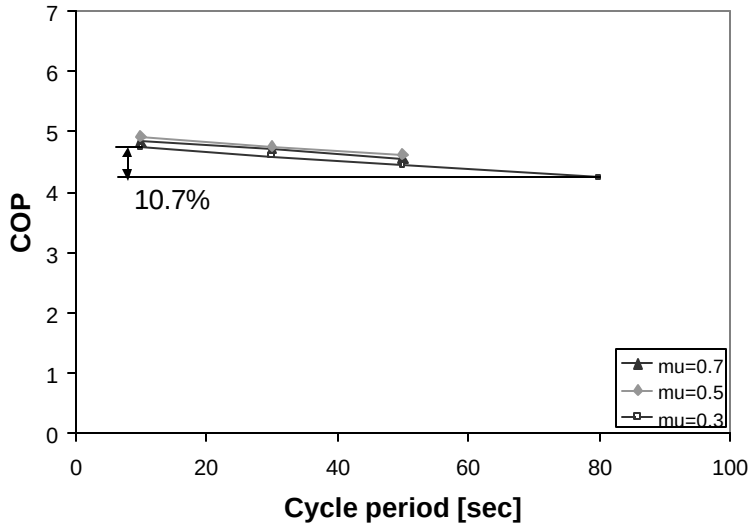

Figure 3.20 COP degradation with cycle period for wet coil experiments

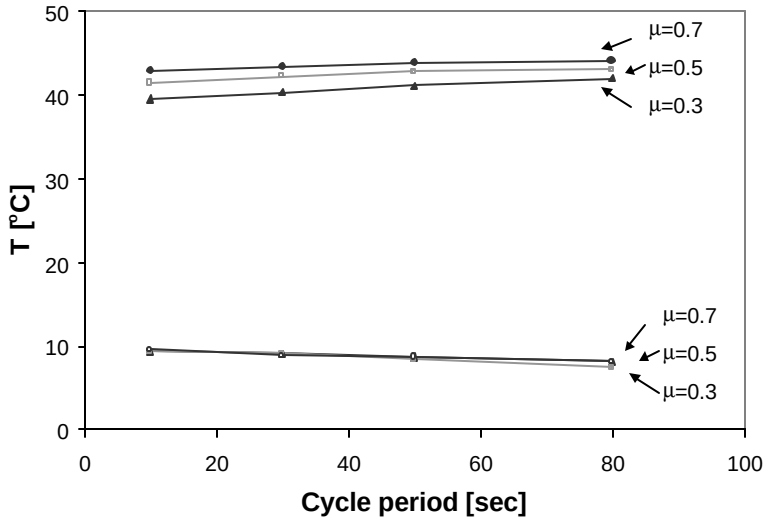

Figure 3.21 On-cycle average saturation temperatures for dry coil experiments

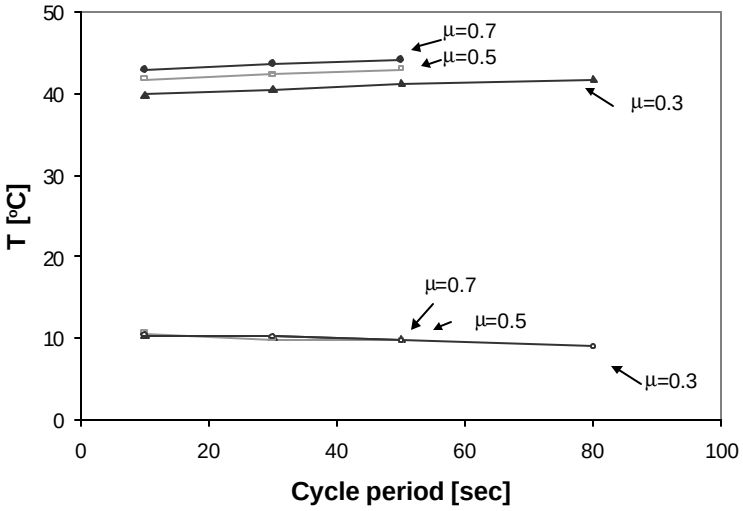

Figure 3.22 On-cycle average saturation temperatures for wet coil experiments

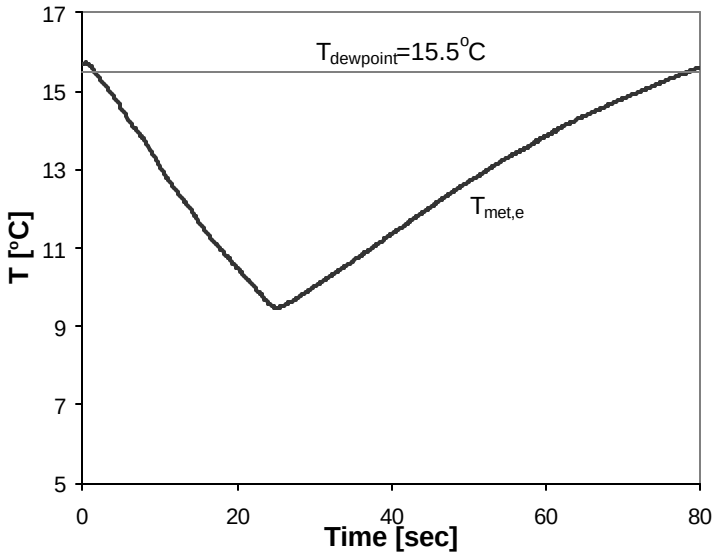

Figure 3.23 Evaporator metal and dew point temperature at μ=0.3 and τ=80 sec

3.6 Open vs. closed valve operation

To understand the effect of isolating the evaporator during the off-cycle, the solenoid valve (solenoid valve was installed upstream of the expansion device as explained in section 2.1 of Chapter 2) was disabled so refrigerant could flow continuously through the expansion valve during the off-cycle.

It was expected that the open valve (OV) operation would have lower COP than closed valve (CV) operation due to possible condensation in evaporator during off-cycle. The evaporator refrigerant temperature rose quickly to the evaporator metal temperature during first few seconds of the off-cycle for both OV and CV operation due to quick pressure rise caused by continued evaporation in the limited low side volume. In the CV case the metal-to-refrigerant heat transfer terminated when the ΔT vanished. However in the OV case, the off-cycle refrigerant flow into the evaporator was expected to continue increasing the saturation pressure, which would cause the evaporator metal to be heated from the refrigerant side while at the same time absorbing heat from the air. Thus, during OV operation, refrigerant could start condensing on the metal, causing additional COP degradation. The difference between saturation and metal temperatures would never get very high because the metal temperature rises slowly as it soaks up heat from the refrigerant.

In order to compare the OV and CV strategies, the system was run at μ= 0.5 and τ=30 seconds for both. Experiments were done with a dry evaporator surface. The air flow rate over the condenser was kept at $\dot{V}$ =1.180 m^3/s. The air flow rate over the evaporator was $\dot{V}$ = 0.184 m^3/s, about 49% of the design air flow rate, to hold the evaporator surface temperature at the desired 12° C.

Figure 3.24 shows the refrigerant mass flow rates, measured upstream of the expansion device, for two strategies. The cumulative refrigerant flow into the evaporator during cycle period was the same to achieve equal capacities.

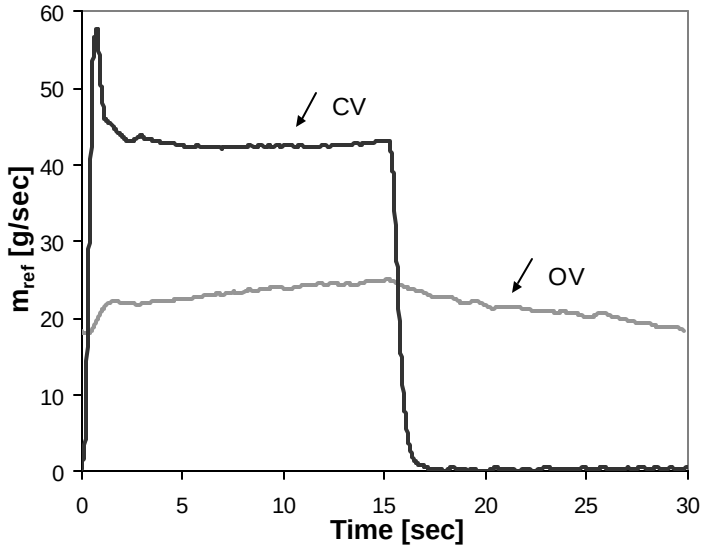

Figure 3.24 Refrigerant mass flow rate into the evaporator overlaid for OV and CV

Evaporator capacity (Q_e) and compressor power (W_{cp}) were monitored and COP was calculated for both experiments. Table 3.2 also shows, along with on-cycle average evaporator and condenser saturation temperatures ($T_{sat,e,on,avg}$ and $T_{sat,c,on,avg}$), and cycle average evaporator metal temperatures ($T_{met,e,avg}$). COP was only 1% lower for OV operation due to the slightly higher compressor power during the OV experiment. Figure 3.25 and Table 3.2 show that the on-cycle average evaporator saturation temperature was slightly lower and condenser saturation temperature slightly higher for OV operation, which increased compressor power about 1%.

Table 3.2 Experimental results compared for OV and CV operation

	μ	τ [sec]	W_{cp} [W]	Q_e [kW]	COP	$T_{sat,e,on,avg}$ [^oC]	$T_{sat,c,on,avg}$ [^oC]	$T_{met,e,avg}$ [^oC]
CV	0.5	30	755.4	3.38	4.47	9.1	42.3	12.0
OV	0.5	30	760.1	3.37	4.43	8.8	42.6	12.2

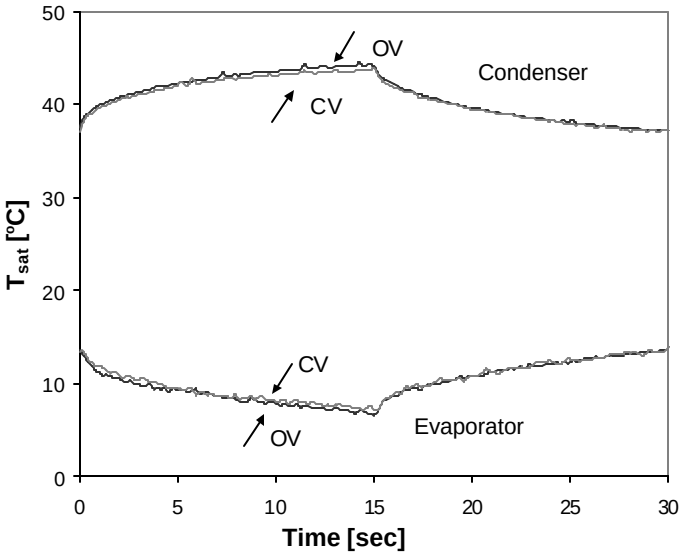

Figure 3.25 Evaporator and condenser saturation temperatures overlaid for OV and CV

Closer inspection of the data revealed that the 0.3 C higher on-cycle average condenser saturation temperature is totally due to the 0.3 C warmer air temperature in the outdoor chamber during the OV experiment. After adjusting for this experimental error it is clear that COP differences are almost negligible when off-cycles are as short as 15 seconds. To see bigger differences between OV and CV, one would need to look at longer cycle periods. A detailed analysis of the temperature lift degradation term for this 30-second cycle is presented for both strategies in Appendix D.

Chapter 4: Short-cycling comparison to continuous operation

4.1 Short-cycling losses at m=0.56 compared to continuous operation

To obtain data for steady state operation, a small rotary compressor was installed and the degradation from ideal performance was measured in the same manner as for short-cycling. Then short-cycling (SC) experiments were done with originally installed two-ton compressor at the run time fraction μ=0.56, which provided the same capacity as the steady state one-ton compressor.

System efficiencies were compared by monitoring the difference between the whole-cycle mean tube temperature ($T_{m,avg}$) and the on-cycle mean saturation temperature ($T_{sat,on,avg}$) in the evaporator and condenser. The larger those differences, the greater the COP degradation relative to the ideal baseline operation at a given capacity. Figure 4.1 shows how temperature lift increases with cycle period. Evaporator and condenser temperature lift degradation terms (ΔT_e and ΔT_c) were compared at five different cycle periods (τ=10, 30, 50, 65 and 80 seconds).

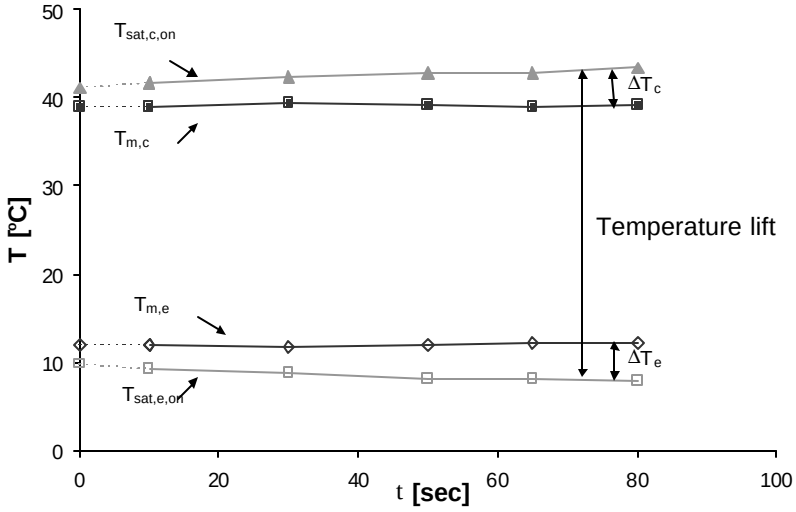

Figure 4.1 Saturation temperature lift and degradation terms increase with τ

In order to compare cycle COP's, the effect of potentially different compressor efficiencies was eliminated by calculating the smaller compressor's steady-state specific power using steady-state compressor calorimeter data provided by the manufacturer of the larger scroll compressor. The experimental points at τ=0 represent continuous operation, and the calculated COP's are based on the assumption that steady-state compressor efficiencies are equal. The temperature lift degradation for continuous operation relative to ideal baseline operation is 2.0^o C on evaporator and 2.1^o C on condenser side (as can be seen in Figures 4.1, 4.3 and 4.4).

Short-cycling operation was compared to the ideal baseline operation in Chapter 3 using the temperature lift degradation term as the measure of degradation from ideal baseline defined by the evaporator and condenser surface temperatures. In this chapter we will focus on the incremental increase in temperature lift attributable to short-cycling relative to variable-speed operation, where continuous operation of the smaller compressor simulates

theoretical variable-speed (VS) operation without inverter losses. This incremental temperature lift term is defined as the difference between the short-cycling lift degradation term at given cycle period and variable-speed lift degradation term, $\Delta T_{e,loss} = \Delta T_{e,sc}(\tau) - \Delta T_{e,vs}(\tau=0)$. This term represents the temperature lift degradation of short-cycling operation at given cycle period compared to the variable-speed operation at $\tau=0$.

The lift loss term can be seen in Figures 4.3 and 4.4 as the temperature lift degradation term increases 0.7^{o} C on evaporator and 0.6^{o} C on condenser side as cycle period increases from 0 to 10 seconds. Compared to continuous operation, short-cycling at this relatively high frequency degrades COP by approximately 2.5% as shown in Figure 4.2.

As shown in Chapter 3, this additional degradation occurred because the higher refrigerant mass flux increased pressure drop. There was also a net increase in ΔT on refrigerant side because the increase, required by the shorter runtime ($\mu<1$), was not fully offset by the increase in heat transfer coefficient. Thus, requirement for a higher on-cycle ΔT on refrigerant side, due to negligible off-cycle heat transfer rate, was dominant over the reduction in refrigerant side ΔT caused by the decrease in the refrigerant side heat transfer resistance with a higher refrigerant mass flux. As cycling period increased to 80 seconds, the COP degradation reached 7.5% due to the "lift loss" of 2.3^{o} C on evaporator and 2.1^{o} C on condenser side shown in Figures 4.3 and 4.4.

The increase in temperature lift caused COP degradation to increase with cycle period at this dry coil $80/95^{o}$ F operating condition. Similar observations for wet surface operation were described in section 3.5 of Chapter 3, and wet and dry operation at $80/82^{o}$ F is compared in Appendix C. All these results are consistent and lead to the same general conclusions.

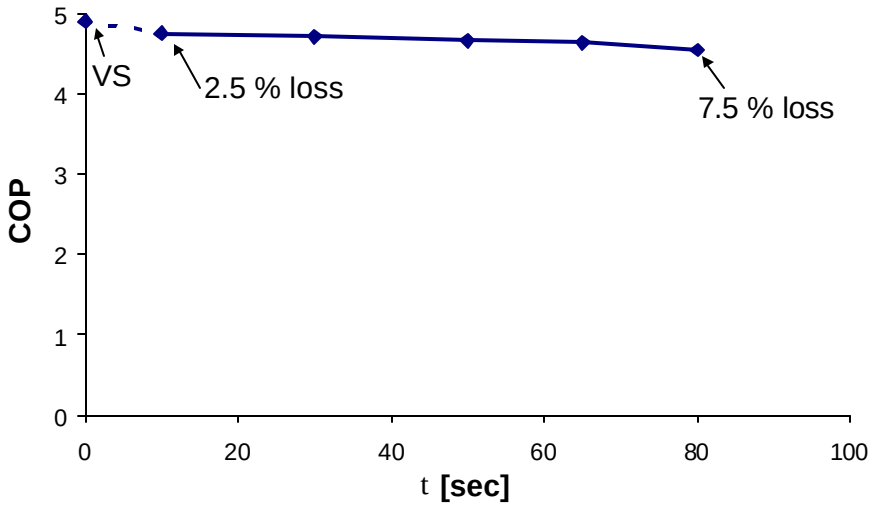

Figure 4.2 Coefficient of performance decrease with τ

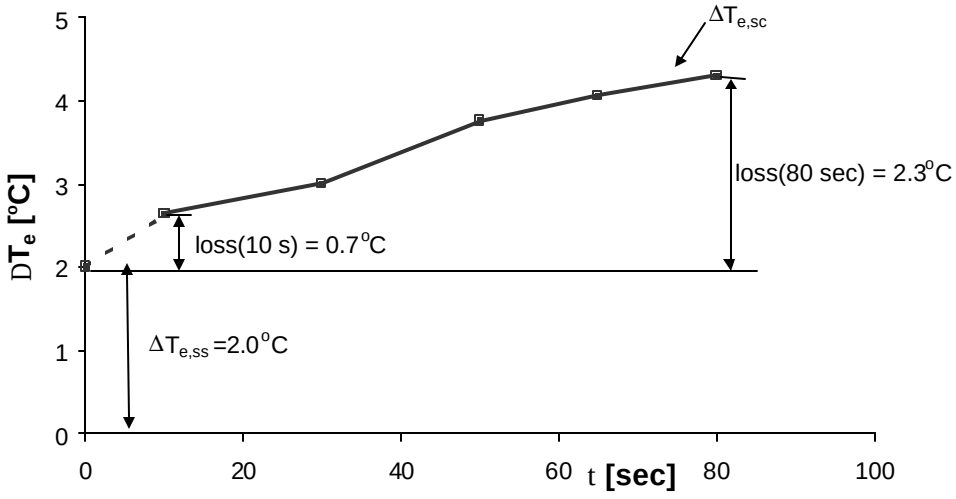

Figure 4.3 Evaporator side lift degradation term increase with τ

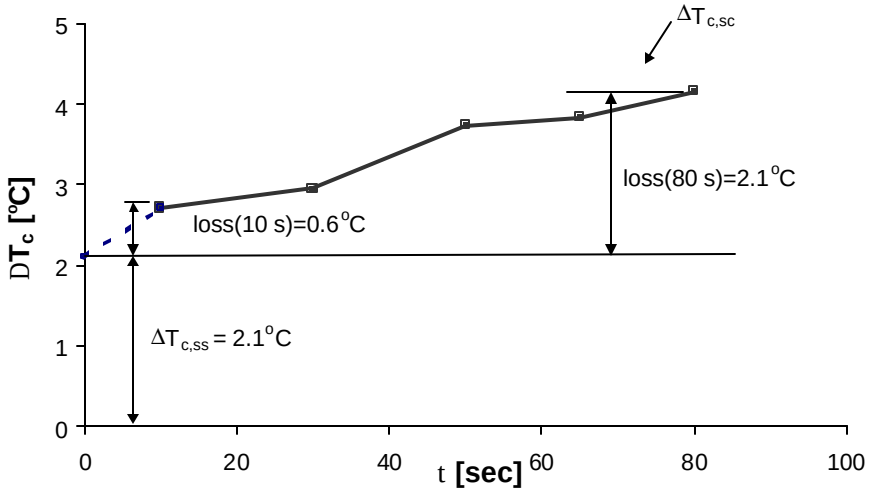

Figure 4.4 Condenser side lift degradation term increase with τ

4.2 Lift degradation terms breakdown for t=0, 10 and 80 seconds at m=0.56

Recall from Chapter 3 that three factors cause degradation of temperature lift: refrigerant heat transfer (rht) resistance, pressure drop and nonlinearity due to thermal capacitance (nonlin). Figures 4.5 and 4.6 quantify these effects for the evaporator and condenser respectively. The effect of thermal capacitance (nonlinearity of temperature oscillations) is by definition zero for continuous operation at τ=0, and negligible for short-cycling operation at 10 seconds. It becomes significant for evaporator at long cycle periods (τ=80 seconds), and earlier for

the less massive condenser. Figures 4.7 to 4.9 illustrate how these degradation terms are calculated for the evaporator at τ=0, 10 and 80 seconds, respectively.

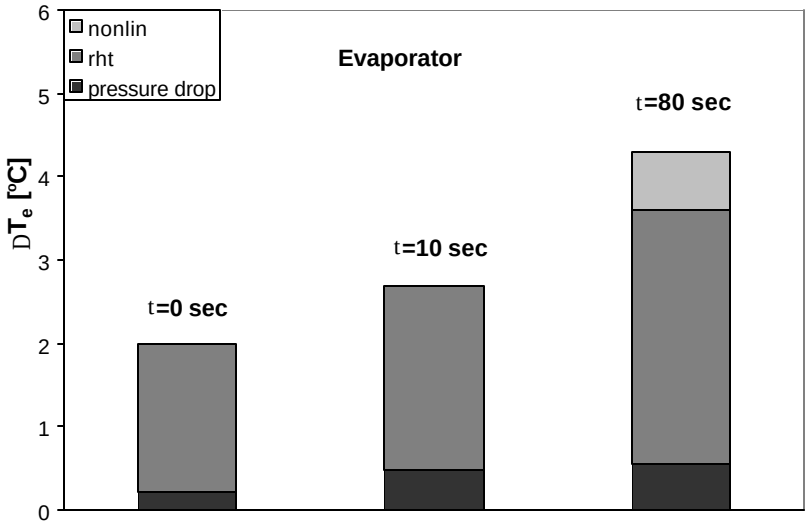

Figure 4.5 Lift degradation term breakdown on evaporator side

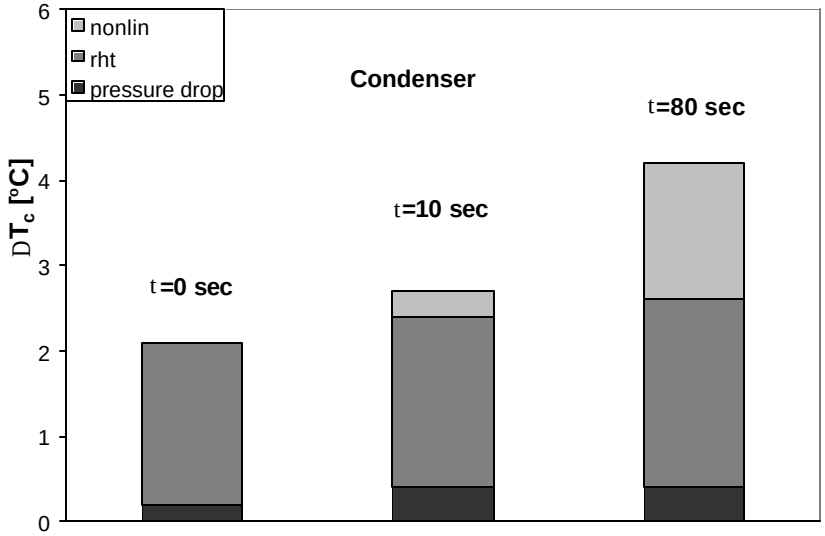

Figure 4.6 Lift degradation term breakdown on condenser side

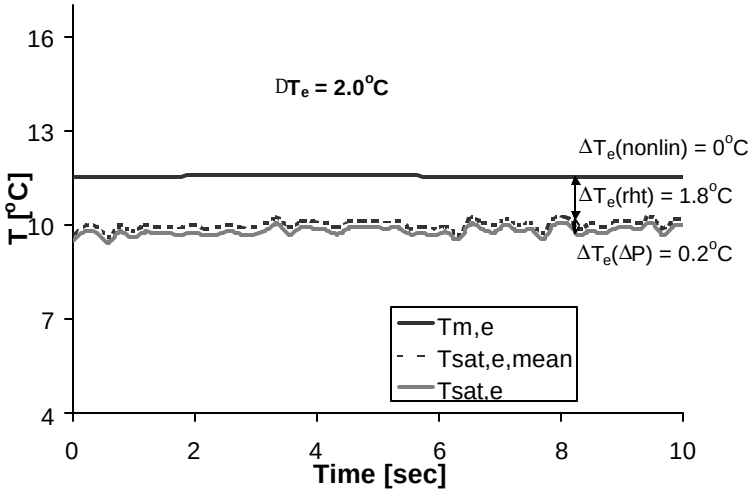

Figure 4.7 Evaporator degradation term for VS operation (τ=0)

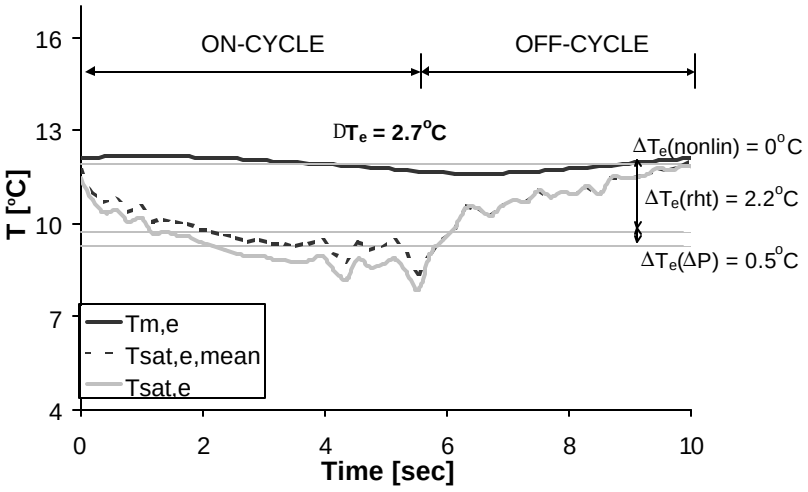

Figure 4.8 Evaporator degradation term for SC at τ=10 sec

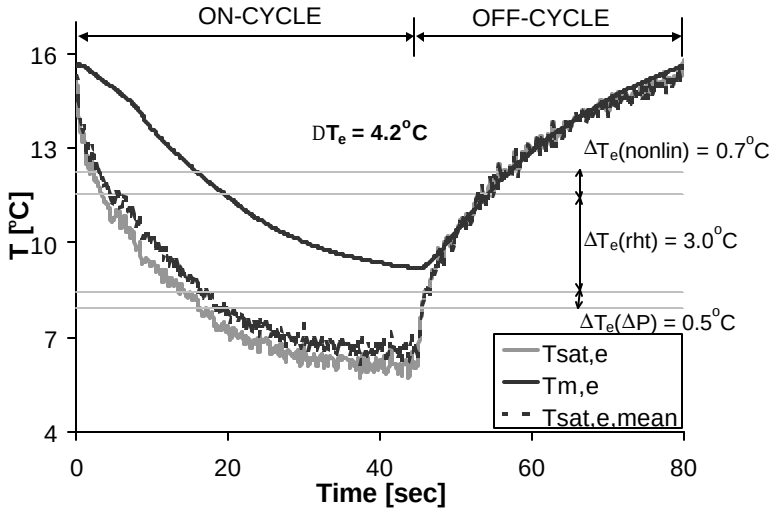

Figure 4.9 Evaporator degradation term for SC at τ=80 sec

4.3 Lift loss for τ=10 and 80 seconds at μ=0.56

This section focuses on the incremental degradation of temperature lift due to short-cycling. Figures 4.10 and 4.11 show the detailed breakdown of this lift loss term at τ=10 and τ=80 seconds on condenser and evaporator side. It is by definition zero for continuous operation. Recall from Figure 4.2 that this additional temperature "lift loss" caused COP losses of about 2.5% and 7.5% at τ=10 and τ=80, respectively, compared to continuous operation.

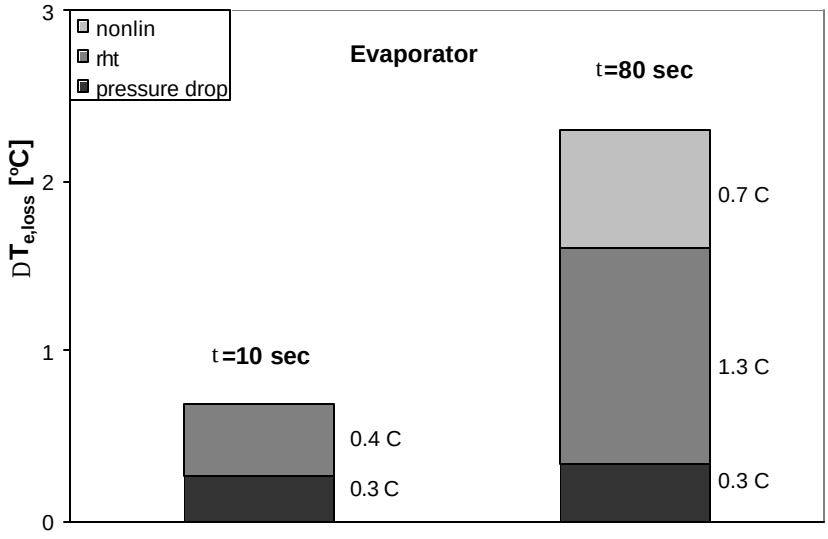

Figure 4.10 Breakdown of the lift loss term on evaporator side

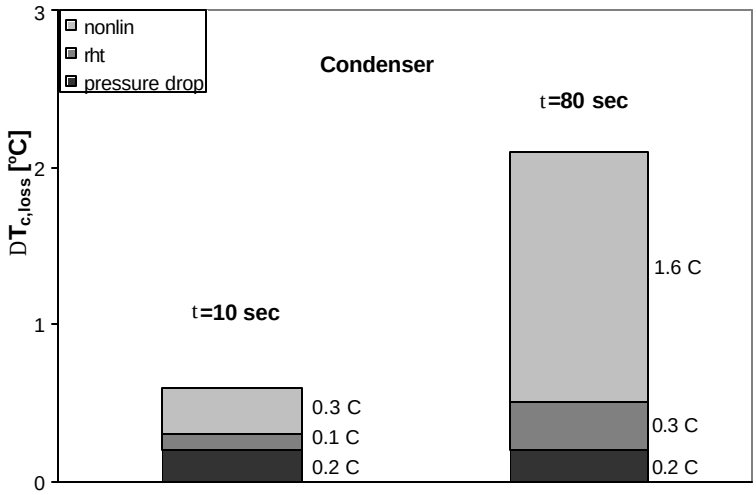

Figure 4.11 Breakdown of the lift loss term on condenser side

4.3.1 Losses due to short-cycling at τ=10 seconds

Figure 4.10 and 4.11 show that losses at τ=10 seconds are caused primarily by the refrigerant side parameters, refrigerant side heat transfer resistance and pressure drop, while the effect of thermal capacitance is small due to the shortness of the on-cycle.

Compared to continuous operation the refrigerant side ΔT (difference between the on-cycle average metal and mean saturation temperatures - rht) is 0.4^{o} C and 0.1^{o} C higher, respectively, for evaporator and condenser. The low off-cycle refrigerant side heat transfer rate required a higher on-cycle ΔT to achieve the same capacity. The higher on-cycle refrigerant side heat transfer coefficient only partially offset this requirement. This trade-off has been explained in Chapter 3.

Pressure drop increased temperature lift by 0.3^{o} C on the evaporator side and 0.2^{o} C on the condenser side, compared to the case of continuous operation. The reasons for this difference are apparent from Figure 4.12 for the evaporator. Similar trends were observed on the condenser side.

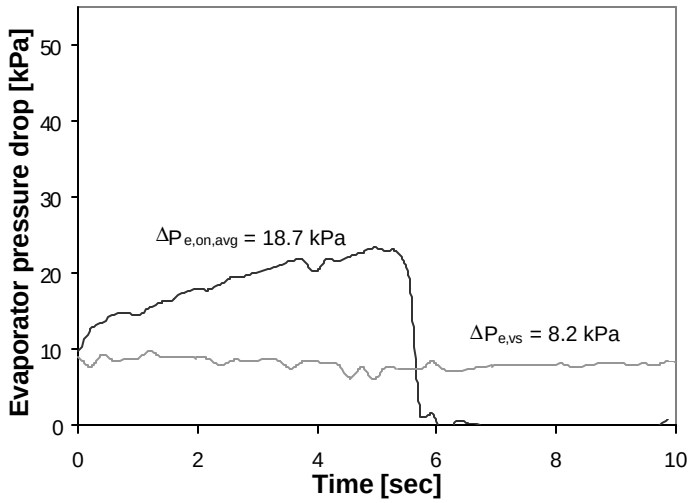

Figure 4.12 Evaporator pressure drop at τ=10 sec (short-cycling) and τ=0 sec (continuous)

The nonlinearity of evaporator surface temperature fluctuation is negligible, and is 0.3^{o} C on the condenser side for this short cycle period (10 sec). However it is significant for longer cycle periods as shown in next section.

4.3.2 Losses due to short-cycling at longer cycle periods (τ=80 seconds)

As expected, short-cycling losses due to pressure drop relative to continuous operation are essentially independent of cycle period because the mass flux is the same for all cycling conditions. For τ=80 seconds, Figures 4.10 and 4.11 show that the longer cycle period losses are dominated by refrigerant side heat transfer resistance and the nonlinearity of heat exchanger surface temperature oscillations.

The losses due to refrigerant side heat transfer were about equal at τ=10 seconds in the evaporator and condenser. However at τ=80 seconds, the on-cycle average heat transfer resistance in the evaporator increased much more than in the condenser. One possibility is that off-cycle heat transfer persists for short time after compressor shut-off, which may have a significant effect at τ=10 but is clearly negligible for τ=80 seconds as shown in Figure 4.9. A more reasonable hypothesis is that dry-out occurs over most of the evaporator during the longer off-cycles, resulting in a lower heat transfer rate during the first part of the on-cycle. Such an effect would not be expected in the condenser, where the walls would always be wet during the on and off-cycles, and even the normally superheated zone would be condensing during the off-cycle. Figure 4.11 shows only a small increase in condenser side ΔT, from 0.1^{o} C at τ=10 to 0.3^{o} C at τ=80 seconds, consistent with this hypothesis.

As expected, the effect of heat exchanger thermal capacitance becomes dominant as $\tau \rightarrow 80$ seconds. The on-cycle average evaporator surface temperature was 0.7^{o} C lower than the cycle-average (Figure 4.10), and the effect was 1.6^{o} C in the condenser (Figure 4.11).

As expected, the temperature lift penalty due to nonlinearity was greatest on the condenser side. The increased magnitude of metal temperature oscillations and increased exponential rate quotient, hA_{air}/C_m, are the causes of increased nonlinearity, as explained in section 3.4.2 of Chapter 3. The thermal capacitance of the condenser was about equal to that of the evaporator, but its 25% higher capacity increased the magnitude of metal temperature oscillations by the same percentage. The condenser side hA_{air} was about 4 times greater than the evaporator side at μ=0.56, so the correspondingly higher exponential rate quotient hA_{air}/C_m increased metal temperature curvature which caused higher nonlinearity. However this temperature lift penalty was more than offset by the beneficial effect of this quadrupled hA_{air}, which decreased temperature substantially (order of magnitude higher beneficial effect). Therefore, maximization of hA_{air} on condenser side is beneficial because it decreases temperature lift by minimizing air side ΔT, even though it slightly increases nonlinearity of surface temperature oscillations.

In summary, the refrigerant side heat transfer and pressure drop are main contributors to short-cycling temperature lift losses at τ=10 seconds causing about 2.5% COP loss. The metal temperature nonlinearity and refrigerant side heat transfer are primary contributors to short-cycling temperature lift losses at τ=80 seconds, causing the largest part of 7.5% COP loss.

4.4 Short-cycling comparison to conventional cycling

As a point of reference, Figure 4.13 shows an 11.5% COP difference (at τ=0) between continuous operation of the small 1-ton compressor, simulating the variable-speed case, and the nominal 2-ton compressor, simulating conventional cycling. It also shows how short-cycling reduced this loss to 2.5% and 7.5% at cycle periods of 10 seconds and 80 seconds, respectively. Of course this comparison is approximate, since it neglects cycling losses in the CC case, and difference between blower power requirements, both of which should favor SC over CC.

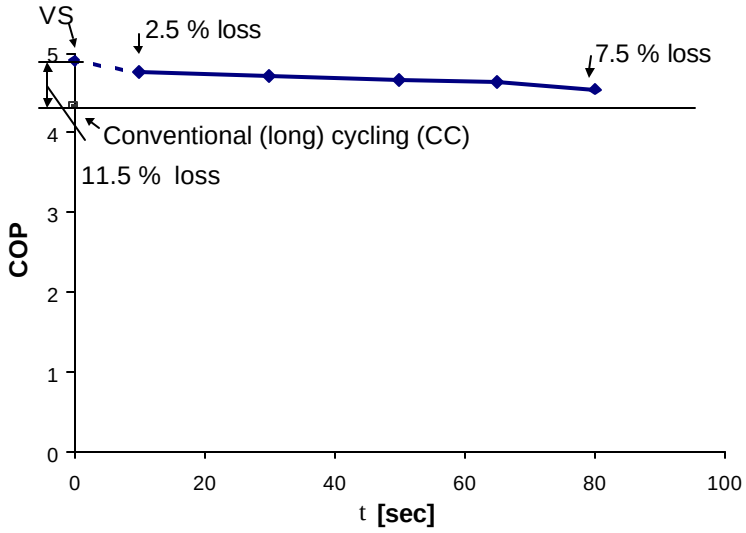

Figure 4.13 COP comparison to conventional cycling

Chapter 5: Conclusions

5.1 Defining an ideal baseline for comparing capacity regulation methods

System cooling capacity during short-cycling is regulated by changing the compressor run time fraction, μ, for a given short cycle period τ. Short-cycling capacity regulation method tends to approach variable-speed continuous operation, as $\tau \rightarrow 0$. Experiments with an automobile a/c system showed that short-cycling COP's are nearly equal to variable-speed operation as long as cycle periods are not very long (5-15 sec).

The short-cycling experiments were done for a typical residential a/c system over the range of run time fractions, and several cycle periods from τ=10 to 80 sec, in order to identify the most important factors affecting short-cycling performance.

An "ideal" baseline system was defined as a system operating – continuously – between heat source and sink temperatures defined by the tube temperatures of real heat exchangers, which have finite size and finite airflow rate. Three methods of capacity regulation: conventional cycling, variable-speed, or short-cycling, were compared to this ideal. Viewed from the air side, the requirement for sensible and latent cooling capacities to be equal for all three systems implies that the cycle time averaged sink (evaporator) temperatures must also be equal. Since the numerator of COP is therefore constant, the amount of degradation depends solely on the power, which in turn is a function of on-cycle temperature lift. Therefore to compare short-cycling system efficiencies with those of ideal system, and with other systems, we monitored the increase in temperature lift. In the evaporator and condenser, the increase is equal to the difference between the whole-cycle mean tube temperature and the on-cycle mean saturation ($\Delta T_e = T_{m,e} - T_{sat,e,on}$ and $\Delta T_c = T_{sat,c,on} - T_{m,c}$). Analysis focused on the ways in which pulsing the flow from the compressor affected the performance of the rest of the system. Differences in compressor efficiencies were outside the scope of the study.

5.2 Factors affecting short-cycling COP degradation

Detailed analysis of ΔT_e identified the three most important factors affecting COP as capacity is modulated by short-cycling. The lift degradation term was separated into three terms, each representing one major factor increasing the temperature lift.

5.2.1 Refrigerant side heat transfer resistance

The on-cycle refrigerant side temperature difference, $\Delta T_{ref}(t)=T_{m,on}(t) - T_{sat,on}(t)$, was identified as one factor increasing the average on-cycle temperature lift. This term is by definition zero for ideal baseline system. For variable-speed system it also has a finite value degrading COP. During short-cycling, on-cycle refrigerant side heat transfer rate was greater, by almost a factor of $1/\mu$ than in the case of variable-speed at the same capacity, due to the low refrigerant side heat transfer rate during the off-cycle. However the penalty in terms of increase in on-cycle ΔT_{ref} did not increase by the same amount ($1/\mu$), since the on-cycle refrigerant side heat transfer coefficient was larger than for variable-speed. The experiments showed that the evaporator refrigerant heat transfer resistance part of COP degradation term increased significantly at longer cycle periods. This may have been due to tube dry-out over most of the evaporator during the longer off-cycles resulting in lower heat transfer rate during the first part of the on-cycle. Therefore evaporators for short-cycling should be designed to minimize dry-out during longer off-

cycles possibly by focusing on tube orientation and circuiting. Moreover the use of microchannel tubes, with their higher refrigerant side surface to volume ratio, may help minimize the magnitude of ΔT_{ref}.

5.2.2 Pressure drop

Since the short-cycling compressor operates at full speed, it has higher on-cycle refrigerant side pressure drop than in the case of variable-speed. Refrigerant pressure drop increases temperature lift by $\Delta T_{sat}(\Delta P_{ref})$. Since pressure drop in a crossflow heat exchanger also increases capacity, the net effect of pressure drop on system temperature lift is approximately $\Delta T_{sat}(\Delta P_{ref}/2)$. It was shown that this pressure drop term was almost independent of cycle period, due to the almost constant on-cycle refrigerant mass flux resulting from the constant on-cycle compressor speed. For the same reason, the temperature lift degradation term due to the pressure drop is also nearly independent of run time fraction. Knowing that variable-speed systems have lower pressure drops at lower run time fractions due to lower mass fluxes, pressure drop losses relative to variable-speed systems worsen at lower run time fractions. The heat exchangers for short-cycling systems should be designed to operate at the optimal design pressure drop for full speed operation.

5.2.3 Heat exchanger thermal capacitance

Due to the inherently exponential nature of the heat transfer process, the evaporator metal temperature during the off-cycle approaches the air temperature nonlinearly. The same phenomenon occurs during the on-cycle as the evaporator surface temperature is pulled down towards the steady-state refrigerant saturation temperature. As a result, the on-cycle average metal temperature is always less than the whole-cycle average, and this difference was defined as the temperature lift degradation due to nonlinearity. Short-cycling truncates these processes, but the fundamental asymmetry remains. Since the compressor sees only the lower on-cycle metal temperature, there is a penalty in pressure lift for long cycle periods where the nonlinearities are the greatest. The curvature of the evaporator surface temperature oscillation depends on its time constant (C_m/hA_{air}), and the magnitude of oscillation is inversely proportional to the evaporator's thermal capacitance, $C_m=mc$. This leads to two design recommendations for minimizing COP degradation during short-cycling: 1) heat exchangers more thermally massive; and 2) increase hA_{air}. The latter strategy is counterintuitive, because the lower time constant increases the curvature of the temperature oscillations, thus increasing the temperature lift by a few tenths of a degree. However the same increase in hA_{air} has a beneficial effect that is an order of magnitude larger; it decreases temperature lift by several degrees, by reducing the air side ΔT. Therefore air side heat transfer surface enhancements provide a net benefit for short-cycling heat exchangers, as they do for a variable-speed systems.

5.2.4 Other effects

Theoretical analysis showed that there are benefits in isolating the evaporator during the off-cycle, so a solenoid valve was installed upstream of the expansion device to disable the refrigerant flow into the evaporator during off-cycle. This operation was compared to open-valve operation which allowed off-cycle refrigerant flow into the evaporator. An experiment conducted at 50% run time fraction and a cycle period of 30 seconds showed no significant change in energy efficiency and saturation temperature lift. Additional experiments at longer cycle periods are needed to measure the capacity degradation, which is expected as off-cycle pressure equalization causes

evaporator saturation temperature to exceed the tube temperature, thus heating the evaporator mass from the refrigerant side.

No significant difference in the COP degradation was observed for the wet and dry coil experiments. Virtually identical increases in on-cycle temperature lift for wet and dry coil experiments caused essentially identical decreases in COP.

5.3 Short-cycling compared to variable-speed meeting ~1/2 of design load

To compare short-cycling and continuous operation directly, a nominal 1-ton rotary compressor was installed, and degradation from ideal baseline performance was measured in the same manner as for short-cycling. Then short-cycling experiments were done with the originally installed two-ton compressor at the run time fraction of 0.56. In both experiments, system capacities were the same: about 4.0 kW.

Cycle efficiencies were compared by monitoring the difference between the whole-cycle mean tube temperature ($T_{m,avg}$) and the on-cycle mean saturation temperature ($T_{sat,on,avg}$) in the evaporator and condenser, and neglecting differences in compressor efficiency. The focus was on the incremental increase in temperature lift attributable to short-cycling relative to variable-speed operation, where continuous operation of the smaller compressor represented variable-speed operation without inverter losses. The temperature lift loss term was defined as the difference between the short-cycling lift degradation term at given cycle period and variable-speed lift degradation term, $\Delta T_{e,loss} = \Delta T_{e,sc}(\tau) - \Delta T_{e,vs}(\tau=0)$. This lift loss term increased 0.7^{o} C in evaporator and 0.6^{o} C in the condenser as cycle period increased from 0 to 10 seconds. Compared to continuous operation, short-cycling at this relatively high frequency degraded COP by approximately 2.5%. As cycling period increased to 80 seconds, the COP degradation reached 7.5% due to temperature lift losses of 2.3^{o} C on evaporator and 2.1^{o} C on condenser side.

5.3.1 Losses for 10-second cycle period

The relatively small cycle COP losses at τ=10 seconds, compared to continuous operation of about 2.5 %, were caused primarily by higher refrigerant side heat transfer resistance and pressure drop. The effect of thermal capacitance (nonlinearity of temperature oscillations) is by definition zero for continuous operation at τ=0, and negligible for short-cycling operation at 10 seconds. The losses due to refrigerant side heat transfer resistance in the evaporator and condenser were about equal at τ=10 seconds. The same was the case for pressure drop losses, which were almost equal in the condenser and evaporator.

5.3.2 Losses for 80-second cycle period

At longer cycle periods, short-cycling losses are dominated by refrigerant side heat transfer resistance, and by the nonlinearity of heat exchanger surface temperature oscillations. As expected, pressure drop losses, relative to variable-speed, were essentially independent of cycle period because the mass flux did not change. At τ=80 seconds, the refrigerant side heat transfer resistance in the evaporator increased much more than in the condenser. This was probably due to already mentioned dry-out, which occurs over most of the evaporator during the longer off-cycles, causing a lower heat transfer rate during the first part of the on-cycle. Such an effect is not expected in the condenser, where the walls are always wet during the on and off-cycles, and even the normally superheated zone condenses during the off-cycle. The effect of thermal capacitance becomes significant for evaporator at long cycle periods (τ=80 seconds), and earlier for the condenser. The on-cycle average evaporator surface temperature was

0.7°C lower than the whole-cycle average, and in the condenser the effect was 1.6° C. The degradation due to nonlinearity was greatest on condenser side since its time constant was four times higher than the evaporator. C_m was almost the same for both heat exchangers, causing almost the same metal temperature magnitude (really slightly higher on condenser side due to 25% higher condenser capacity).

5.4 Short-cycling compared to conventional cycling

The short-cycling loss of 2.5% and 7.5% at τ=10 and 80 seconds, respectively, can be compared to the maximum 11.5% COP loss that would occur for large τ, corresponding to conventional (long) cycling operation. The 11.5% COP loss difference between two compressors (continuous operation of the small 1-ton simulating the variable-speed, and the nominal 2-ton, simulating conventional cycling without cycling losses) is due mainly to the savings on condenser side, since the requirement of keeping the constant latent/sensible ratio of ~25/75% required maintenance of a constant evaporator surface temperature.

The experiments reported here were conducted under controlled conditions to explore the effects of short-cycling on the rest of the system, outside the compressor. For experimental purposes a switch was used to control the compressor, and the resulting startup power spikes were excluded from the reported results (they accounted for up to ~10% of total energy at τ=10 sec, and ~1% at τ=80 seconds). Other short-cycling compressors use a clutch mechanismand run the motor at lower power during the off-cycle, and therefore incur a different kind of power penalty. Similarly, our reported comparisons to variable-speed systems neglected any speed dependence of isentropic efficiency, and inverter losses. Such all compressor-specific parasitic power losses must be included, along with fan and blower powers, when comparing performance of capacity-modulated systems. Isentropic efficiency of the variable-speed compressor was assumed to be unaffected by speed.

References

Bahel, V., and S.M. Zubair. 1989. An assessment of inverter-driven variable-speed air-conditioners: sample performance comparison with a conventional system. *ASHRAE Transactions* 95(1): 455-464

Coulter, W.H., and C.W. Bullard. 1997. An experimental analysis of cycling losses in domestic refrigerator-freezers. *ASHRAE Transactions* 103(1): 587-596

Krause, P.E., and C.W. Bullard. 1996. Cycling and quasi-steady behavior of a refrigerator. *ASHRAE Transactions* 102(1): 1061-1070

Marquand, C.J., S.A. Tassou, Y.T. Wang, and D.R. Wilson. 1984. An economic comparison of a fixed speed, a two speed and a variable speed vapor compression heat pump. *Applied energy* 16(1): 59-66.

Mulroy, W.J., and D.A. Didion. 1985. Refrigerant migration in a split-unit air conditioner. *ASHRAE Transactions* 91(1A): 193-206

Murphy, W.E., and V.W. Goldschmidt. 1986. Cycling characteristics of a residential air-conditioner – modeling of shutdown transients. *ASHRAE Transactions* 92(1A): 186-202

Parken, W.H. Jr., R.W. Beausoliet, and G.E. Kelly. 1977. Factors affecting the performance of a residential air-to-air heat pump. *ASHRAE Transactions* 83(1): 839-849.

Tassou, S.A., C.J. Marquand, and D.R. Wilson. 1983. Comparison of performance of capacity controlled and conventional on/off controlled heat pump. *Applied energy* 14(4): 241-256.

Toshiba (UK) Limited. 1987. Toshiba inverter aided air-conditioner. Survey, United Kingdom.

Umezu, K., and S. Suma. 1984. Heat pump room air-conditioner using a variable capacity air-conditioner. *ASHRAE Transaction* 90(1A): 335-349.

Wang, J., and Y. Wu. 1990. Start-up and shut-down operation in a reciprocating compressor refrigeration system with capillary tubes. International Journal of Refrigeration 13(3): 187-190

Watlow Electric Manufacturing Company. 1995. SCR Power control. Book six of the Watlow Educational Series. St. Louis, United States.

Watlow Electric Manufacturing Company. 1995. Temperature control. Book five of the Watlow Educational Series. St. Louis, United States.

Appendix A: Short-cycling experiments on R134a mobile a/c system

A.1 Purpose

The purpose of this experiment was to determine coefficient of performance (COP) for short-cycling (SC) and variable speed (VS) capacity regulation method for several evaporator capacities (Q_e) lower than the design evaporator capacity, which was chosen to be the capacity of the continuous system operation at the compressor speed of 1700 rpm.

A.2 Experimental setup

The mobile air conditioning system in the Air Conditioning and Refrigeration Center (ACRC) at the University of Illinois is equipped with an open scroll compressor having both clutch and compressor motor frequency controller, enabling experiments by regulating evaporator capacity using both short-cycling (SC) and variable speed (VS) capacity regulation method.

Condenser for experiments had micro-channel, brazed Al tube heat exchanger. Evaporator was brazed Al plate and fin heat exchanger. Refrigerant was R134a. The system also included, suction line heat exchanger and high-side refrigerant receiver.

The mobile air conditioning experimental facility (Nelson, 2001) was designed to allow three procedures to determine evaporator capacity: refrigerant side, air side, and calorimetric chamber energy balance. During short-cycling experiments, refrigerant side energy balance cannot be used due to intermittent flow and system operation. Analyzed parameters were changed very quickly during experiments (on the order of seconds), so the chamber balance also is not useful for short periods of time, which are on the order of a few cycle duration, due to the thermal capacitance of the chamber. However, the chamber balance could be useful when integrated over long time periods. The air side energy balance was used to determine evaporator capacity during the mobile a/c system experiments. Air side evaporator capacity integrated over a cycle ($Q_{e,avg}$), was calculated from the air side energy balance.

Power was calculated every 0.1 seconds by measuring compressor speed (rpm) and torque. The compressor torque was measured during the experiments by torque meter and the compressor speed by tachometer.

A.3 Experiment description

Short-cycling experiments was done at 1700 rpm. It should be mentioned that 1700 rpm was not necessarily been optimized rpm for SC operation but arbitrarily chosen for the experiment.

The system was run at three run time fractions (μ=0.8, 0.6 and 0.35). Run time fraction μ=1 corresponds to the baseline continuous operation for this experiment (chosen as the design, maximum capacity operation). The baseline continuous operation (100% on) was at the compressor speed of 1700 rpm. Three cycle periods were tested (τ=15s, 10s, and 5s) for each run time fraction.

For comparison with the variable speed capacity regulation method three additional steady-state experiments were conducted at 1350 rpm, 1000 rpm and 700 rpm using a VS frequency controller. The baseline continuous operation (chosen as the design, maximum capacity operation) was chosen to be at the compressor speed of 1700 rpm.

All experiments were conducted with constant air inlet temperature in the evaporator of 32 C. The condenser air inlet temperature was 38 C. Experiments were done with a dry evaporator surface to facilitate repeatability. The air flow rates over condenser and evaporator were kept constant for all experiments ($\dot{V}_e$ =0.129 m^3/s and $\dot{V}_c$ =0.406m^3/s).

A.4 Experimental results and analysis

Evaporator capacity and compressor power were measured and calculated for all run time fractions and cycle periods of short-cycling operation at 1700 rpm and shown in the top section of Table A.1. Evaporator capacity and compressor power have been calculated for different speeds (rpm) as well, and shown in the bottom section of Table A.1.

Table A.1 Experimental results for short-cycling and variable speed capacity regulation method

Short-cycling (1700 rpm)				
run time fraction μ	cycle period τ [s]	COP	W_{cp} [kW]	Q_e [kW]
1	no cycles	2.32	1.42	3.30
0.8	15	n/a	n/a	n/a
0.6	15	3.16	0.83	2.63
0.35	15	3.90	0.49	1.92
1	no cycles	2.32	1.42	3.30
0.8	10	2.62	1.13	2.95
0.6	10	3.23	0.83	2.70
0.35	10	4.01	0.48	1.93
1	no cycles	2.32	1.42	3.30
0.8	5	2.68	1.11	2.97
0.6	5	3.19	0.83	2.65
0.35	5	4.20	0.47	1.98
rpm	**Variable-speed**			
1700	2.32	1.42	3.30	
1350	2.69	1.10	2.95	
1000	3.27	0.77	2.53	
700	4.02	0.51	2.06	

Note: the results for SC operation at τ=0.8 and t=15 sec are not available due to errors in the experimental procedure for this experimental point.

After obtaining the evaporator capacity and the compressor power, coefficient of performance for cycle was calculated as the ratio of the two: $COP=Q_e/W_{cp}$. The coefficients of performance calculated for cycle are shown in Figure A.1 as a function of evaporator capacity Q_e. COP is shown with three lines for short-cycling, and one bolded line for variable speed (VS) capacity regulation method. SC experimental points are connected for run time fractions μ=1.0, 0.8, 0.6 and 0.35 at a constant cycle period (one line). There are three lines, each for different cycle period (τ=5,10 and 15 sec). The fourth line, which is bold, connects VS experimental points obtained for 1700 rpm,

1350 rpm, 1000 rpm and 700 rpm. The VS point at 1700 rpm is SC experimental point at μ=1.0. The lines are shown in Figure A.1 only to connect experimental points and emphasize a trend of increase in COP with decreasing Q_e.

In all cases, the measured efficiency (increase in COP) results from increasing the evaporating temperature from approximately 0 C at the maximum capacity condition (3.3 kW) to about 13^o C as capacity is reduced to about 2 kW. This was the effect of keeping the evaporator air flow rate constant with decreasing capacity (which will not be the case in the residential a/c experiments).

It is obvious from Figure A.1 that coefficient of performance of VS operation is almost the same as a coefficient of performance of SC operation for the range of capacities tested, and COP increases as capacity is reduced. A COP decrease was expected for longer cycle periods, but these results suggest that the longest cycle period tested (τ=15 sec) is still not long enough to degrade the system performance.

COP increase at lower capacities comes from the highest percentage decrease in compressor power than in evaporator capacity. Figures A.2 and A.3 show, for a 10 second cycle period, that compressor power decreased by about 65%, while the capacity decreased by only 40%, increasing COP by about 70%.

Coefficient of performance COP increases with decreasing capacity due to decreased pressure lift (condenser and evaporator saturation pressure difference) at lower capacities. The measure of a COP increase for VS operation is a decrease in the condenser and evaporator saturation temperature (pressure) difference ($\Delta T_{sat,vs}$). COP increases at lower speeds for VS operation, since the saturation temperature difference decreases. The reason for COP increase is in lower compressor work required for each unit of refrigerant mass compressed, when compressor operates in between lower pressure difference (lower pressure lift). The measure of a COP increase for short-cycling (SC) operation is a decrease in the condenser and evaporator saturation temperature (pressure) difference during the on-cycle ($\Delta T_{sat,on,sc}$), not the whole cycle period. One would expect that the condenser and evaporator saturation temperature (pressure) difference during the on-cycle for SC operation ($\Delta T_{sat,on,sc}$) is the same as $\Delta T_{sat,vs}$ during VS operation since COP for SC and VS operation are the same. This is shown for SC at τ=10 sec and VS operation in Figure A.4. Saturation temperatures used in Figure A.4 are shown in Table A.2.

It is also important to mention that COP of conventional cycling (CC) operation (τ~20-30 min in residences) wouldn't increase at lower capacities and would stay approximately constant if CC cycle losses were neglected. The reason is in on-cycle operation between maximum saturation pressure (temperature) difference. Thus CC on-cycle capacity and power are equal to design values while almost no heat is exchanged during off-cycle.

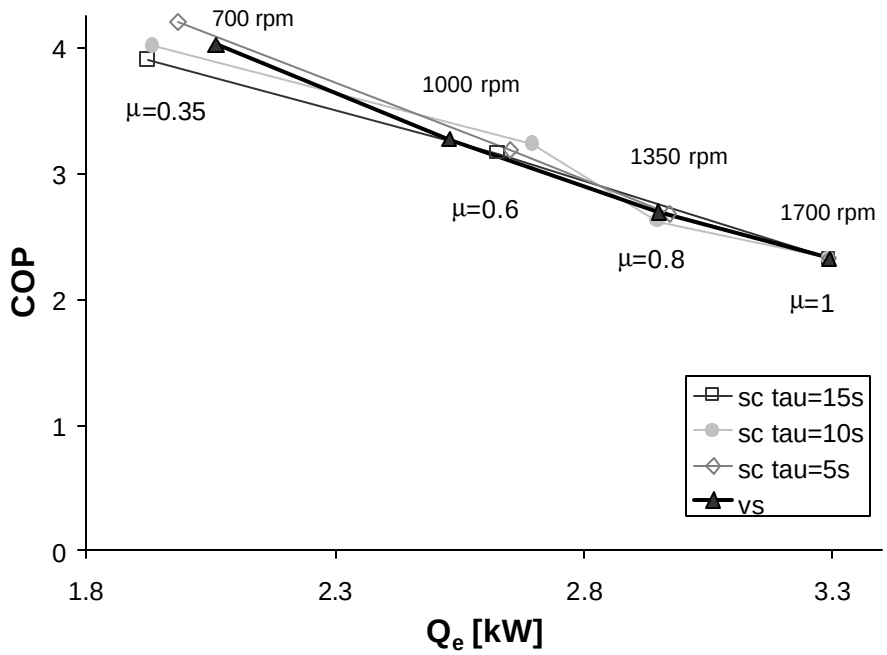

Figure A.1 Experiment results for short-cycling (SC) and variable speed (VS) capacity regulation method

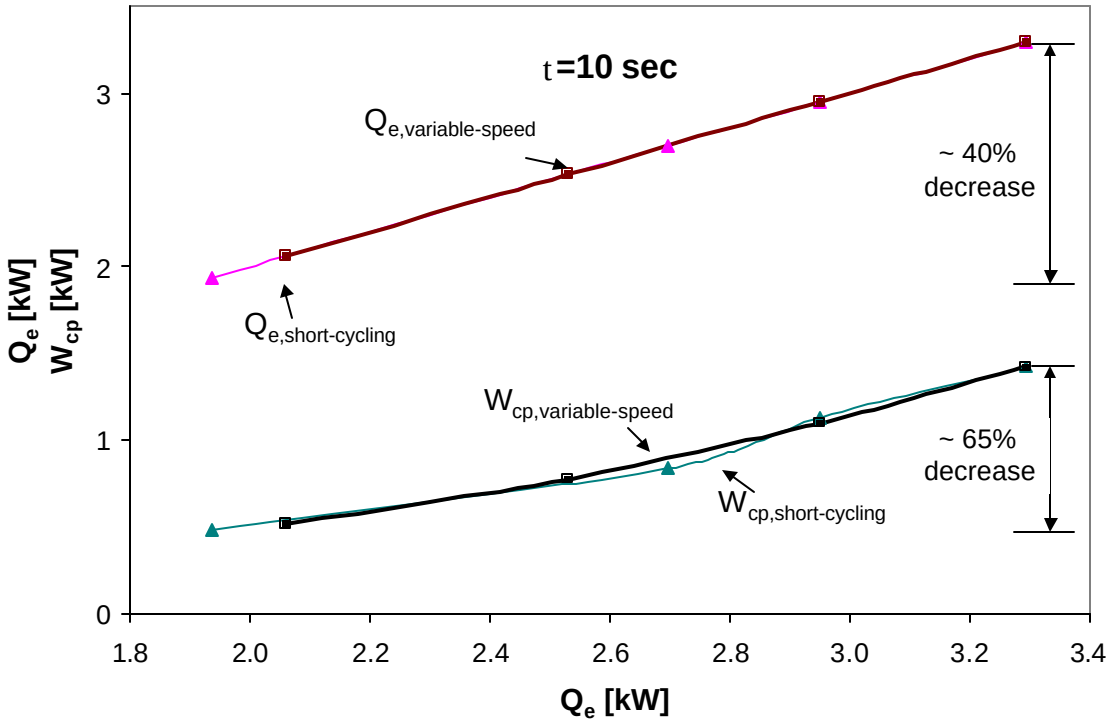

Figure A.2 Change of compressor work and evaporator capacity for SC at τ=10 sec and VS

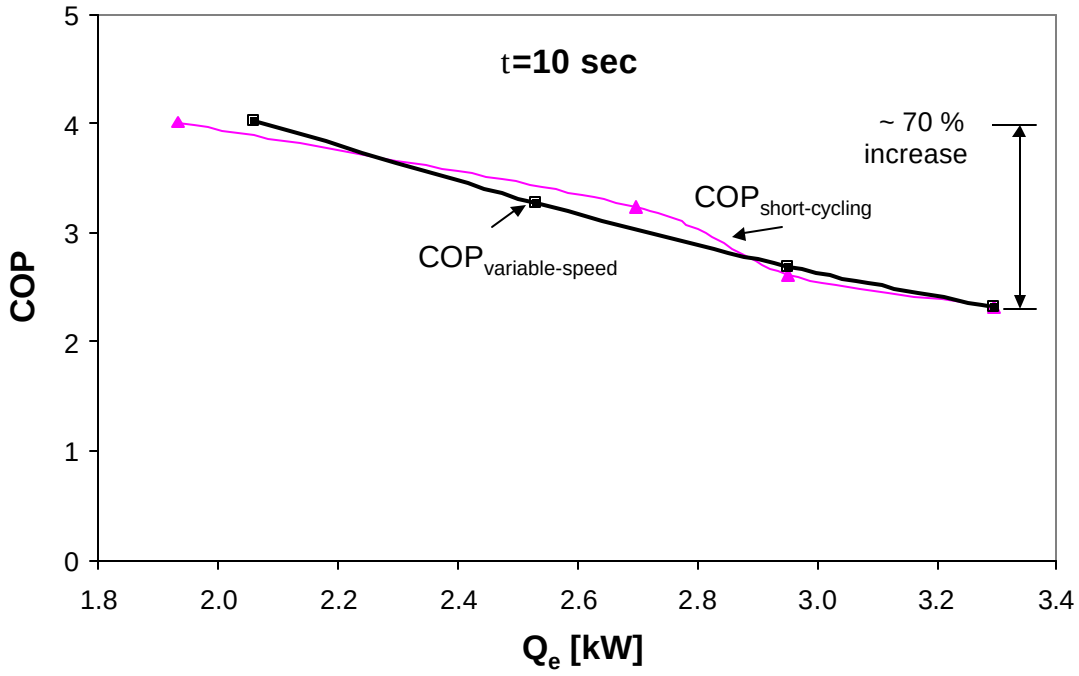

Figure A.3 Change of coefficient of performance of cycle for SC at τ=10 sec and VS

Table A.2 Condenser and evaporator saturation temperatures for VS and SC operation (τ=10s)

Compressor speed	Q_e	$T_{sat,e}$	$T_{sat,c}$
rpm	[kW]	[C]	[C]
1700	3.30	-0.5	50.6
1350	2.95	1.8	49.1
1000	2.53	4.7	47.1
700	2.06	8.9	45.0

run time fraction μ	cycle period τ	Q_e	$T_{sat,e,on}$	$T_{sat,c,on}$
	[s]	[kW]	[C]	[C]
1	10	3.30	-0.5	50.6
0.8	10	2.97	2.1	49.3
0.6	10	2.71	5.1	47.3
0.35	10	1.95	10.1	44.4

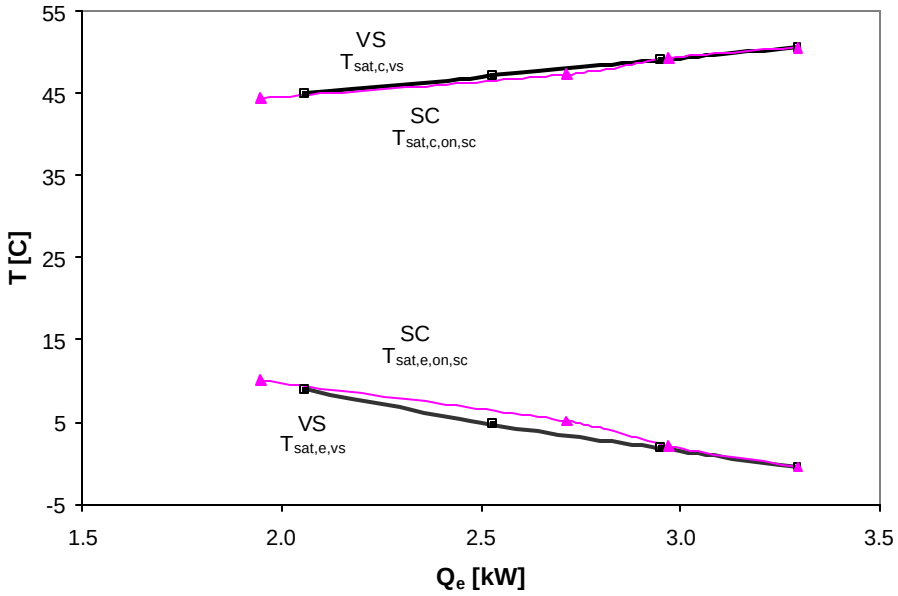

Figure A.4 Saturation temperatures averaged over on-cycle for VS and SC

A change in evaporator and condenser saturation temperatures during two cycles of short-cycling operation is shown in Figure A.5 for μ=0.35 and τ=10 sec. Constant saturation temperatures integrated over whole cycle period, and integrated over only on-cycle are shown by using straight lines.

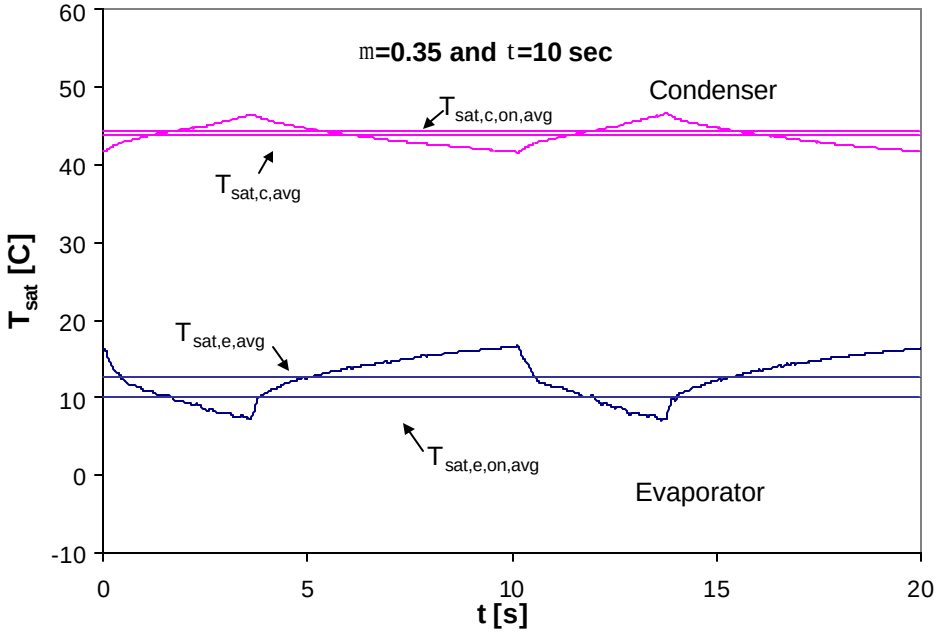

Figure A.5 Change in evaporator and condenser saturation temperatures for two cycles of short-cycling operation at μ=0.35 and τ=10 sec

Change in evaporator and condenser saturation temperatures for two cycles (τ=10 seconds cycle period) is shown for run time fractions μ=0.8, 0.6 and 0.35 in Figure A.6. Straight lines represent integrated values of the corresponding saturation temperatures over the on-cycle only, since these integrated temperatures, serve as a measure of COP increase. It is obvious that the system was operating at the lowest on-cycle saturation temperature difference for the smallest μ=0.35, resulting in the highest efficiency (COP_{cyc}). Furthermore, the efficiency was almost the same as the efficiency of VS operation providing the same capacity, due to establishing almost the same integrated condenser and evaporator saturation temperature during on-cycle as the condenser and evaporator saturation temperature during VS operation. The main reason for this is in using heat exchangers during the off-cycle, which can be seen by comparing the air inlet temperature (32 C) and refrigerant temperature during the off-cycle in Figure A.6 for different run time fractions.

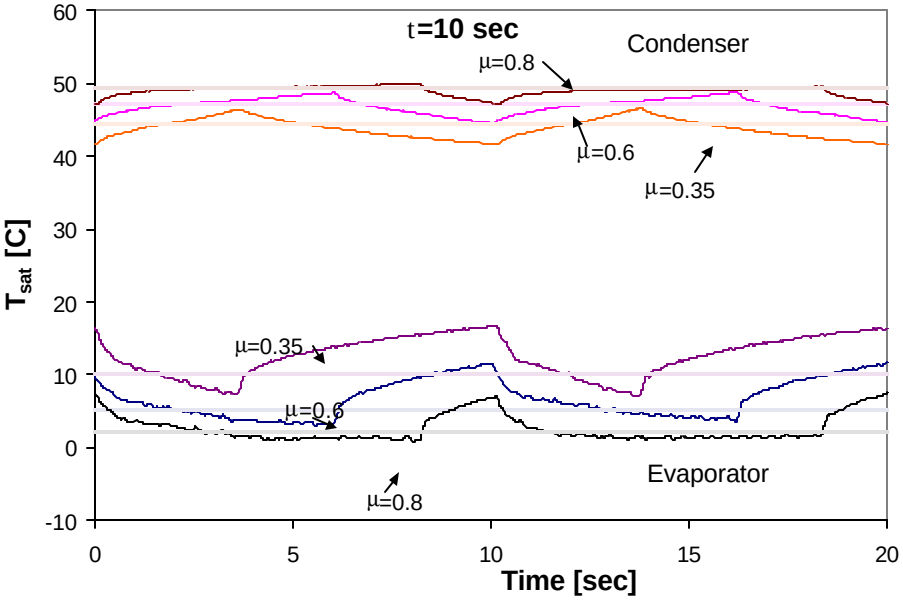

Figure A.6 Change in evaporator and condenser saturation temperatures for two cycles (τ=10 seconds) for run time fractions μ=0.8, 0.6 and 0.35

A.5 Conclusions

It can be concluded that energy efficiency of short-cycling (SC) operation can be almost the same as energy efficiency of variable speed operation (VS) for the mobile a/c system experimented under conditions explained in previous paragraphs and cycle period of 15 seconds. The measure of an energy efficiency increase for variable speed (VS) operation (at lower capacities) is a decrease in condenser and evaporator saturation temperature (pressure) difference ($\Delta T_{sat,vs}$). The capacity of a/c system could be regulated by short-cycling (SC) method with the same energy efficiency as by VS method if the integrated condenser and evaporator saturation temperature (pressure) difference over the on-cycle ($\Delta T_{sat,on,sc}$) is the same as the condenser and evaporator saturation temperature (pressure) difference during VS operation. The main reason for establishing lower saturation temperature difference ($\Delta T_{sat,on,sc}$) is in using heat exchangers during the off-cycle. Heat exchangers are used

effectively for the cycle periods experimented in analyzed experiment. One could expect $\Delta T_{sat,on,sc}$ increase (for the same required capacity) with increasing cycle period to be on the order of minutes. When $\Delta T_{sat,on,sc}$ increases for the same required capacity, COP decreases (for required capacity) since higher compressor work is required for each unit of refrigerant mass compressed during the on-cycle.

Appendix B: Experimental setup for residential a/c system

B.1 A/C refrigeration loop and components

The main components of a residential air conditioning system tested are condenser, evaporator, compressor and expansion valve (Figure B.1). Heat exchangers (condenser and evaporator) were taken from a two-ton R-22 unitary rooftop air conditioning system (Trane model TCH024100A). Heat exchangers for this system are made of copper tubing and plate fins. The heat exchangers were not modified from Trane's original unitary a/c design in any way, but compressor, piping and expansion device were.

The system contains Copeland 2-ton hermetic scroll compressor (model ZR22K3-TF5) with added dynamic valve so the discharge plenum would not equalize with suction during off-cycle time of short-cycling operation. Compressor is connected to a timer, which controls lengths of on and off compressor operation during short-cycling.

The system has a manually adjusted expansion device instead of the TXV, which was installed in Trane's original unitary a/c. The experiments with a TXV showed significant TXV lags and unrepeatable saturation temperature fluctuation, which made accurate averaging over a cycle impossible. Therefore, the experiments were done by using the expansion valve, which had manually adjusted opening for each test. The solenoid valve was installed in series with the expansion device. While in operation, the solenoid valve was fully closed simultaneously with compressor shut-off in order to disable the refrigerant flow into the evaporator during the off-cycle of compressor operation.

In addition to the main components of the a/c system loop, a receiver was installed at the exit of the condenser (high side). The system is designed to enable liquid flow into the evaporator during the entire off-cycle, by using the receiver holding enough liquid refrigerant to last during entire off-cycle of up to 40 seconds.

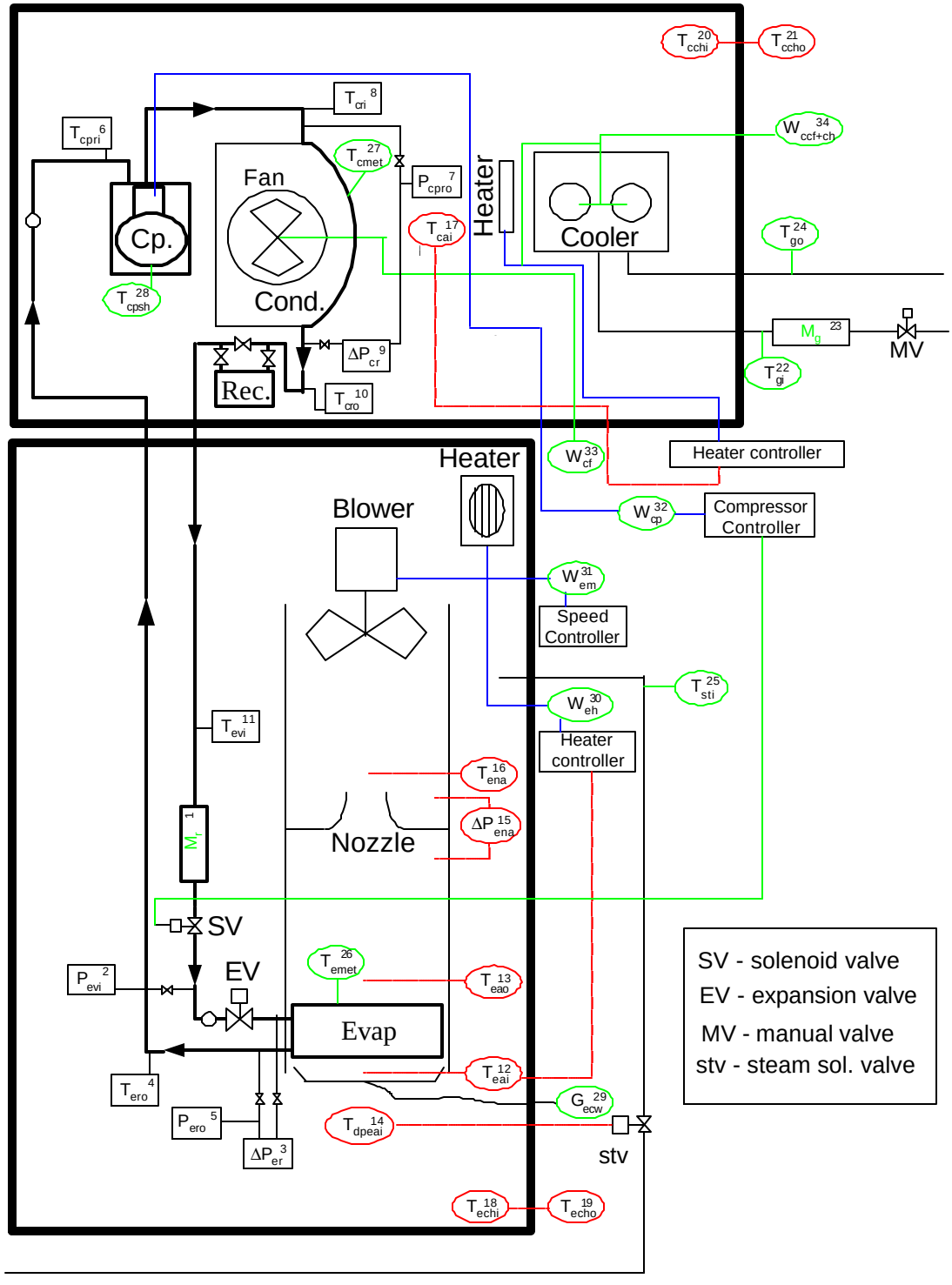

Figure B.1 Residential a/c facility for short-cycling

Table B.1 Short-cycling parameters and instruments used for measurements

Symbol	Number	Measurement	Instrument	Brand	Range	Accuracy	Description/Location
M_r	1	Mass flow rate	Model D25 mass flow meter	Micro Motion	0 to 680 kg/h	+/- 0.15% of reading	Refrigerant mass flow rate (expansion device inlet)
P_{evi}	2	Pressure	Model TJE pressure transducer	Sensotec	0 to 500 psia	+/- 0.1% FS	Expansion valve refrigerant inlet pressure
ΔP_{er}	3	Pressure drop	Model Z differential pressure transducer	Sensotec	0 to 50 psid	+/- 0.25% FS	Evaporator refrigerant pressure drop
T_{ero}	4	Temperature	T type thermocouple probe (Model GTMOSS)	Omega	-200 to 350 C	+/- 0.1°C	Evaporator refrigerant outlet temperature
P_{ero}	5	Pressure	Model 280E pressure transducer	Setra	0 to 500 psia	+/- 0.11% FS	Evaporator refrigerant outlet pressure
T_{cpri}	6	Temperature	T type thermocouple probe (Model GTMOSS)	Omega	-200 to 350 C	+/- 0.1°C	Compressor refrigerant inlet temperature
P_{cpro}	7	Pressure	Model 280E pressure transducer	Setra	0 to 500 psia	+/- 0.1% FS	Compressor refrigerant outlet pressure
T_{cri}	8	Temperature	T type thermocouple probe (Model GTMOSS)	Omega	-200 to 350 C	+/- 0.1°C	Condenser refrigerant inlet temperature
ΔP_{cr}	9	Pressure drop	Model Z differential pressure transducer	Sensotec	0 to 50 psid	+/- 0.25% FS	Condenser refrigerant pressure drop
T_{cro}	10	Temperature	T type thermocouple probe (Model GTMOSS)	Omega	-200 to 350 C	+/- 0.1°C	Condenser refrigerant outlet temperature
T_{evi}	11	Temperature	T type thermocouple probe (Model GTMOSS)	Omega	-200 to 350 C	+/- 0.1°C	Expansion valve refrigerant inlet temperature
T_{eai}	12	Temperature	T type welded thermocouple	Omega	-200 to 350 C	+/- 0.1°C	Evaporator air inlet temperature
T_{eao}	13	Temperature	T type welded thermocouple	Omega	-200 to 350 C	+/- 0.1°C	Evaporator air outlet temp. (10 t/c's on a probe)
T_{dpeai}	14	Dew point	Model D-2 chilled mirror dew point sensor	General Eastern	-35 to 25 C	+/- 0.2°C	Evaporator air inlet dew point
ΔP_{ena}	15	Pressure drop	Model 239 pressure transducer	Setra	0 to 1" water	+/- 0.4% FS	Air pressure drop across the nozzle
T_{ena}	16	Temperature	T type welded thermocouple	Omega	-200 to 350 C	+/- 0.1°C	Evaporator air exit temperature at the nozzle
T_{cai}	17	Temperature	T type welded thermocouple	Omega	-200 to 350 C	+/- 0.1°C	Condenser air inlet temperature

Table B.1 continued

Symbol	Number	Measurement	Instrument	Brand	Range	Accuracy	Description/Location
T_{echi}	18	Temperature	T type welded thermocouple	Omega	-200 to 350 C	+/- 0.1°C	Evaporator chamber inside walls temperature
T_{echo}	19	Temperature	T type welded thermocouple	Omega	-200 to 350 C	+/- 0.1°C	Evaporator chamber outside walls temperature
T_{cchi}	20	Temperature	T type welded thermocouple	Omega	-200 to 350 C	+/- 0.1°C	Condenser chamber inside walls temperature
T_{ccho}	21	Temperature	T type welded thermocouple	Omega	-200 to 350 C	+/- 0.1°C	Condenser chamber outside walls temperature
T_{gi}	22	Temperature	T type thermocouple probe (Model GTMQSS)	Omega	-200 to 350 C	+/- 0.1°C	Glycol inlet temperature
M_g	23	Mass flow rate	Elite CMF050 mass flow meter	Micro Motion	0 to 6800 kg/h	+/- 0.1% of reading	Glycol mass flow rate
T_{go}	24	Temperature	T type thermocouple probe (Model GTMQSS)	Omega	-200 to 350 C	+/- 0.1°C	Glycol outlet temperature
T_{sti}	25	Temperature	T type thermocouple probe (Model GTMQSS)	Omega	-200 to 350 C	+/- 0.1°C	Steam inlet temperature
T_{emet}	26	Temperature	T type welded thermocouple	Omega	-200 to 350 C	+/- 0.1°C	Evaporator metal temp. (12 t/c's on U-bends)
T_{cmet}	27	Temperature	T type welded thermocouple	Omega	-200 to 350 C	+/- 0.1°C	Condenser metal temperature
T_{cpsh}	28	Temperature	T type welded thermocouple	Omega	-200 to 350 C	+/- 0.1°C	Compressor shell temperature
G_{ecw}	29	Condensate weight	Model 31 load cell (tension)	Sensotec	0 to 1000 gr	+/- 0.15% FS	Evaporator condensate weight
W_{eh}	30	Power	Model GW5 Watt transducer	Ohio Semitronics	0 to 8 kW	+/- 0.2% of reading	Evaporator chamber heater power (2 heaters)
W_{em}	31	Power	Model GW5 Watt transducer	Ohio Semitronics	0 to 8 kW	+/- 0.2% of reading	Evaporator chamber blower power
W_{cp}	32	Power	Model PC5 Watt transducer	Ohio Semitronics	0 to 8 kW	+/- 0.5% FS	Compressor power
W_{cf}	33	Power	Model GW5 Watt transducer	Ohio Semitronics	0 to 2 kW	+/- 0.2% of reading	Condenser fan power
W_{ccf+ch}	34	Power	Model GW5 Watt transducer	Ohio Semitronics	0 to 8 kW	+/- 0.2% of reading	Condenser chamber cooler fan and heater power

B.2 Environmental chambers and evaporator wind tunnel

The environmental chambers are constructed of 4-inch, class 1, urethane panels with galvanized stucco embossed on interior and exterior of the panels

2.1 (W) x 4.6 (L) x 2.5 (H) m for the evaporator chamber, and 1.8 (W) x 3.7 (L) x 2.5 (H) m for the condenser chamber. The chambers have one thermocouple located on the inside and outside of the walls, floor and ceiling. The temperatures yield a temperature drop across each wall, which is used to find transmission losses.

The evaporator is installed in the duct, which is positioned in the evaporator chamber. Air from the chamber is circulated through the duct and over the evaporator using a Dayton evaporator air blower. The evaporator air blower is not installed from the Trane's unitary system due to a need for experiments with changed air flow rates over evaporator. Changing air flow rate over evaporator is possible by using blower frequency controller which changes a frequency of 3-phase air blower motor (Trane's blower was single phase). Air flow rate and the evaporator air temperature difference are measured during the experiments. In order to calculate air flow rate, a Helander 6 inch nozzle is installed in the duct and connected to the low range differential air pressure transducer measuring air pressure drop through the nozzle (ΔP_{ena}). Discussion about measured parameters will be presented in section B.3, and the complete list of all measured parameters in Table B.1. A nozzle is positioned about 1 meter downstream of the evaporator, and the nozzle temperature, measured by a T thermocouple. positioned in the throat of the nozzle, is used as the measure of evaporator air exit temperature (T_{ena}). Two Marley 3.2 kW heaters are installed in the evaporator chamber for maintaining constant temperature in the chamber. Generally, this evaporator chamber temperature, is the same which is measured at the inlet of the evaporator (T_{eai} is kept constant for each experiment). One of the two heaters has manual on/off control while the other one is connected to Watlow SCR heater power controller and Watlow microprocessor-based PID controller providing continuous change in power requirement depending on the temperature sensor reading. More detailed explanation of the system of chamber air (evaporator inlet) temperature control will be presented in section B.3.1.2.1.

The condenser and condenser fan from the Trane's unitary system are put in a condenser chamber and not in a duct. Air is sucked through the condenser and exits through the condenser fan, towards the ceiling where a Bohn cooling coil is installed to maintain constant temperature in the outdoor chamber. Glycol entering the chamber at 6^{o}C is circulated from a central chiller in the building. Three PID controlled Vulcan trim heaters (3 x 0.7 kW), are installed between exit of the condenser and inlet to the cooler, for the purpose of easier maintenance of the constant air temperature in the condenser chamber. The temperature at the inlet of the condenser (T_{cai}), is measured by a T type thermocouple and kept at constant value.

B.3 Measured parameters

The most important parameters to monitor during short-cycling operation are those needed for calculation of COP. In addition, the purpose of experiments is not only in calculating COP, but also trying to understand system parameters, which influence degradation or improvement of system COP. Therefore, much more parameters were monitored than needed for only calculation of COP. See Table B.1 for complete list of measured parameters and information about instruments used for measurements, and Figure B.1 for instrument locations. Absolute pressure

transducers were used to measure a pressure at the evaporator exit, the condenser inlet, the expansion device inlet and differential pressure transducer to measure pressure drop through the condenser and the evaporator.

The air and refrigerant mass flow rates were measured by using a mass flow meter and the nozzle, which was installed in the duct. Coriolis type mass flow meter, consisting of sensor and transmitter was used for measuring the refrigerant mass flow rate. Watt transducers were used to measure power of the compressor, the blowers and the heaters. The sampling frequency of data acquisition system was consistent with width of power pulses measured by Watt transducers as explained in next section (B.3.1)..

B.3.1 Measured parameters providing information about COP

Main parameters providing information about the system performance are evaporator capacity (Q_e) and compressor power (W_{cp}). Q_e and W_{cp} were measured and calculated in order to obtain information about coefficient of performance (COP): $COP=Q_e/W_{cp}$.

The Copeland hermetic scroll compressor power was measured by using Watt transducer. It was very important to capture very quick changes in the compressor power measurement during short-cycling, especially during transient periods. Installed Ohio Semitronics Watt transducer averages the reading over 0.2 seconds. Therefore, the rate of data acquisition sampling during experiments was chosen to be about 0.2 seconds per sample which consisted not only of the compressor power but of about additional 50 measurements. The shortest compressor on-cycle tested was 3 seconds, for which 15 samples was obtained providing enough information for accurate compressor power averaging included in calculation of COP.

The existing commercial implementation of the short-cycling concept has the mechanical clutch mechanism installed in the compressor for the purpose of engaging and disengaging scrolls enabling short-cycling without high starting currents and potential reliability risk which exist when a switch is used. A switch was used in our experiment since our focus has been on the influence of short-cycling on the rest of the system. The high starting currents were excluded from the analyses presented in the report. The starting currents increased the measured power about 2.5 times during initial moments of the on-cycle; the rate of data acquisition sampling during experiments was about 0.2 seconds per sample; the data acquisition system dwelling time on specific measurement channel is on the order of milliseconds; however the watt transducer averages the reading over also 0.2 seconds which suggests that the measured start-up power peak lasted about 0.2 seconds and this accounted for about 0.5 – 10 % for the longest (56 sec) and shortest (3 sec) on-cycle on-cycles respectively.

The evaporator blower power was measured by using separate Watt transducer and can be used in COP calculation. The experimental facility was designed to provide three procedures to determine evaporator capacity: air side, calorimetric chamber and refrigerant side energy balance. Each balance yields its own energy balance calculation to find the capacity of the system. The air side and chamber balances are usually only available balances during short-cycling (SC) operation. The air side balance was the only one providing the fast response needed for detailed analysis of cycling phenomenon during all experiments.

B.3.1.1 Air energy balance

Measurements of the air flow rate and enthalpies of the air at the inlet and the exit of the evaporator are needed for determining evaporator capacity by using air energy balance. Air flow rate and the evaporator air temperature difference are measured during the experiments. Air flow rate is known by measuring pressure drop

across the nozzle, knowing the enthalpies of the air at the inlet and exit of the evaporator and atmospheric pressure. For "the wet evaporator surface" experiments, the air temperatures are used in conjunction with inlet and outlet relative humidity to find the air enthalpies and specific heats. The relative humidity in the evaporator chamber is maintained by setting required dew point temperature in a PID controller. The PID controller controls a solenoid valve opening of the steam supply line, which adds a steam that covers for a water removed from the air on the evaporator surface (the evaporator latent load). The evaporator air inlet enthalpy is determined by using the evaporator air inlet temperature (T_{eai}) and the evaporator air inlet dew point (T_{dpeai}). The evaporator air inlet humidity is calculated by knowing inlet dew point measured by using a chilled mirror dew point meter. The evaporator air exit enthalpy is determined by obtaining information about a condensate removal rate by the means of a scale measuring weight of condense (G_{ecw}). The change in weight of condensate over time yields the condensate removal rate needed for calculation of the evaporator latent load.

B.3.1.2 Chamber energy balance

To determine cooling (evaporator) capacity by the chamber energy balance, all chamber energy inputs and outputs were measured. Two electrical heaters and the blower motor provide a sensible load. SCR heater power controller and electronic microprocessor based PID controller control the heater power and maintain the temperature in the chamber at constant value. Process of the temperature control in environmental chambers will be explained in more detail in section B.3.1.2.1.

Three electrical sources going into the chambers, two electrical heaters and blower power were measured by three separate Watt transducers. The change of state of the steam (needed for keeping constant relative humidity in the chamber) is also a part of energy input to the chamber and can be calculated by knowing temperature and pressure of the steam supply and condensate removal rate. The transmission losses through the evaporator chamber walls, for a system operating at 26.7 C indoor temperature, are approximately 70 W, which is only about 1% of a chamber energy balance during continuous operation at full speed.

B.3.1.2.1 Process of the temperature control in environmental chambers The system of temperature control in the environmental chambers consists of:

1) Temperature sensor (T type welded thermocouple) for measuring process temperature
2) Electronic PID temperature controller (Watlow microprocessor-based Series 93 PID controller)
3) Power controller output device (Watlow DIN-a-mite SCR power controller)
4) Heater

The input is the part of the PID controller, which receives and interprets the temperature sensor information. After interpreting the input signal, the input part of PID controller sends this information as a temperature value to the control block of PID controller. The control block of PID controller receives the input information and compares it to the set point temperature. It then uses a control algorithm to tell the power controller what to do. More on control algorithm and theory of PID (proportional-integral-derivative) control can be read in Book 5 of the Watlow Educational Series (Temperature Control).

The output of Watlow Series 93 temperature controller is continuous, variable current signal in the range of 4-20 mA, and it is called a process output. For say a 25% power requirement, an 8 mA continuous signal, [((20 - 4 mA) x 25%) + 4 mA], is sent to the power controller.

The PID controller's process output (4-20mA) is connected to SCR power controller (Watlow DIN-a-mite). Based on the value of the process output signal received, the power controller sends the appropriate amount of power to the heater. So, depending on what the PID process output signal signals, the SCR power controller rapidly switches the heater ON and OFF accordingly (on the order of tens of milliseconds). When the output is switching so fast, heater life increases. The slower ON and OFF switching would cause the resistance element inside of a heater to go through a continuous heating and cooling cycle. The large temperature swings would accelerate the oxidation of the resistance element in a heater. SCR power controller is used in the system to reduce temperature swings of the resistance element in heater. This switching is so fast, that the resistance element experiences very little temperature fluctuation. A SCR power controller is made up of 3 distinct parts: the silicon controlled rectifier (SCR), sophisticated electronics which switch the SCR ON and OFF and a heat sink to dissipate the heat a SCR produces. The electronics use the signal from the process output to calculate how often the SCR must switch the heater ON and OFF. The electronics then adjust load current by very rapidly switching the SCR ON and OFF.

The Watlow DIN-a-mite power controller installed in our system is a zero crossing SCR controller used to regulate the power by using detector which detects the zero crossing of the AC voltage input and allows the SCR to conduct starting with a zero crossing of the voltage. So, controller is always fired (switched ON) at the lowest possible voltage - zero. Switching the SCR ON when the AC sine wave crosses zero voltage is called zero-cross switching. This eliminates electrical noise (also known as radio frequency interference or RFI) associated with the phase angle fired SCR controller. More can be read about both zero-cross firing and phase angle firing in Book 6 of the Watlow Educational Series (SCR Power Control).

B.3.1.3 Refrigerant energy balance

Measurements of the refrigerant mass flow rate and the evaporator inlet and exit refrigerant enthalpies are needed for determining evaporator capacity by using refrigerant energy balance. The refrigerant mass flow rate (M_r) is measured by using the mass flow meter. The refrigerant enthalpies at the inlet and exit of the evaporator are calculated by using measurements of temperatures and pressures at the inlet and the exit of the evaporator. Temperatures are measured by using thermocouples. Thermocouples placed in the refrigerant loop are T-type immersion thermocouple probes placed directly into the refrigerant flow. The Omega low noise thermocouple probes with miniature size connectors were used, which assure high accuracy measurements, providing protection against electrical noise. They maintain an electrical connection from the sheath of the probe, through the connectors, all the way to instrumentation. Pressures at the inlet and exit of the evaporator are measured by using pressure transducers. Three absolute and two differential pressure transducers are used in order to get information about pressures at several positions in the refrigerant loop (along with inlet and exit of the evaporator). More on all measurements, instruments and their locations can be seen in Figure B.1 and Table B.1.

B.4 Data acquisition

All data is taken with Hewlett-Packard data acquisition system which used HP E1313A A/D converter. Data acquisition software was programmed for scanning samples of about 50 parameters in 0.2 seconds. Very fast scanning speed was needed to capture quick changes in measured parameters during short-cycling. Special 7 Hz fixed filters capable of filtering noise on thermocouple measurements were installed since electric noise makes

readings erroneous during very fast scanning without filters. All data were monitored via graphic windows using slow sampling program and after reaching repeatable steady condition fast sampling was used to store data in one-dimensional textual file for further analysis. Data was then transferred to an Excel data sheet and stored for further analysis. Data stored in Excel were transferred to Engineering Equation Solver (EES) using a Visual Basic program.

B.4.1 Data acquisition system

In order to capture the rapidly changing conditions in the refrigerant's temperature, pressure, compressor power, etc., it was determined that a fast sampling data acquisition system was needed with a capability of filtering electrical noise on temperature readings while fast sampling. For this, a HP data acquisition system with listed components was installed:

-HP Mainframe (E1300B)

-64 Channel A/D Converter w/ Filters (E1313A)

-Five 1508 Filters and two 1501 Filters

-GPIB Communications Card

-PC with Windows NT software (Service Pack 4.0)

This data acquisition system itself outperformed needs this project had with respect to required speed of about 250 readings per second (maximum speed capability - 100 K readings per second). This allows for greater flexibility and usefulness of the system after the completion of the project.

There are two types of filters which are used with this system. The E1501 is a signal conditioning plug on (SCP). The E1508 is another SCP, which has a fixed filter and amplifier. E1508 is special 7 Hz fixed filter capable of filtering noise especially on thermocouple measurements, since electric noise makes noisy temperature readings during very fast scanning without filters. The system's speed capabilities were exploited for the purpose of reducing noise on readings, in addition to using filters. The E1313A sampled every channel 64 times and averaged the readings. It then provided output of group of about 50 channels (each averaged over 64 readings) every 0.2 seconds. This type of averaging very fast readings helps in eliminating 60 Hz noise as suggested by manufacturer. The settings for sampling time are input in HPVee panels as shown in Figures B.11 and B.12.

The E1300B is a 9-slot HP mainframe. The E1300B features a built-in command module, GPIB interface, and Resource Manager. Attached to the mainframe is the E1313A, which is a 64 channel A/D converter. The E1313A allows high speed scanning, 16-bit resolution, 4mV to 16V full-scale input, dual-ported FIFO buffer with size of 64k samples for block transfers, current value buffer for on-line monitoring, and automatic self calibration. The GPIB is the PC interface card. The GPIB has built in buffering, which provides the system with performance superior to that of direct memory access.

Two data acquisition programs were written using HPVee. First, slow data sampling (speed of about 1.5 seconds per sample consisting of about 50 variables) program used for instant on-screen monitoring while reaching continuous repeatable operation of the system. Second, fast data sampling (speed of about 0.2 seconds per sample consisting of about 50 variables) program useful for acquiring data to be analyzed.

B.4.2 Slow data sampling for instantaneous display

One of the HPVee visual program capabilities is that it enables writing programs for instant on-screen monitoring by the means of graphical windows. For sampling at speeds slower than 1 sample per second, the programming is rather straightforward. In this version of the sampling program, it is not very useful for acquiring data to be analyzed. However, it is very useful to instantaneously display data when attempting to reach steady state. Here the channels are scanned and formulas are used to convert the measurements to real time data. These values are either viewed numerically or graphically. The program itself is documented in screen dumps for further explanation. The screen in Figure B.2 shows the basics of the program from labeling of variables to storing the data in the FIFO buffer. Figure B.3 shows the E1313A Direct I/O boxes (HPVee programming boxes) opened.

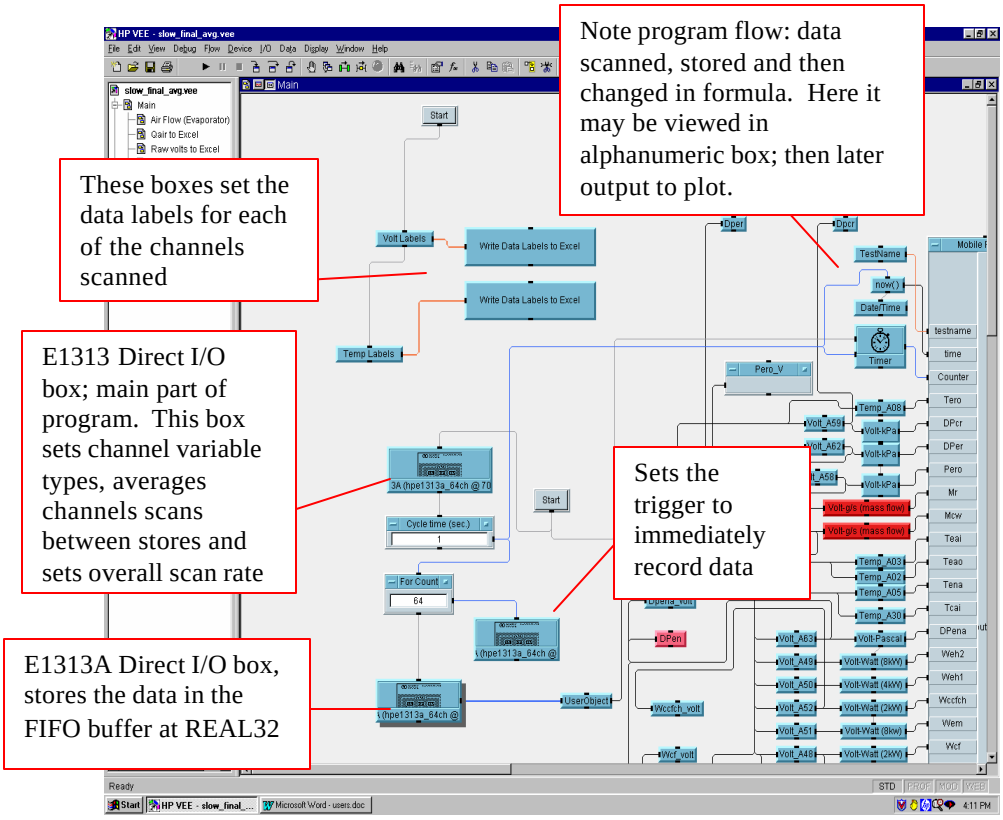

Figure B.2 1st slow sampling and averaging program screen shot.

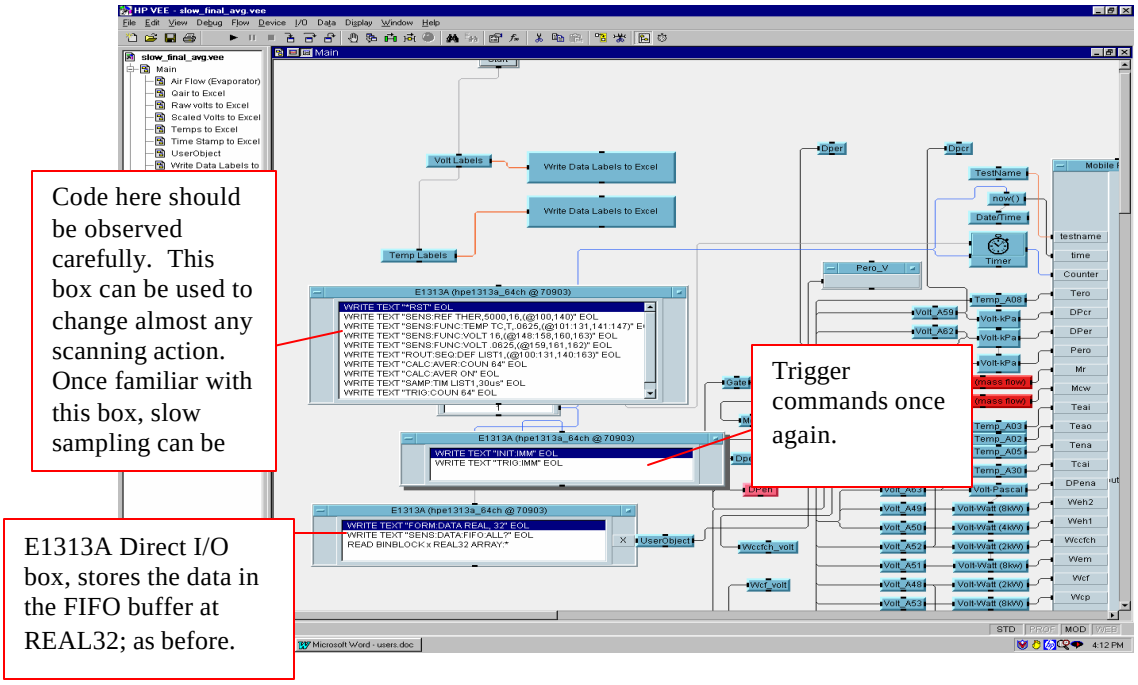

Figure B.3 2nd Slow sampling and averaging program screen shot.

The Figure B.4 shows the bottom of the program and demonstrates how raw data can be stored to MS Excel.

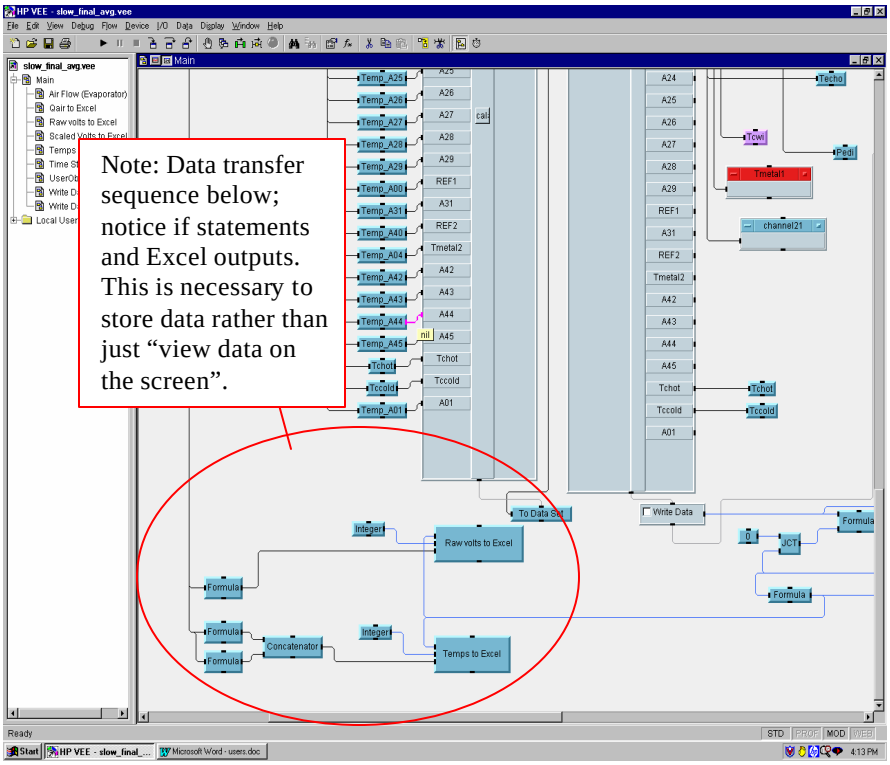

Figure B.4 3rd slow sampling and averaging program screen shot

Figure B.5 follows from the B.2, and shows the flow of data along the top of the program.

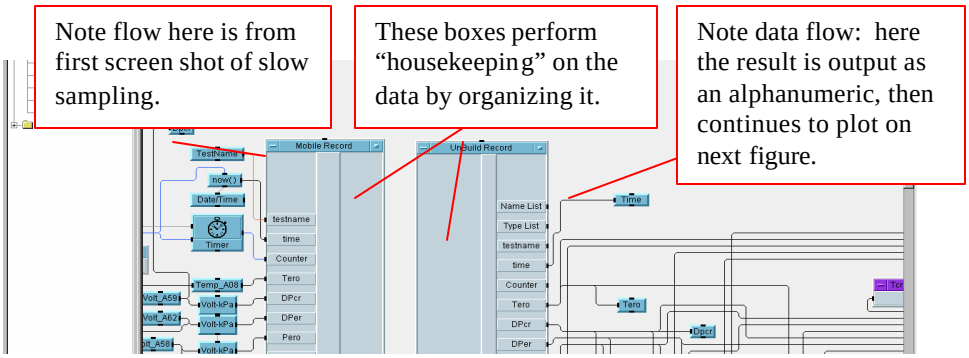

Figure B.5 4th slow sampling and averaging program screen shot

The screen shot shown in Figure B.6 demonstrates the final step of producing graphical view by slow sampling program

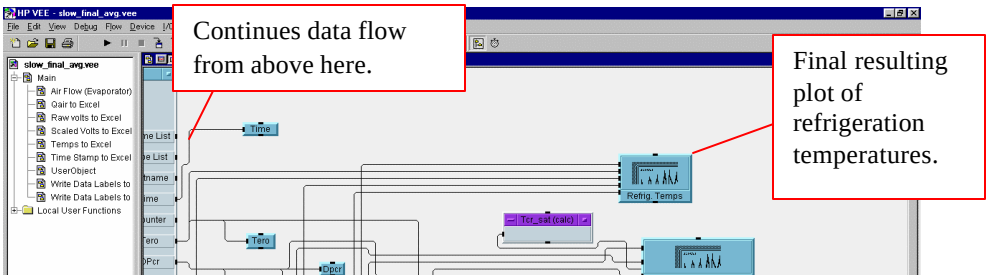

Figure B.6 5th slow sampling and averaging program screen shot

B.4.3 Fast data sampling

To samp le at speeds greater than 1 sample per second, several methods exist. However, these methods are used to push the system to very high sampling rates (up to 100,000 readings per second). Due to the nature of this very high sampling, the program becomes difficult. Each of these methods depends on the speed requirements of the measurement and the noise in the system. For instance, the system can sample each channel every 15 ms, however, if a noisy signal is present, this value may need to be held up to 16 times before it can be averaged and output. Appendix E of the E1313A User's Manual demonstrates 4 versions of this type of programming. A few of these sample programs are available on the manufacturer's website as well. However, these programs are written to be used with the E1413A and require some heavy editing.

A method of sample and hold was used, to enhance noise reduction in the system. This method sampled every channel 64 times and averaged the readings. It then provided output of group of about 50 channels every 0.2 seconds. The Figures B.7 to B.12 show screen dumps of the fast sampling program specifically written for this project's requirements, including several text boxes that explain what some formulas, loops and output scenario are used for. Figure B.7 shows overall program and B.8 program with important text boxes opened for viewing (Note: trigger, error, data storage loop). The panel in Figure B.9 configures the filters on each set of eight channels. The panel in Figure B.10 designates Type-T thermocouples. The panel in Figure B11 shows sets of the channel lists to

scan and their order and sets the sample timer and sets-up averaging. The panel in Figure B.12 sets-up the trigger source and timer, which is the actual scan rate of any individual channel.

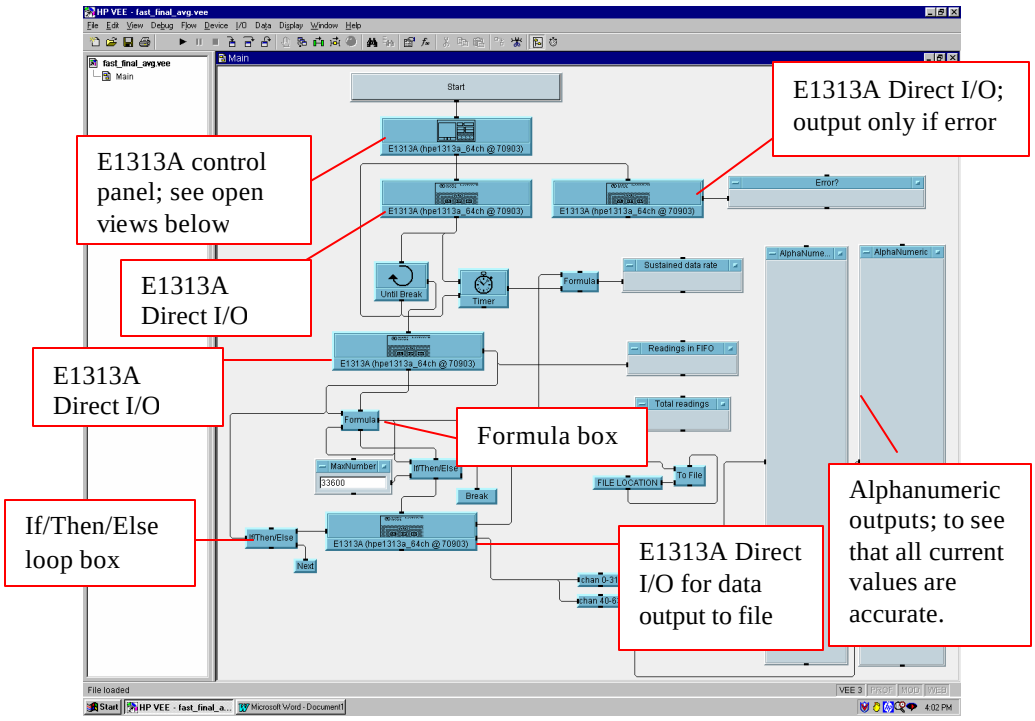

Figure B.7 1st screen shot of entire fast sampling and averaging program.

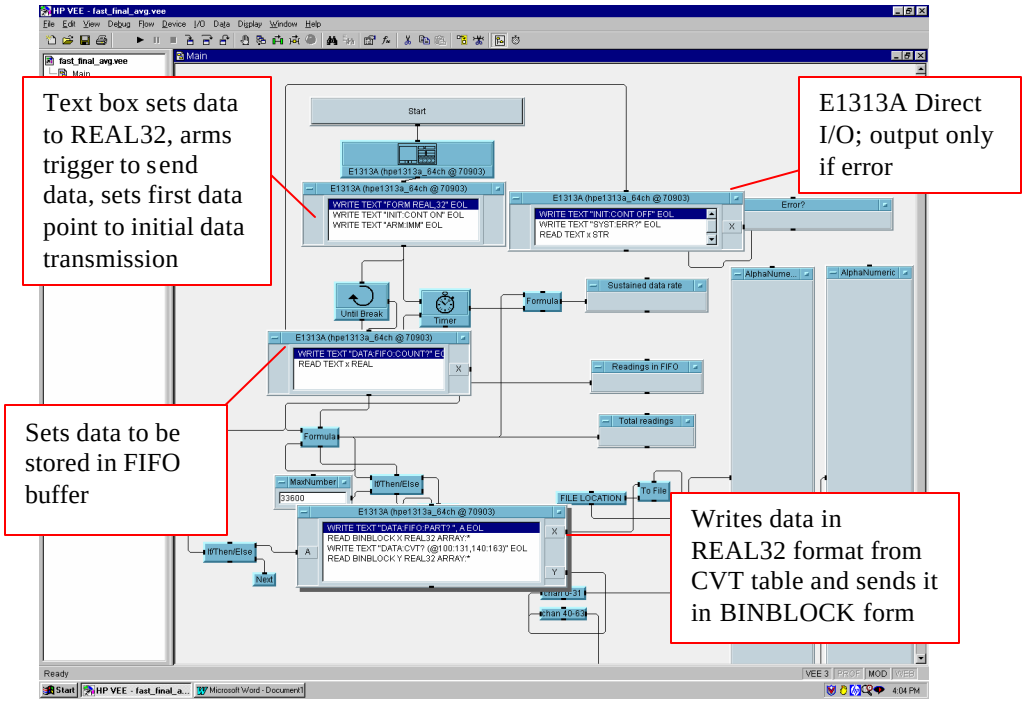

Figure B.8 2nd screen shot of fast sampling and averaging program

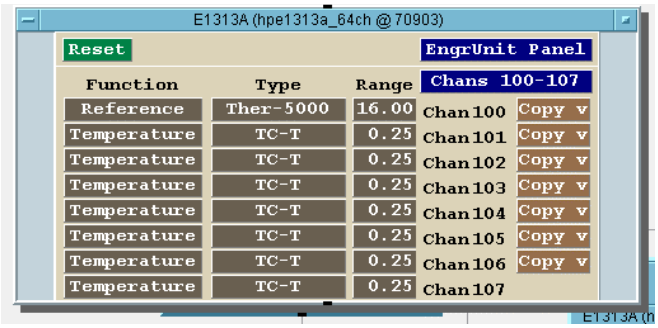

Figure B.9 E1313A Direct I/O control panel, configuration panel.

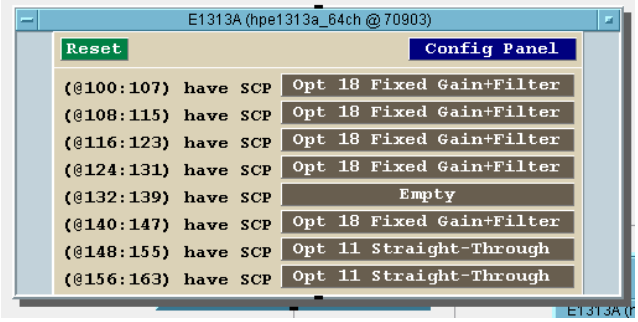

Figure B.10 E1313A Direct I/O control panel, engineering units panel.

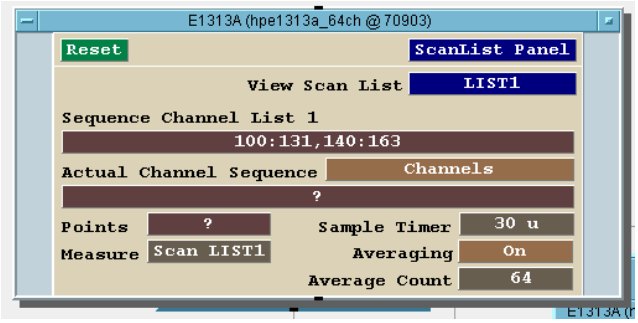

Figure B.11 E1313A Direct I/O control panel, scan-list panel.

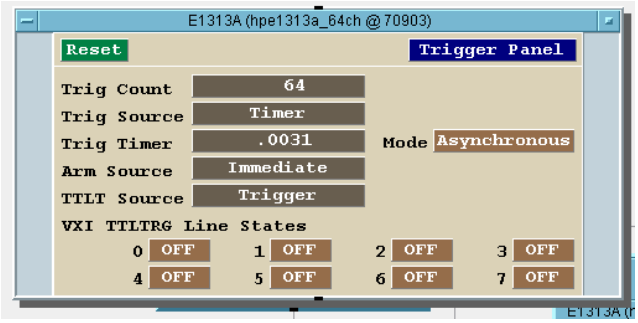

Figure B.12 E1313A Direct I/O control panel, trigger panel.

Appendix C: Short-cycling experiments at 26.7/27.7^{o} C (80/82^{o} F)

The increase of temperature lift with cycle period caused COP degradation, which was analyzed for the dry and wet coil at 80/95^{o} F operating condition in Chapter 3 and 4. Similar analysis for dry (section C.1) and wet (section C.2) operation at 80/82^{o} F will be presented in this Appendix. All results are consistent with results in Chapter 3 and 4 and lead to the same general conclusions.

C.1 Dry coil experiments

C.1.1 Short-cycling losses at μ=0.57 compared to continuous operation

System efficiencies were compared by monitoring the difference between the whole-cycle mean tube temperature ($T_{m,avg}$) and the on-cycle mean saturation temperature ($T_{sat,on,avg}$) in the evaporator and condenser. The larger those differences, the greater the COP degradation relative to the ideal baseline operation at a given capacity. Figure C.1 shows how temperature lift increases with cycle period. Evaporator and condenser temperature lift degradation terms (ΔT_e and ΔT_c) were compared at two different cycle periods (τ=10 and 50 seconds).

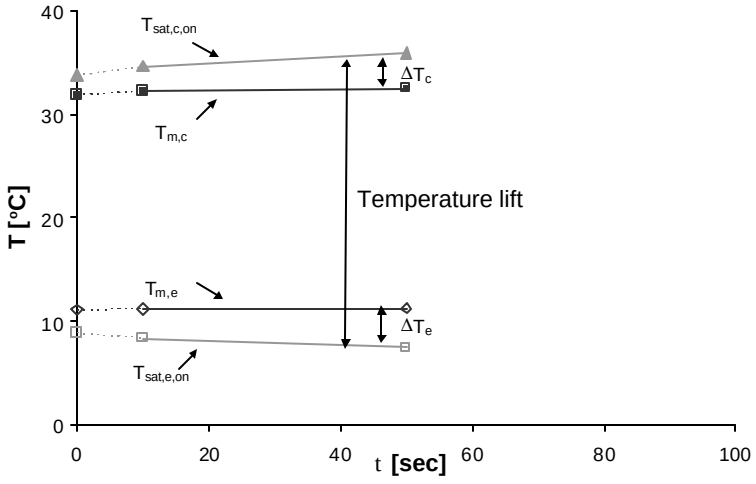

Figure C.1 Saturation temperature lift and degradation terms increase with τ

In order to compare cycle COP's the effect of potentially different compressor efficiencies was eliminated by calculating the smaller compressor's steady-state specific power using steady-state compressor calorimeter data provided by the manufacturer of the larger scroll compressor. The experimental points at τ=0 represent continuous operation of the smaller compressor. The temperature lift degradation for continuous operation relative to ideal baseline operation is 2.3^{o} C on evaporator and 1.9^{o} C on condenser side (as can be seen in Figures C.1, C.3 and C.4).

In the same way as in the Chapter 4 the focus in this Appendix is on the incremental increase in temperature lift attributable to short-cycling (SC) relative to variable speed (VS) operation, where the continuous operation of smaller compressor represents theoretical VS operation without inverter losses. This incremental temperature lift term is defined as the difference between the short-cycling lift degradation term at given cycle

period and continuous operation lift degradation term, $\Delta T_{e,loss} = \Delta T_{e,sc}(\tau) - \Delta T_{e,vs}(\tau=0)$. This term represents the temperature lift degradation of short-cycling operation at given cycle period compared to the operation at τ=0.

The lift loss term can be seen in Figures C.3 and C.4 as the temperature lift degradation term increases 0.5° C on evaporator and 0.4° C on condenser side as cycle period increases from 0 to 10 seconds. Compared to continuous operation (VS), short-cycling at this relatively high frequency degrades COP by approximately 2% as shown in Figure C.2.

As cycling period increased to 50 seconds, the COP degradation reached about 5.5% due to the "lift loss" of 1.5° C on evaporator and 1.5° C on condenser side shown in Figures C.3 and C.4.

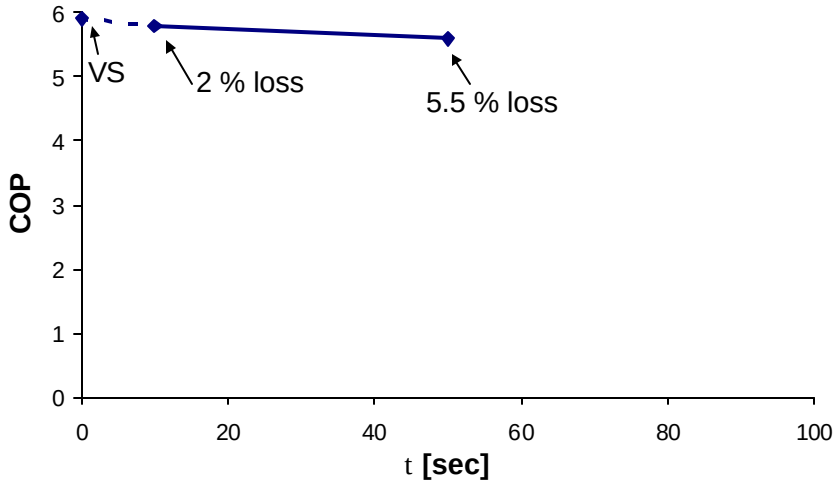

Figure C.2 Coefficient of performance decrease with τ

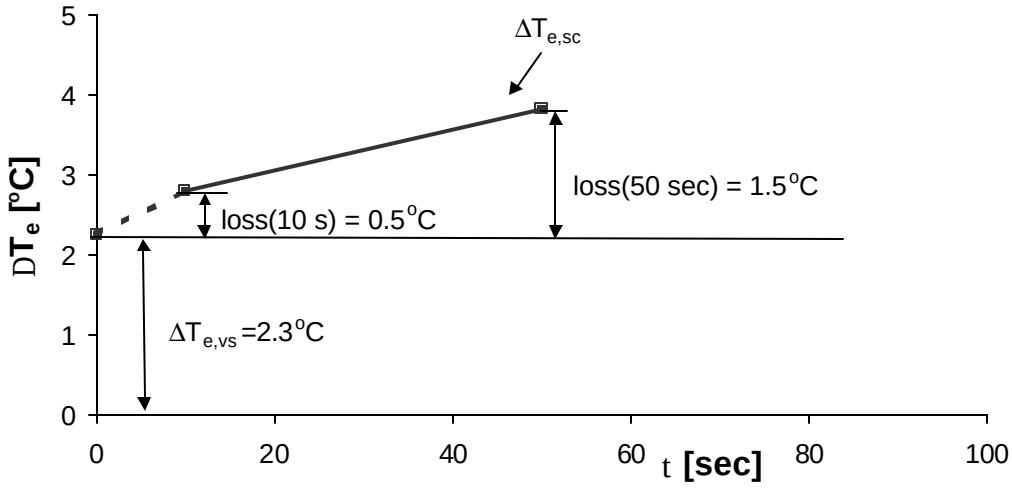

Figure C.3 Evaporator side lift degradation term increase with τ

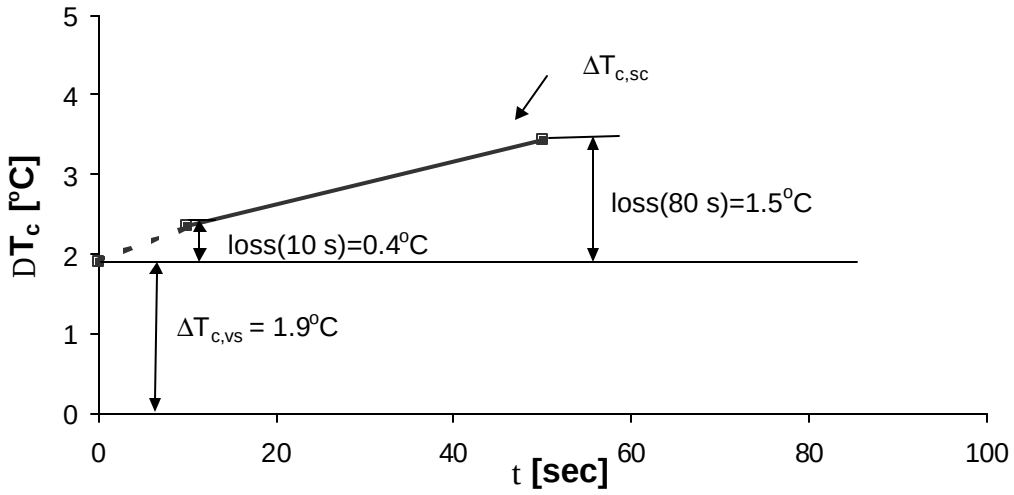

Figure C.4 Condenser side lift degradation term increase with τ

C.1.2 Temperature lift degradation breakdown for τ=0, 50 seconds at μ=0.57

Recall from Chapter 3 and 4 that three factors cause degradation of temperature lift: refrigerant heat transfer (rht) resistance, pressure drop and nonlinearity due to thermal capacitance (nonlin). Figures C.5 and C.6 quantify these effects for the evaporator and condenser respectively. The effect of thermal capacitance (nonlinearity of temperature oscillations) is by definition zero for continuous operation at τ=0, and negligible for short-cycling operation at 10 seconds. It becomes significant for evaporator at long cycle periods (τ=50 seconds), and earlier for the less massive condenser.

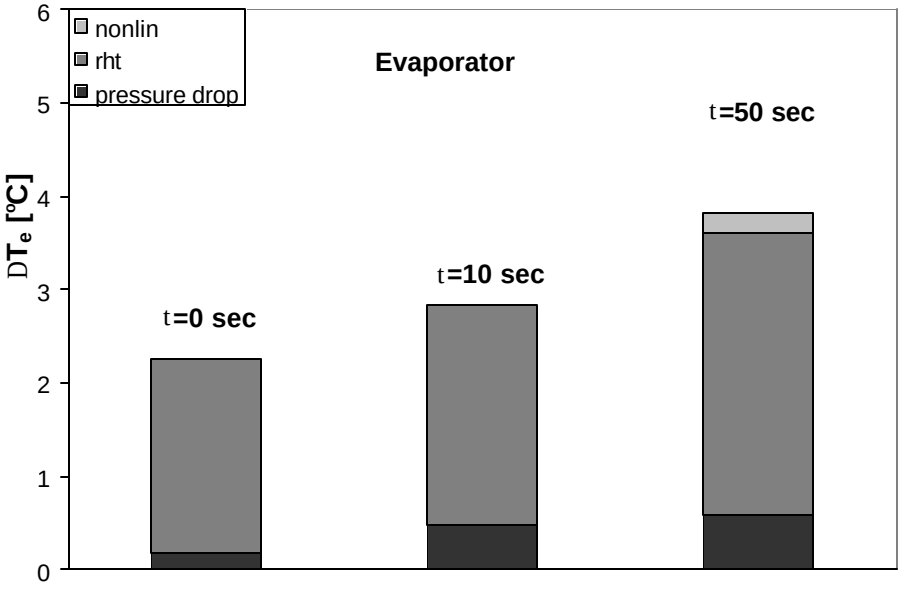

Figure C.5 Lift degradation term breakdown on evaporator side

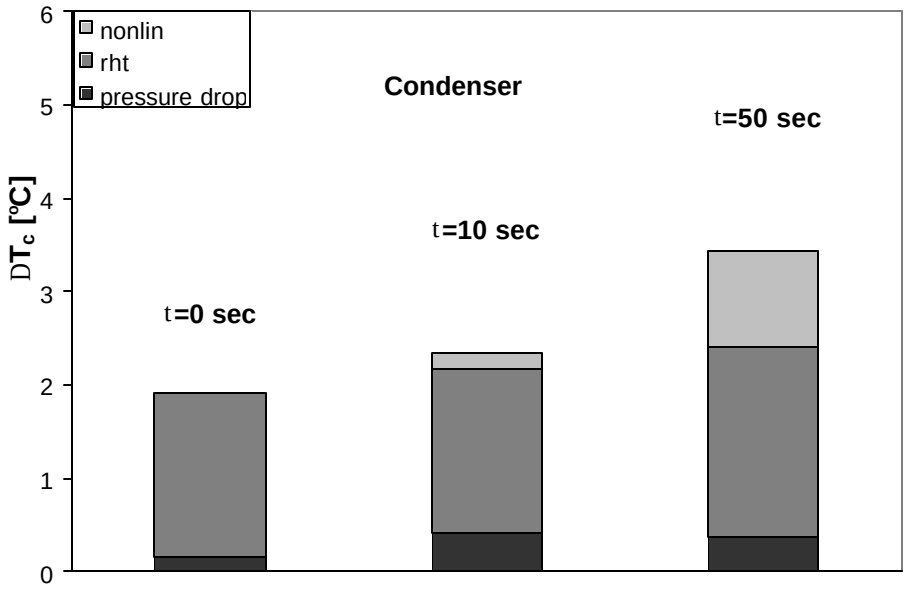

Figure C.6 Lift degradation term breakdown on condenser side

C.1.3 Lift loss for τ=10 and 50 seconds at μ=0.57

The graphs in this section focus on the incremental degradation of temperature lift due to short-cycling. Figures C.7 and C.8 present detailed analysis of this lift loss term at τ=10 and τ=50 seconds on condenser and evaporator side. It is by definition zero for continuous operation. Recall from Figure C.2 that this additional temperature "lift loss" caused COP losses of about 2% and 5.5% at τ=10 and τ=50, respectively, compared to VS operation.

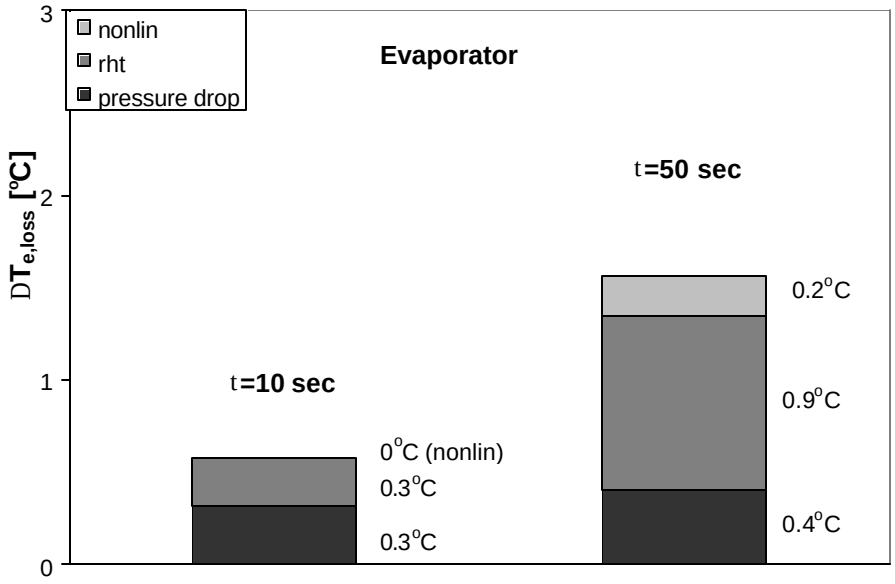

Figure C.7 Breakdown of the lift loss term on evaporator side

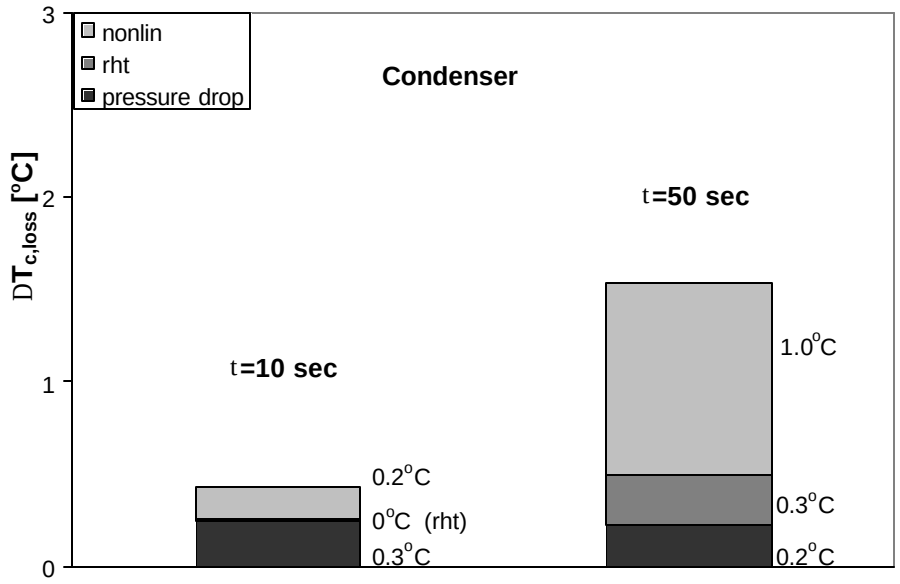

Figure C.8 Breakdown of the lift loss term on condenser side

C.1.4 Short-cycling comparison to conventional cycling

Figure C.9 shows an 9% COP difference (at τ=0) between continuous operation of the small 1-ton compressor simulating the variable-speed case, and the nominal 2-ton compressor, simulating conventional cycling. It also shows how short-cycling reduced this loss (cycling relative to VS operation) to 2% and 5.5% at cycle periods of 10 seconds and 50 seconds, respectively. As in Chapter 4 for 80/95° F operating condition, the comparison is approximate, since it neglects cycling losses in the CC case, and difference between blower power requirements, both of which should favor SC over CC.

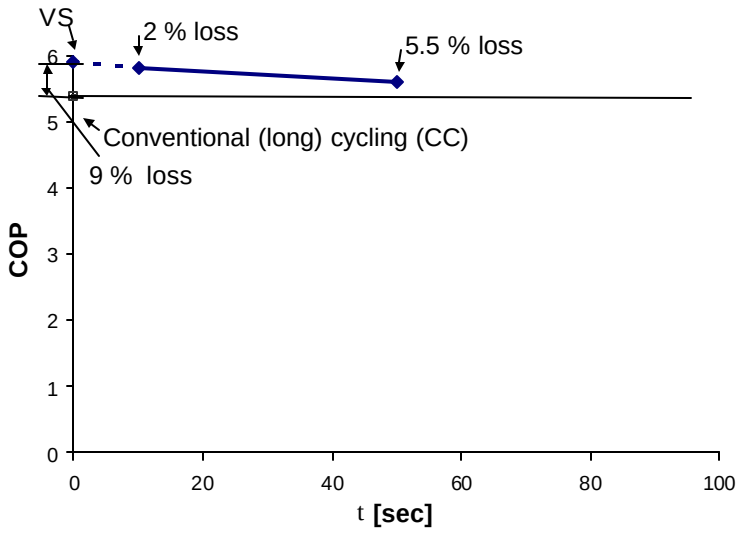

Figure C.9 COP comparison to conventional cycling

C.2 Wet coil experiments at 26.7/27.7 C (80/82 F)

The purpose of the wet surface experiments at 80/82^{o} F was to determine whether the latent load had any effect on COP degradation caused by short-cycling. Results presented in section 3.6 of Chapter 3 showed that there was no significant difference in between wet and dry coil tests at 80/95^{o} F operating condition.

Almost the same COP degradation for wet and dry experiments at the 80/82^{o} F operating condition was expected, since the refrigerant sees only the constant tube wall temperature, which is nearly identical for both cases.

Virtually identical increases in on-cycle temperature lift for wet and dry coil experiments caused essentially identical decreases in COP. The experimental results showing an increase in the on-cycle temperature lift with cycle period, for a given run time fraction were almost the same for both dry and wet coil experiments as shown in in Figures C.1 and C.10, respectively. There is no significant difference in COP degradation observed, for the wet and dry coil experiments, as shown in Figures C.2 and C.11.

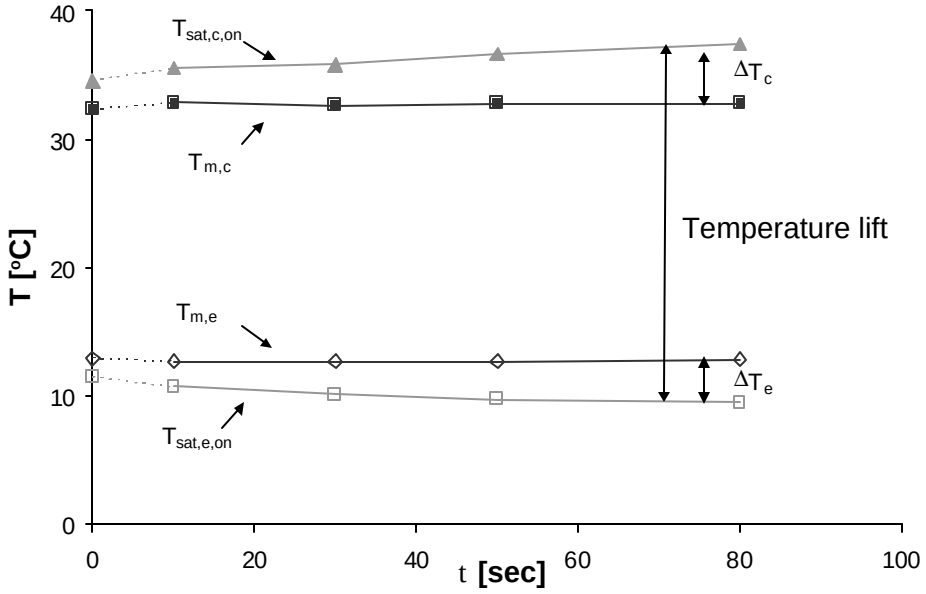

Figure C.10 Saturation temperature lift and degradation terms increase with τ

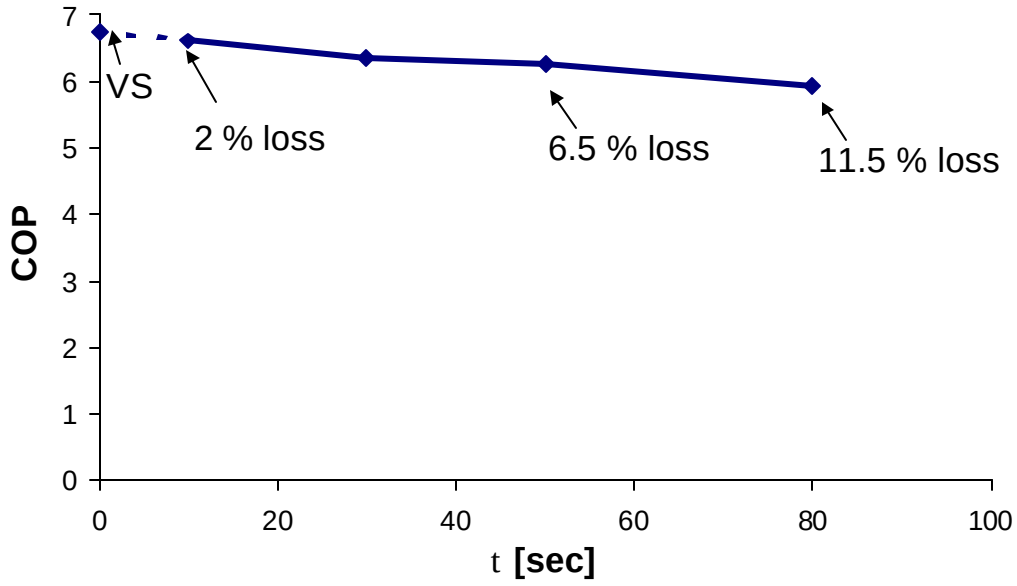

Figure C.11 Coefficient of performance decrease with τ

APPENDIX D: Temperature lift degradation for open vs. closed valve

Table D.1 shows the three components of the evaporator lift degradation term, ΔT_e, for both OV and CV operation. For the OV strategy ΔT_e was 0.5 C higher, refrigerant side heat transfer term was 0.9 C higher, and the nonlinearity term was negative, suggesting the possibility of experimental error.

Table D.1 Lift degradation term and its components for OV and CV operation

	μ	τ [sec]	ΔT_e [^{o}C]	ΔT_e(rht) [^{o}C]	ΔT_e(nonlin) [^{o}C]	ΔT_e(ΔP) [^{o}C]
CV	0.5	30	2.9	2.2	0.2	0.6
OV	0.5	30	3.4	3.1	-0.2	0.5

Figures D.1 and D.2 show evaporator saturation and metal temperatures for CV and OV operation respectively. Off-cycle evaporation persisted a few seconds longer in the OV case, and the on-cycle metal temperature fluctuation differed between two experiments. Measured on-cycle refrigerant ΔT was much higher during OV operation, due to higher on-cycle metal temperature, not lower saturation temperature. It is possible that the valve opening was not set properly for OV causing difficulty maintaining the no-superheat condition at the exit of evaporator. On the other hand, the repeated transient in the superheat shown in Figure D.3 may reflect the existence of a transient or even periodic two-phase flow regime during OV operation. Whatever the causes, the result was a higher weighted on-cycle average metal temperature. higher ΔT_e(rht), and negative ΔT_e(nonlin) for the OV operation.

The pressure drop part of temperature lift degradation term was apparently not affected, as shown in Figure D.5. The equality of refrigerant side pressure drops may seem surprising for such radically different flow management strategies. Near the evaporator inlet the off-cycle flow velocities are obviously different. However, most of the pressure drop in an evaporator occurs in the high-quality regions where the velocities are up to 5 times higher than at the inlet. At the evaporator exit, refrigerant velocity is determined by the compressor, and is by definition zero during the off-cycle for both strategies. Therefore it should be expected that the pressure drops would be almost equal for OV and CV operation as shown in Figure D.5.

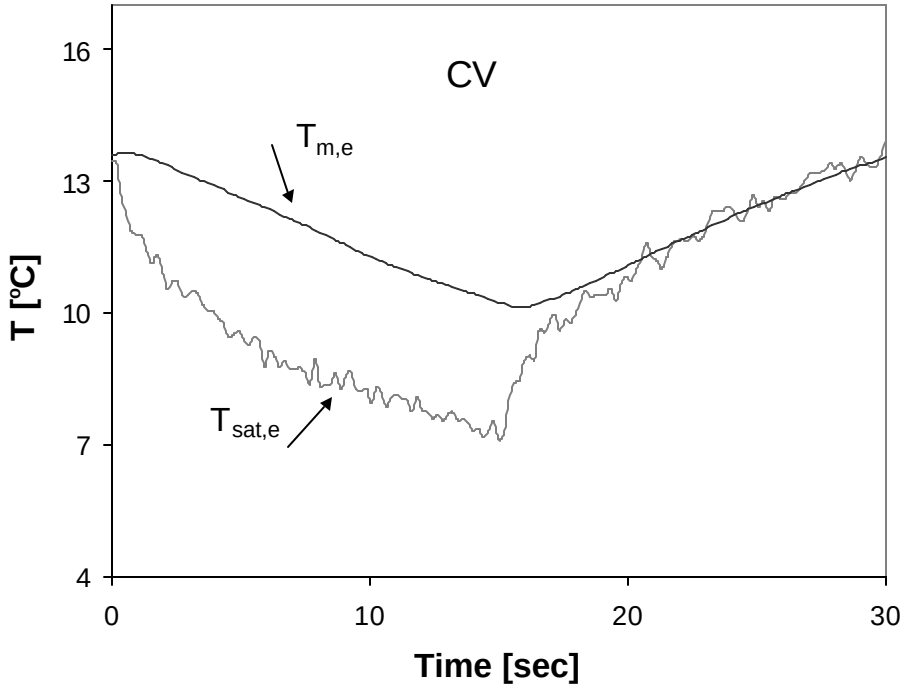

Figure D.1 Evaporator metal and saturation temperature for CV

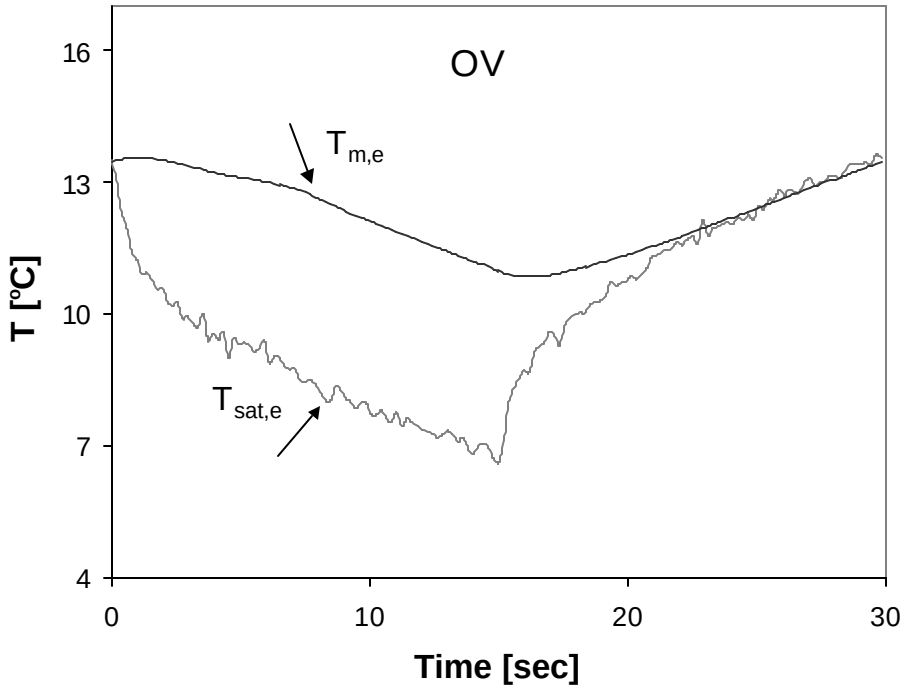

Figure D.2 Evaporator metal and saturation temperature for OV

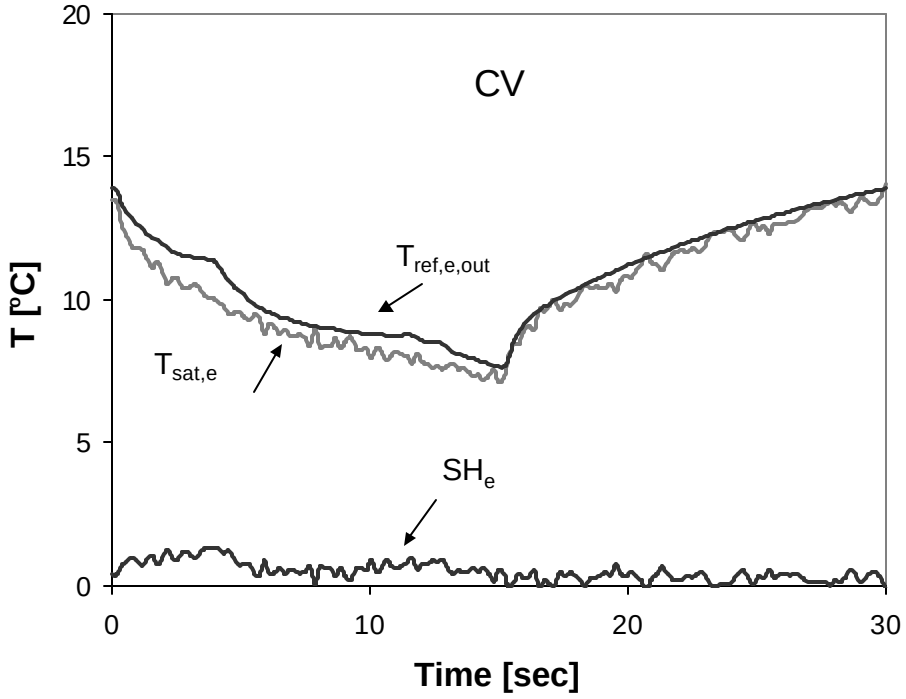

Figure D.3 Evaporator superheat for CV

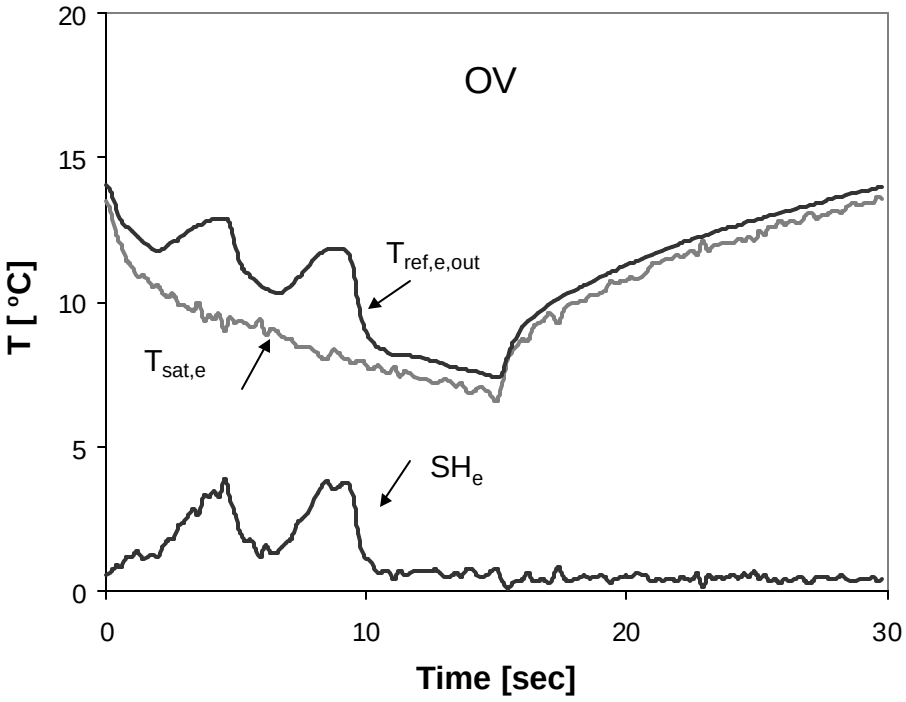

Figure D.4 Evaporator superheat for OV

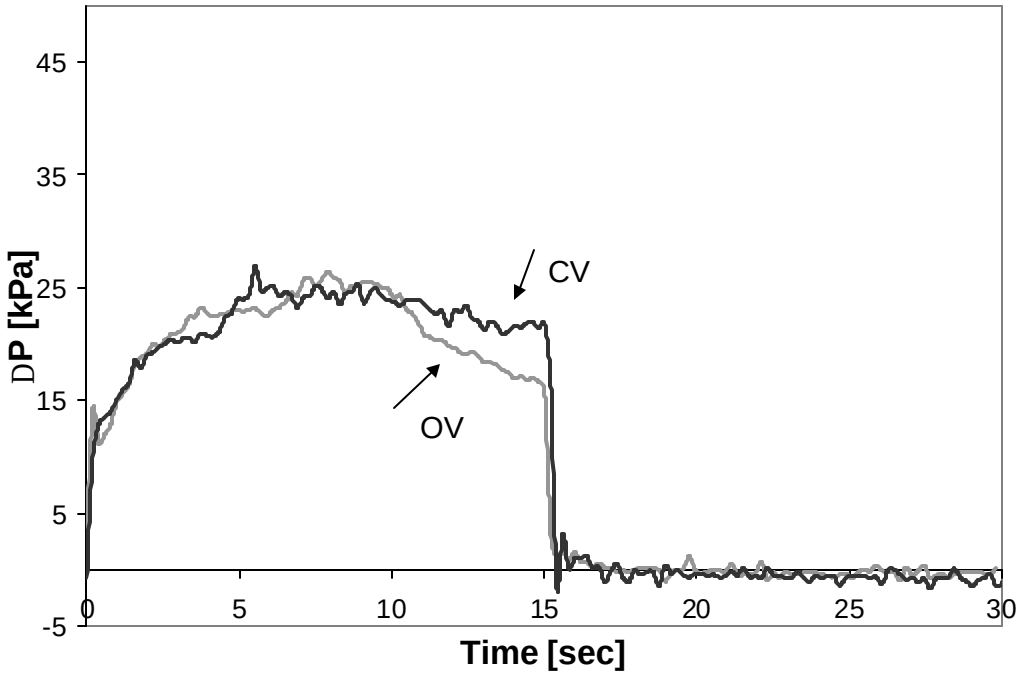

Figure D.5 Evaporator pressure drop overlaid for OV and CV operation

It is clear from the analysis done in section 3.6 of Chapter 3, that COP differences are almost negligible when off-cycles are as short as 15 seconds. The conclusion was that to see bigger differences between OV and CV, one would need to look at longer cycle periods.

The experiments at τ=80 seconds and μ=0.5 were conducted for both OV and CV operation, but the maintenance of compressor inlet superheat at the same level for both strategies was impossible using available expansion device and tape heater (EEV and tape heater use was explained in section 2.2 of Chapter 2). Therefore experiments were incomparable, and better superheat management at longer cycle periods is recommended for future tests. Ideally, fast electronic expansion device without time lags between the superheat sensor and valve controller is recommended. Time lags in superheat response to the valve opening may be an issue as well.